A Geometric Morphometric Study of Sexual Dimorphism in the Human Hip Bone

by

Heather Isobel Robertson
Bachelor of Arts, Simon Fraser University, 2004

A Thesis Submitted in Partial Fulfillment
of the Requirements for the Degree of

MASTER OF ARTS

in the Department of Anthropology

Supervisory Committee

A Geometric Morphometric Study of Sexual Dimorphism in the Human Hip Bone

by

Heather Isobel Robertson
Bachelor of Arts, Simon Fraser University, 2004

Supervisory Committee

Dr. Helen Kurki, (Department of Anthropology)
Supervisor

Dr. Lisa Gould, (Department of Anthropology)
Departmental Member

Abstract

Supervisory Committee
Dr. Helen Kurki, Department of Anthropology
Supervisor
Dr. Lisa Gould, Department of Anthropology
Departmental Member

The purpose of this study was to use geometric morphometrics (GM) to investigate the relationships between non-metric traits of the human hip bone: the greater sciatic notch (GSN), the ventral arc (VA), the subpubic contour (SPC), and the ischiopubic ramus ridge (IPRR), estimated skeletal sex, and shape. Fifty-nine undocumented left hip bone specimens were visually assessed for skeletal sex using recognized standards of sex estimation for the GSN (Buikstra and Ubelaker, 1994). The VA, SPC, and IPRR were assessed according to Klales et al., (2012). The Non-metric traits were scored on a five-scale scheme. Skeletal sex was classified as either male, possible male, indeterminate sex, possible female, or female. Three-dimensional computer models were created of the hip bones using the NextEngine 3D desktop surface scanner. Thirty landmarks were selected to represent the hip bone in three-dimensional shape for GM analysis. Twenty-seven of the selected landmarks were reliable according to suggested digitizing error measurements. The apex of the auricular surface, the arcurate eminence, and the anterior gluteal line were the least precise in the test for digitizing error. Geometric morphometric analysis of the computer models were performed using MorphoJ software. Principal component analysis identified the patterns of hip bone shape within the sex categories. A Procrustes ANOVA and a Spearman's correlation tested the significance between hip bone shape and estimated skeletal sex, and between hip bone shape and non-metric trait morphology.

Patterns of hip bone shape in the ischium could not be identified by sex, however sex differences were identified in ischium size. Patterns of hip bone shape in the whole hip bone, segmented ilium and segmented pubis were distinguishable by larger sex groups (males = male and possible male categories; females = female and possible female categories). Shape patterns alluded to differences between females and possible females,

however, shape patterns did not distinguish males from possible males. Individuals of indeterminate sex shared similar hip bone shapes as males and were therefore included in that larger sex group. Hip bone shape was also correlated with GSN, SPC, IPRR, and VA. However, the strength of the correlation differed between non-metric traits and certain components of hip bone shape. The GSN and SPC had the strongest correlation ($p=<0.01$) with the whole hip bone, the ilium and the pubis at distinguishing between larger male and female sex groups. The IPRR, and GSN had the strongest correlation ($p=<0.01$) with the pubis at distinguishing females and possible females.

The results of the study suggest that non-metric traits can discern patterns of female shape better than patterns of male shape. Further research into discerning patterns of male hip bone shape and non-metric trait variation using GM is suggested. The results of the study also suggest that patterns of pubis shape might exist among females and could be identifiable using pubis non-metric trait scores. This result lends credence to the practice of estimating sex on a five-scale gradient rather than on a male/female dichotomous division, in order to capture the morphological variation of female hip bone better.

Table of Contents

List of Tables

List of Figures

Acknowledgments

There are many people I wish to acknowledge who were involved in the success of this thesis both directly and indirectly. I wish to thank my family and my friends who supported and encouraged my decision to commute to a University over 100km away from home. I especially acknowledge the patience of Dr. Douglas Ross and Anika Robertson who lived with my many incarnations throughout this process. To those in the Department of Anthropology at the University of Victoria who inspired and instructed me, I thank you for your wisdom and for your knowledge. I especially wish to acknowledge the insights of Dr. Helen Kurki and Dr. Lisa Gould that guided me along this journey. Thanks also to Shannon Wood and Dr. Barbara Winter in the Department of Archaeology at Simon Fraser University, and Dr. Danmei Liu from the Centre for Hip Health and Mobility who in their different ways inspired, prepared, and encouraged me to begin this journey. This research would not have been possible if not for those who helped facilitate it. The Department of Cellular and Physiological Sciences at the University of British Columbia, thanks to Dr. Claudia Krebs, Ciaran Connolly, Erin Gloeden, Heather Farnden, and Alan Gilmour, provided the time and the specimens needed to see the fruits of this research.

Dedication

For:

Doug and Anika;

Julia and Sasha

Chapter 1 : Introduction and Background

1.1. Introduction

Sex estimation and categorization is easily accomplished in human osteology when there are clear size and shape difference between the hip bones of males and females (Buikstra and Ubelaker, 1994; Listi, 2010; Phenice, 1969; Walker, 2005). Problems occur in sex estimation when there is little sexual dimorphism within a population (Rosenberg, 2002). When sexual dimorphism is limited, it has the potential to conflate sex identification by making size differences and morphological sex traits indistinguishable, resulting in "possible" or "indeterminate" sex determinations if applying visual methods to estimate sex (Buikstra and Ubelaker, 1994). Regardless of the level of size dimorphism in a population, shape-based sex differences are retained because obstetric capacity is constant in females (Gustafson and Lindenfors, 2004; Kurki, 2007, 2011, 2013; Ridgeway et al., 2011; Tague, 2000). Therefore, sex-based shape differences should be discernible even if sexual dimorphism and non-metric trait discrimination are limited. The purpose of this research is to gain new insight into human hip bone morphology and its relationship with non-metric sex traits using a new method of analysing shape differences in bone, geometric morphometrics (GM). This research has two goals. The first goal is to investigate the morphological characteristics that distinguish sex in whole and partial hip bone shapes using GM analysis. This goal is important for understanding the variations of hip bone shape among males and females in both whole and partial hip bones. The second goal of this research is to explore the relationships between non-metric trait morphologies and hip bone shape in whole and

partial hip bones. It is important for broadening our understanding of non-metric trait patterns among male and female groups in order to gain new insights into using non-metric traits when estimating the sex of individuals from populations with limited sexual dimorphism between males and females, or between populations.

Sex differences in human osteology are predicated by anatomical differences in the human skeleton, such as non-metric traits and reproductive capability (Buikstra and Ubelaker, 1994; Gellar, 2005; Phenice, 1969; Walker, 2005. In order to understand how morphological variability in humans could influence sex differences in the human hip bone it is important to review the evolutionary life history of the hip bone (Buikstra and Ubelaker, 1994; Nordbladh and Yates, 1990). The shape of human hip bone is a product of bipedalism, and the shape of the human female pelvis is a negotiation of the biomechanical needs of bipedalism and the obstetric capacity to give birth to large brained human infants (Grabowski et al., 2011). Environmental adaptation generates population variation in the size of the hip bone, whereas genetic variations in the form of timing and rate of adolescent growth influence hip bone size and shape variation among individuals. Evolutionary, environmental, and genetic factors are also important to consider when conceptualizing of sexual dimorphism in the human skeleton. Skeletal sex is understood as an extension of biological sex, is observable in phenotypic and genotypic traits, and is categorized dichotomously (Geller, 2005). However, when considering the factors that contribute to hip bone morphology, the dichotomous categorization might not represent that complexity adequately (Blackless et al., 2000; Fausto-Sterling, 2000; Nordbladh and Yates, 1990). A range of sex categories might be a better approach to represent both sex and shape variation.

The conceptualization of sex is evident in the methods human osteologists use to estimate sex. Ordinal methods of sex estimation involve visually assessing skeletal morphology and scoring, or ranking, non-metric traits such as the ventral arc, subpubic contour, ischiopubic ramus ridge, and the greater sciatic notch along a shape continuum from hyper-male to hyper-female (Buikstra and Ubelaker, 1994; Byers, 2002; Klales et al., 2012; Phenice, 1969; Walker, 2005). Metric methods of sex estimation rely on absolute measurements to determine sexually dimorphic size and shape (Arun et al., 2012; Luo, 1995; Washburn, 1948). Both methods have an array of strengths that make them suitable for estimating sex on the human hip bone, however, they also have their limitations. A common limitation found in both sex estimation methods is remaining useful or applicable when estimating sex from fragmented hip bones (Arun et al., 2012; Brůžek, 2002; Buikstra and Ubelaker, 1994; Rogers and Saunders, 1994). Geometric morphometrics (GM) is a relatively new method of investigating sex differences using landmarks to represent object shape and size as Cartesian coordinates in tangent space. Applied to the understanding of sex-based shape differences, GM combines the strengths of ordinal sex estimation methods as it captures bone shape variation, and metric sex estimation methods as it captures bone size and Euclidian distances (Gómez-Valdés et al., 2012; Pretorius et al., 2006; Slice, 2007; Zelditch et al., 2004). Geometric morphometrics also addresses the limitations of ordinal methods by being a more objective assessment of shape than visual assessments, and the limitations of metric methods by being a more accurate measure of sex. For these reasons, GM is an ideal technique to use to investigative sex-based shape differences in the human hip bone as a whole and in isolated shapes. Until now GM has been used to determine sex

dichotomously, however, this research will attempt to isolate the sex-based shape differences on a five-scale sex continuum.

1.1.1. Theory of skeletal sex in human osteology

According to Geller (2005), skeletal sex is conceived of as a natural biological division within a species for the purpose of reproduction, is observable in phenotypic and genotypic traits, and is categorizable into binaries. Geller goes on to critique the analytical rigidity created by a biologically defined sex binary, a sentiment that is shared by a few other authors (Nordbladh and Yates, 1990; Hollimon, 2011; Sørensen, 2000), and proposes analysing sex as separate from biology. The result is a new concept of gender theory that includes sexuality to illustrate the multifaceted movement of societal roles, sexuality, and identity that are independent of biology (Geller, 2005). Although Geller's proposed view of gender provides a fluid and retrospective theoretical foundation, it shifts the gaze away from the arguments that review and critique dichotomous sex classification in human osteology and in biology (Blecher and Erickson, 2007; Nordbladh and Yates, 1990; Sitek et al., 2012). Arguably, a continuum of sex categorization proposed by Nordbladh and Yates (1990) and Blecher and Erickson (2007) is a justifiable concept of skeletal sex. Using Geller's model of how sex is conceived of in human osteology, I will outline an alternative view of how sex can be conceived of in biology, not as a binary, but as a continuum. Evolutionary and adaptive forces mitigate size and shape differences in the hip bone rather than define natural dimorphism of the human species; phenotypic and genotypic traits do not separate the sexes clearly in

biology, and are less clear in human osteology; and categorization of sex needs confident terminology in order to be divided along a continuum.

1.1.1.1. Reproduction, evolution, and adaptation

In Geller's critique of how sex is conceived of in human osteology, she claims that human osteologists perceive biology as unchanging, subjected to western ethnocentrism, and positivistic epistemologies. As such, she divorces sex from biology by suggesting that sex, like gender, is a cultural construct in the way science, medicine, and society take the binary division of sex for granted (Geller, 2005). This idea persists among some human osteologists in the way sex is interpreted and categorized, but it is sometimes tempered with the recognition that sex is also variable between populations (Byers, 2002; Mays, 2010; Sofaer, 2006; White, 2000). Other human osteologists suggest alternative methods to the classic division of sex as binaries (Agarwal, 2012; Hollimon, 2011; Klales et al., 2012; Nordbladh and Yates, 1990). If we, human osteologists, deepen our perception of how "biological sex" came to be in modern humans by reviewing the evolutionary life history of the hip bone, we can begin to see that biology and sex are not static, but dynamic. Sexual dimorphism of the human hip bone is a reflection of the reproductive mechanics of parturition and body size in a large brained bipedal primate (Arsuaga and Carretero, 1994; Grabowski et al., 2011; Lovejoy, 2005; Plavcan, 2011; Tague, 1991). Habitual bipedalism is possible due to changes in the shape of the sacrum, spine, and hip bones to accommodate the muscles that maintain an upright posture (Lovejoy, 2005). Over time, the morphology of the pelvis (articulated sacrum, coccyx, and hip bones) widened antero-posteriorly to accommodate the expanding hominin brain

(Lovejoy, 2005). In humans, the biomechanical demands of bipedalism on the human hip bone favour a narrow pelvis, and the cephalo-pelvic demands of birthing a large brained baby encourage a wider female pelvic complex (Grabowski et al., 2011; Lovejoy, 2005). Together, these two forces have generated a hip bone morphology that is uniquely human. In a reproductive framework, dimorphism of the hip bone is clear, females must give birth and the hip bone shape must accommodate this, males do not give birth so the hip bone shape is free to conform to only the biomechanical needs of bipedalism. However, dimorphism of the hip bone becomes more complex when factoring in theories of mate selection and environmental adaptation.

The measure of sexual dimorphism in body size between males and females of a species is believed to be influenced by the pattern of mate competition and mate selection adopted by that species (Badyaev, 2002; Plavcan, 2011). For example, among mixed-sex primate groups, where males compete for mating privileges, males tend to be larger than females in body size and secondary sex characteristics especially among anthropoids (Badyaev, 2002; Plavcan, 2011). Body size differences among "monogamous primates," primates who tend to form long-term mating partnerships with one mate and arguably include humans, are less contrasting between males and females than among mixed-sex primate groups. One possible reason for this is that the males are not competing for mating privileges, but rather males and females are selecting desirable traits in the opposite sex that lead to variations in body size selection in both sexes (Plavcan, 2011). Plavcan (2011) suggests that low female metabolic demands during pregnancy, and high fecundity due to a younger reproductive age are desirable traits found in smaller sized females (Gluckman and Hanson, 2006; Nettle, 2002b). However, mate selection is not

the only factor to influence body size variations. Adaptation to differences in climate can also influence body breadth and size, which are reflected in hip bone shape differences in human populations because of thermoregulation (Ruff, 1991; 2002). Wider and shorter pelvic complexes are generally characteristic of colder climates because they have less surface area for heat exchange, whereas taller and narrower hip bones have more surface area to facilitate heat loss and are generally characteristic of warmer climates (Ruff, 1991; 2002).

By acknowledging the complexities of change that has taken place in human evolution, we can see that dimorphism, as it manifests in the skeleton, has a complicated past rooted in biology. Dimorphism is a product of the reproductive mechanism of childbirth in females and patterns of mate selection, while environmental adaptation generates size and shape variability within human females and males. Size and shape variability within sex groups does not pose a *prima facie* problem for sex estimation until the morphology of one sex group resembles the morphology of the other sex group, creating an overlap between the sexes (Bidmos et al., 2010; Phenice, 1969; Steyn and Patriquin, 2009; Rosenberg, 2002; Washburn, 1948). One way of investigating the male/female overlap of size and shape is to understand other sources of size and shape variability in the hip bone.

1.1.1.2. Genotypic and phenotypic sex traits

Genotypic and phenotypic sources of hip bone size and shape variation can contribute to male/female morphological overlap. Typically, genital form and function, primary sex characteristics, are derived from allosomal combinations (Stone, 2008).

Ovaries develop from an XX allosome pair while testes develop from an XY combination (Blecher and Erickson, 2007; Fausto-Sterling, 2000). Secondary sex characteristics develop during adolescence, and endocrine secretions from sex organs govern their development (Blecher and Erickson, 2007; Wilson, 1981). Typical allosome combination, creating typical gonad form and function, lead to typical skeletal sex characteristics, such as a larger and narrower hip bone in males and a smaller and wider hip bone in females. However, in rare cases, multiple chromosomes combine in the fertilized ovum, or there is an absence of an autosome after fertilization, which affect gonadal development and endocrine secretion such as Turner Syndrome (XO) or Klinefelter Syndrome (XXY). The endocrine changes related to chromosomal changes influences the shape of the hip bone away from the typical phenotype (Fausto-Sterling, 2000; Stone, 2008). It has been suggested that androgens influence the shape of the male hip bone during adolescence, and the presence of androgen receptors in females could influence the shape of the female hip bone closer to a male shape (Sitek et al., 2012; Iguchi et al., 1995). In animal trials, the absence of androgen production due to castration resulted in female like hip bones (Iguchi et al., 1995; Uesugi et al 1992).

However, new research into the genetic influences of the development of secondary sex characteristics has suggested that sex-determining factors in the allosomes, and possibly in the autosomes, is what stimulates the development of sex characteristics into male and female forms rather than simply endocrine secretions derived from allosomes combination (Blecher and Erickson, 2007). This could explain why individuals with Turner Syndrome, who have limited ovarian function and endocrine levels, develop phenotypically female characteristics. It could also explain why

individuals who are XXY and have limited endocrine function, produce a smaller and wider hip bone, similar to the female shape, in spite of having a XY allosome combination (Blackless et al., 2000; Blecher and Erickson, 2007; Uesugi et al., 1992). Sex-determining factors also explain why individuals with typical sex chromosome parings can develop intersexed phenotypes (Blecher and Erickson, 2007). The most common type of phenotypic intersexuality, congenital adrenal hyperplasia (CAH), occurs in roughly 1.5 percent of the population (Fausto-Sterling, 2000). Congenital adrenal hyperplasia causes the growth of masculine like genitalia in infants with XX chromosomes (Blackless et al., 2000). The factors that promote masculine like genitalia in XX individuals could very likely influence the shape of the hip bone. Primary sex characteristic morphologies could be the result of more male sex-determining factor in the individual, which could in turn influence the morphology of secondary sex characteristics including the hip bone. The degree to which the hip bone could change in intersexed individuals and individuals with gonadal dysgenesis is unknown, it could resemble a more masculine hip bone or it could resemble a female/male hybrid shape if obstetric capacity is maintained in females.

Sex-determining factors could be an important cause of morphological variation that explains male/female overlap of hip bone non-metric traits. The combined prevalence of Turner Syndrome, Klinefelter Syndrome, and CAH intersexuality is roughly 2% of the population. In the hip bone that could mean 2% of all skeletal specimens could be intersexed and possess a hip bone morphology that is unique to the typical "male" or "female." In the most accurate of current human osteological methods there is a 2% accuracy error that is attributed as an artifact of method quality resulting in

hip bone misclassification (Brůžek, 2002). However, it could also be the result of trying to fit three morphological types into two categories. It is not the goal of this thesis to uncover the causes of hip bone misclassification or intersexuality, however, it is important to consider what might be occurring in 2% of the population when interpreting the accuracies of sex estimation methods that will be introduced later in this chapter. Sitek and colleagues (2012) found a pattern of hip bone shape in female to male transsexuals that was different from non transsexual females. Individual hormonal variance could be one of the causes of hip bone shape variance due to sex determining factor (Blecher and Erickson, 2007; Sitek et al, 2012). The biological predictor of sex is therefore more complicated than it once appeared and contributes to the dynamic properties of sex as biology.

Blecher and Erickson (2007) also suggest that sex-determining factors influence sex and growth hormones of males and females of typical chromosomal sex to produce population specific morphological sex characteristics. This would account for the variation in hip bone size and shape seen across populations that lead to the overlap of hip bone size and shape when these populations are compared (MacLaughlin and Bruce, 1986; Patriquin et al., 2005; Washburn, 1948). How genetic and other intrinsic or extrinsic factors influence bone shape differences could be studied in human osteology in more detail if hip bone shapes are distinguished or categorized using a spectrum of morphology. The existence of these and other dynamic properties of bone growth and development are some reasons why it is important to represent the shape differences of the hip bone as a spectrum of morphology within biology.

1.1.1.3. Certainty when estimating sex from the hip bone

Certainty in sex estimation is necessary in human osteology in order to instill confidence in the method of sex estimation used, and because identification of skeletal material in forensic cases require that the results stand up to cross-examination scrutiny (Byers, 2002; Mays, 2010; Nordbladh and Yates, 1990). Phenice (1969) and Brůžek (2002) use inclusive language to describe the morphological overlap between males and females as "intermediate" sex, denoting a place in-between the sexes, rather than the term "ambiguous" sex used by Buikstra and Ubelaker (1994) that depicts an unknown or unclear morphology. The language used by Buikstra and Ubelaker is part of the standard methods of sex estimation and as such, the idea of ambiguity in sex estimation spreads. The response then is to create new methods of sex estimation that attempt to increase certainty of sex estimation in an attempt to conquer the idea of an ambiguous sex (Brůžek, 2002; Rogers and Saunders, 1994).

However, uncertainty in sex estimation might have less to do with the method used and more to do with the specific use of terminology aimed at describing completeness of the bone on which the sex estimation method is being performed (Mays, 2010). The terms used in Brown (1998), in order of most confident to less confident, illustrate the reliability of sex estimation on incomplete skeletal remains: "likely," "possible," or "probable," male or female. The term "probable" is also used by Buikstra and Ubelaker (1994) to distinguish uncertain sex estimations from confident sex estimations. When compared to Brown's terminology, it could be assumed that the level of confidence Buikstra and Ubelaker are referring to in a "probable" sex estimation has the same level of confidence as Brown's "probable" sex estimation. There is no way of

knowing for sure if the two terms are referring to similar levels of confidence. However, the important point is to distinguish, either by nomenclature or in text, when uncertain sex estimation is due to incompleteness of the remains or of the traits used, and when uncertainty is due to the accuracy of the method used to estimate sex. When remains are complete, sex estimation terminology should reflect an inclusive nomenclature for the morphological variation within the study sample. If the terminology of sex estimation categories presented less ambiguous language and use a nomenclature that emphasizes morphological variation, confidence in sex estimation could increase.

1.1.2. How to Categorize sex

What is sex? The idea of sex has gone through a series of incarnations. Beginning as a substitute for "gender" and "sexuality," "sex" was criticized for being a static, polarizing, and confining term (Butler, 1993; Gilchrist, 1999; Lorber, 1996). Sex and gender were later defined separately, sex was defined as pertaining to biology while gender was defined culturally (Gilchrist, 1999). Sex, not separated from sexuality, returned once again to the theoretical realm of a cultural construct as the heterosexual hegemonic structure of sexuality and gender theories began to breakdown (Butler, 1993; Geller, 2005; Gilchrist, 1999; Nordbladh and Yates, 1990). If sex is isolated from ideas of sexuality and gender, and looked upon as the culmination of genes, hormones, genitals, and bones, opposing theories compete to define how sex should be categorized and what the basis of that categorization should be. Sorensen (2000) noted that the issue surrounding sex lies in how sex is classified and not in its manifestation as a cultural or biological construct. Classifying sex dichotomously based on autosomal combination in

the nucleus seems a straightforward approach, XX indicates female XY indicates male. However, nuclear DNA is often degraded in ancient skeletal samples, and the small Y allosome is difficult to amplify making this technique unreliable for skeletal specimens (Brown, 1998; Stone, 2008; Ubelaker, 2008).

As illustrated above, sex based on skeletal morphology is more complicated than a dichotomous model. Sex determining factors affecting endocrine secretion incites morphological variation in the skeleton within male and female groups (Blecher and Erickson, 2007; Fausto-Sterling, 2000; Nordbladh and Yates, 1990). Changes in morphology due to evolution and adaptation create morphological variation between populations and contribute to the morphological overlap between the sexes when populations are examined together (MacLaughlin and Bruce, 1986; Plavcan, 2001; Rosenberg, 2002; Washburn, 1948). In order to assess sex in skeletal remains on a global scale it is important to develop a universal system of categorization that bases skeletal sex on morphology using a terminology that includes variation in shape expression within males and females. The five-sex categorization scheme, described on page 14, accomplishes this. This research will contribute to the discussion of sex categorization, specifically in advocacy of a five-scale categorization scheme for identifying sex by hip bone morphology.

1.2. Sex Estimation Methods

Currently, there are several ways to estimate the sex of an individual using the hip bone. The methods can be either ordinal in nature, meaning sex is estimated based on morphological features and is given a ranked value based on its degree of "maleness" or

"femaleness," or metric in nature, using absolute measurements to classify sex. The following section will outline the benefits and limitations of each sex estimation technique and consider an alternative approach that combines the benefits of both ordinal and metric methods.

1.2.1.1. Ordinal methods

Ordinal methods of sex estimation are the visual assessment and scoring of sexually dimorphic non-metric traits. Skeletal sex is estimated along a continuum of female, possible female, intermediate, possible male, and male, according to the expression of non-metric traits. Traits could be given a number value, or a score, from which sex is estimated, or the presence/absence of a trait indicate "femaleness" or "maleness" (Brůžek, 2002; Buikstra and Ubelaker, 1994; Gómez-Valdés et al., 2012; Phenice, 1969; Walker, 2005). The most sexually dimorphic traits of the adult human hip bone (Figure 1.1) include the ventral arc, ischiopubic ramus ridge, subpubic contour located in the region of the pubic bone, and the shape of the greater sciatic notch in the inferoposterior region of the ilium (Buikstra and Ubelaker, 1994; Klales et al, 2012; Phenice, 1969; Walker 2005).

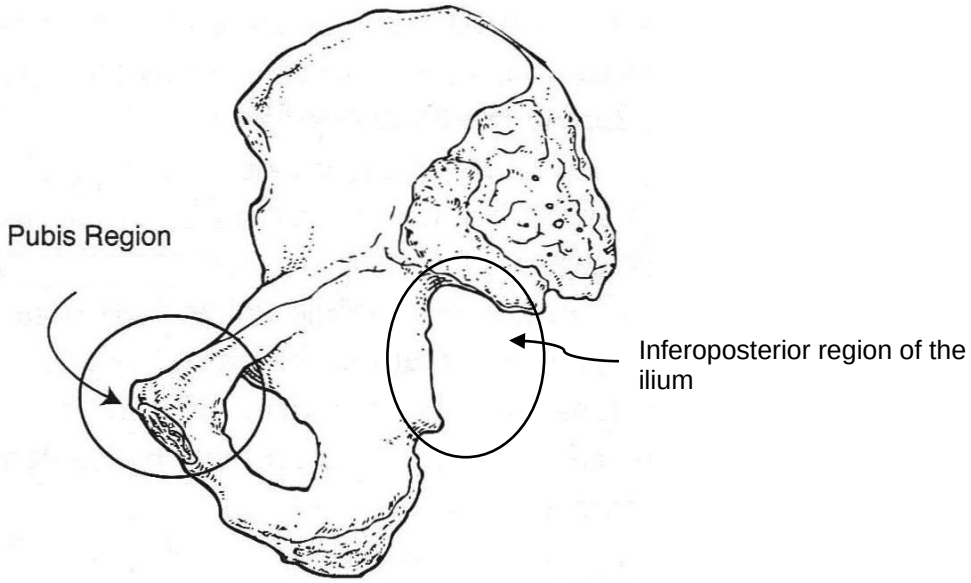

Figure 1.1: Most sexually dimorphic regions of the human hip bone. [Adapted from Buikstra and Ubelaker, 1994:17]

Ordinal methods demonstrated to be highly accurate for determining sex using the hip bone. Phenice (1969) report a 96% accuracy estimating sex in the pubic bone using the ventral arc, the subpubic concavity, and the ischiopubic ramus ridge together. Klales and colleagues (2012) developed a new method of estimating sex using Phenice's pubic bone features to 95% accuracy. However, when only one non-metric trait is used the accuracy of sex estimation declines. Rogers and Saunders (1994) tested 17 sexually dimorphic traits in the hip bone and found that, when used alone, the ventral arc was accurate to 87%, the subpubic contour was accurate to 84%, and the ischiopubic ramus was accurate to 80%. A similar level of accuracy was seen in the greater sciatic notch, which was also tested in isolation, by Walker (2005) although Rogers and Saunders (1994) documented a higher accuracy (86%) for this region using the standard methods outlined by Buikstra and Ubelaker (1994). When non-metric traits of the entire pubic

bone and the greater sciatic notch are used together, sex estimation accuracy is improved to 98% (Brůžek, 2002; Buikstra and Ubelaker, 1994).

High accuracy is a strong benefit of these ordinal methods, however, a drawback to the ordinal method is that accuracy is dependent on the completeness of the hip bone, and the experience or the reliability of the observer (Buikstra and Ubelaker, 1994; Brůžek, 2002; Đurić et al., 2005; Milne, 1990; Rogers and Saunders, 1994). Sex estimation accuracy has been tested between experienced and inexperienced observers in a collection of Baltic skeletons (Đurić et al., 2005). Differences in accuracy between observers (interobserver accuracy) was less than 10% when estimating sex in the hip bone, and not surprisingly, the more experienced observers estimated sex more accurately than inexperienced observers (Đurić et al., 2005). Intraobserver accuracy, the same observer interpreting a single trait multiple times, was as high as 11% for some traits, such as the ischiopubic ramus ridge, but as low as 0% for other traits, such as the ventral arc, indicating that some non-metric traits are easier to interpret than others (Rogers and Saunders, 1994). In the greater sciatic notch, intraobserver error was highest when attributing scores 3 and 4 and lowest when attributing a score of 1 (Walker, 2005). Accurate visual assessment of non-metric traits on the pubic bone and greater sciatic notch requires knowledge of anatomic positions, orientation terminology, and exposure to a range of hip bone morphological variation to distinguish sex differences from age related bone changes, trauma, disease, and taphonomic changes (White, 2000). Klales and colleagues (2012) have produced a very useful technique detailing the morphological variation of the ventral arc, the subpubic contour and ischiopubic ramus ridge, that might help standardize how sex trait morphological variations are interpreted and categorized in

the future. Walker (2005) has also recommended standardized handling procedures to improve interpretation of the greater sciatic notch morphology, however sex estimation was more accurate without it (Rogers and Saunders, 1994). Although these methods attempt to improve the subjective bias of non-metric trait interpretation, it does not replace the benefits that come out of experience and exposure to the morphological variability of osteological collections.

1.2.1.2. Metric methods of sex estimation

Metric methods are useful tools for estimating sex within hip bone assemblages of high morphological variability, because the techniques are reproducible on most complete hip bones and do not require one to identify anomalous features (Brůžek, 2002; Luo, 1995) . There are many different ways to quantify sex differences including individual measurements, the ischiopubic index, and multivariate analysis (Brůžek, 2002; Luo, 1995; Patriquin et al., 2005, Walker 2005; Washburn, 1948). The greatest strength to using a metric method is objectivity and repeatability (Brůžek, 2002; Luo; 1995). The ability to obtain similar results as another researcher consistently are the means to improve intraobserver error through measurement at fixed locations, and are paramount in human osteology when conducting forensic skeletal identifications that will be scrutinized in court (Brůžek, 2002; Byers, 2002). For example, Albanese calculated a lower mean intraobserver error for the superior pubis ramus length (0.6%), compared with 2.7% intraobserver error from what he calls "traditional pubic length measurements" (2003:4). Another strength of the metric method is the capacity to estimate sex in fragmented skeletal material. As with ordinal methods, fragmentary remains limit the

number of highly dimorphic hip bone landmarks, and as a result, sex estimation using metric approaches are not as accurate relative to complete hip bones. Still, metric methods on fragmented hip bones can be useful when the major dimorphic regions of the hip bone, such as the pubic bone and greater sciatic notch, are not present (Arun et al., 2012; Patriquin et al., 2005).

Although it appears that metric techniques would be superior methods of sex estimation to ordinal methods because metric results are more objective, these methods are not without their own set of limitations. There are many different ways of measuring intact and fragmented hip bones, therefore metric methods of sex estimation are not always comparable between studies (Arun et al., 2012). For example, Albanese (2003) applied a revised method of measuring the superior pubis ramus length, which improved the method by decreasing the intraobserver measurement error. Similarly, Washburn (1948) and Patriquin and colleagues (2005) both used the ischiopubic index, but they used different landmarks at the acetabulum to obtain their measurements. In addition, population and temporal variability influence hip bone size and shape, in response human osteologists have created, or suggested the creation of population and temporally specific metric methods (Biwasaka et al., 2012; Luo, 1995; MacLaughlin and Bruce, 1986; Patriquin et al., 2005; Rosenberg, 2002; Washburn, 1948; Zeng et al, 2012). These specific methods of sex estimation are often not appropriate for identifying sex of unknown specimens, and temporally specific metric method of sex estimation might not be applicable to the same population if it experienced environmental or cultural changes over time that influenced hip bone morphology.

Another limitation of metric analyses of sex is that the results of metric analyses of sex estimation are only accurate to around 85%, which is not as high as the accuracies for ordinal methods (Albanese, 2003; Biwasaka et al., 2012; Brůžek, 2002; Milne, 1990; Tague, 2005; Walker, 2005; Washburn, 1948). Metric analyses of sex do not discriminate between male and female hip bone size and shape as well as ordinal methods because considerations for indeterminate sex shape are seldom made. Consequently, male/female morphological overlap registers as error. One reason for this consequence is the attempt to identify sex dichotomously rather than incorporating intra-sex variation into the calculation. As a result, the accuracy of estimated sex, although high in metric analyses, is typically less accurate than ordinal methods of sex estimation.

1.3. Sex Estimation Using Geometric Morphometrics

Geometric morphometrics (GM) is the study of object form (size and shape) using a Cartesian coordinate system in tangent space, which is conceptualized as a grid system in either two or three dimensions (Bookstein, 1991). Landmarks and semi-landmarks represent the shape of the object, or the area of interest, and are positioned on points of biological importance on the object that are easy to locate and are present on every specimen (Richtsmeier et al., 2002; Slice, 2005; Zelditch et al., 2012). The landmark coordinates are recorded in the tangent space, which can then be subjected to multivariate comparative analyses to answer questions about the biological significance of certain shape differences. This technique incorporates the benefits of both ordinal and metric techniques of sex estimation by capturing size and shape of the hip bone at reproducible

points, which is important when approaching new ways to investigate how sex is represented in the human pelvis.

Geometric morphometrics compares the shape and size of skeletal elements in order to assess differences between species, sexes, and populations (Adams et al., 2004; Anastasiou and Chamberlain, 2013; Baab et al., 2012; Betti at al., 2013; Bruner, 2004; Bytheway and Ross, 2010; Franklin et al., 2010; González et al., 2009; Schutz et al., 2009; Slice, 2007). This analysis in humans has predominately focused on cranium morphology (Baab et al., 2012; Bigoni et al., 2010; Bruner, 2004; Franklin et al., 2010; González et al., 2011; Kimmerle et al., 2008; Manzi et al., 2000; Rosas and Bastir, 2002; Sholts et al, 2011; Strand Viðarsdóttir et al., 2002). Although several studies have involved the hip bone (Anastasiou and Chamberlain, 2013; Bytheway and Ross, 2010; González et al., 2009; Lycett and von Cramon-Taubadel, 2013; Wilson et al., 2011). Geometric morphometrics has been very successful in determining shape differences related to sex in the whole hip bone complex, the ischiopubic complex, the greater sciatic notch, and the auricular surface, with accuracies in the 88-95% range (Bilfeld et al., 2012; Anastasiou and Chamberlain, 2013; Bytheway and Ross, 2010; González et al., 2009). Because GM has been successful at capturing and measuring sex-based shape of the human hip bone, it can be used to investigate the relationships between whole and partial hip bone shape, sex-based shape, and non-metric traits.

The landmark points used to gather GM shape data are strategically positioned to capture shape sex-based shape variation and are reproduced exactly on all specimens. The points register three-dimensional coordinates in tangent space: a projection of three-dimensional Euclidean distances (distance between points) on a two dimensional surface

that resembles the distortion of a globe projected as a map (Baab et al., 2012). Positional differences between the same landmark points of different specimens in this tangent space provide the information for measuring shape differences. Once the landmarks are selected and the shape configurations have been made they are adjusted using Procrustes superimposition (see section 2.2.4.1) to ensure all specimens are comparable in size and orientation (Bookstein, 1991; Slice, 2007). A size component, centroid size (the square root of the sum of squared coordinate differences from their centroid) is removed to enable components of shape to be analysed (Bookstein, 1991; Zelditch et al., 2012). However, in some cases allometric size differences remain between landmark configurations even after the objects have been scaled to the unit centroid size (Slice, 2007; Zelditch et al., 2012).

The strength of using GM in analyses of sex estimation is in its similarity with both metric and ordinal methods. Like metric methods, shape differences can be quantified and statistically validated, and, like ordinal methods, areas of morphological significance can be compared in detail (Bilfeld et al., 2012; Bytheway and Ross, 2010; González et al., 2009; Mitteroecker and Gunz, 2009; Richtsmeier et al., 2002; Slice, 2007; Steyn et al., 2004). The benefit of combining the strengths of metric and ordinal methods is the multivariate quantification of non-metric sex trait morphologies that contribute the most to overall sex-based shape differences. For example, the subpubic contour and greater sciatic notch can be quantified through Procrustes coordinates that maintains the shape of the contour and notch in the evaluation of sex-based shape differences in the human hip bone. For the greater sciatic notch, the accuracy of sex

estimation improved 10% using GM relative to both metric and ordinal methods, (Brůžek, 2002; González et al., 2009; Walker, 2005).

Quantifying shape through GM is also beneficial when applying the investigation of sexual dimorphism to partial human remains. Ordinal and metric results identifying sex from partial hip bones have reached accuracies between 80- 90% (Arun et al., 2012; Brůžek, 2002; Patriquin et al., 2005; Rogers and Saunders 1994). Sexually dimorphic shapes have been derived from partial human hip bone shapes using GM to an accuracy of just under 95% (Anastasiou and Chamberlain, 2013; González et al., 2009; Wilson et al., 2011). The superior accuracy of GM in the analysis of sexual dimorphism in partial hip bone suggests that the use of GM could contribute to accurate sex identification of partial human remains that are missing some or all of the standard non-metric traits used to estimate sex of unknown skeletal material.

Considering the successes GM has achieved in determining sex-based shape differences in the human hip bone, it would be interesting to investigate the relationship hip bone shape has with non-metric traits and with sex. Based on my previous argument for how to categorize sex and how terminology could denote confidence, this study will estimate sex using standard ordinal methods and classified as either male, possible male, indeterminate, possible female, and female. The purpose of this investigation would be to determine the relationship non-metric traits have with whole and partial hip bone shapes and to determine whether ordinal categories of sex are discernible using GM representation of whole and partial hip bone shapes.

1.4. Significance of Study

A deeper understanding of how whole and partial hip bone shape influence the expression of non-metric traits will be garnered by this study. It will also contribute to a deeper understanding of the relationship between hip bone shape and sex categorization by identifying the non-metric traits that contribute the most to the sex-based shape and sex categorization. If GM is successful at discerning the shape differences between the hip bones classified as male, possible male, indeterminate sex, possible female, and female in this study, it could contribute valuable knowledge to our understanding of how sex is expressed morphologically in the hip bone. This study will also contribute to the discussion of how to record and categorize sex in human osteology and biological anthropology: is a dichotomous method of sex categorization sufficient, or is a broader categorization scheme, such as the one used in ordinal methods, more appropriate for capturing morphological variation both within sex groups and between populations. This study could lead human osteologists to discern future steps to a more accurate (over 98%) sex categorization, and to more confident category labels that would convey sex identification within varying hip bone morphologies.

Chapter 2 : Materials and Methods

There are two questions driving this research. First, what are the hip bone shape differences, obtained using geometric morphometrics (GM) that contribute to the categorization of sex as female, possible female, intermediate, possible male, or male? Second, what relationships exist between sex-based shape differences of the hip bone and the ordinal traits used to estimate sex? The assumption inherent in these research questions is that the landmarks selected for GM analysis adequately represent the sex differences in hip bone shape.

2.1. Materials

The samples used to answer the research questions consisted of 59 left hip bones obtained from osteological teaching specimens housed by the Life Sciences Department at the University of British Columbia (UBC). These specimens are undocumented, meaning the identity of each individual (age at death, sex, and ancestry) is unknown. Among the specimens available for study, only complete left hip bones were included in the study sample to maximise the potential for landmark selection on the specimens and to maximise the accuracy potential during the sex assessment process.

2.2. Methods

In order to investigate sexual dimorphism in the hip bone and the relationship between components of sex-based shape and the standard non-metric traits used in sex

estimation, two main types of data were collected. The first type is a visual assessment of sexually dimorphism from non-metric traits. The trait scores were recorded and used to assign each specimen to one of five sex categories: female, possible female, indeterminate sex, possible male, or male. The second type of data is landmark coordinate data that was recorded from three-dimensional surface scans of the individual hip bones and used in geometric morphometric (GM) analysis. The NextEngine desktop 3D laser scanner (NextEngine, Inc) was used to capture the hip bone surface and to create a three-dimensional model of a complete hip bone. Landmark 3.6 software (Institute for Data Analysis and Visualization) was used to place landmarks that represent hip bone shape onto the three-dimensional hip bone model and to record the landmark coordinates needed for GM analysis. Geometric morphometric and statistical analyses were performed using MorphoJ software (Klingenberg, 2011) and SPSS 17.0 (IBM SPSS Statistics, 2008).

2.2.1. Sex estimation

Sex estimation on a five-scale scoring system was assessed visually for each hip bone using standard non-metric traits of the pubic bone and greater sciatic notch (Buikstra and Ubelaker, 1994; Klales et al., 2012; Phenice, 1969; Walker, 2005). The non-metric traits of the pubic bone: the ventral arc, subpubic contour and ischiopubic ramus ridge, were evaluated using the scoring system outlined by Klales et al (2012), summarized in table 2.1, which expands the range of morphological variation considered by Phenice (1969). Klales and colleagues' method of estimating sex in the pubic bone was used in this study rather than Phenice's (1969) method because the former makes it

easier to compare pubic bone morphology with greater sciatic notch morphology that also uses a five-scale scoring system and to compare all non-metric traits with five sex categories.

Table 2.1: Morphological description of non-metric trait scores. [adapted from Klales et al., (2012) and Buikstra and Ubelaker (1994)]

Non-metric Trait	Score 1	Score 2	Score 3	Score 4	Score 5
Ventral Arc	40 degrees from the pubic symphyseal face	25 to 40 degrees from the pubic symphyseal face	less than 25 degrees from the pubic symphyseal face	parallel to the symphyseal face	absence of a ventral arc
Subpubic contour	well developed subpubic concavity	slight subpubic concavity	no subpubic concavity/ convexity	small subpubic convexity	large subpubic convexity
Ischiopubic ramus ridge	sharp ridge with a narrow ascending ramus	rounded or flattened ridge with a narrow ramus	narrow ramus with no ridge present	slightly wider ramus with no ridge present	very wide ramus with no ridge present
Greater sciatic notch	Very wide angle	Moderately wide angle	Medium sized angle	Moderately narrow angle	Very narrow angle

The ventral arc, is described as a "slightly elevated ridge of bone, which extends from the pubic crest and arcs inferiorly across the ventral surface of the lateral most extension of the subpubic concavity" and is also the location of the lateral border of the sulcus for the nerves of the penis and clitoris (Phenice, 1969:298; Šedý et al., 2008). The ridge of bone that makes up the nerve sulcus is more medially and inferiorly oriented in male hip bones, a distinct morphology from the more laterally oriented nerve sulcus that is characteristically female (Anderson, 1990; Klales et al., 2012; Šedý et al., 2008). Klales and colleagues (2012) characterize scores 1 and 2 as female ventral arc shape,

while scores 4 and 5 characterize male ventral arc shape. Score 3 incorporates possible ventral arc shape from either sex (Figure 2.1). The subpubic contour is the site of attachment for the gracilis muscle and becomes sexually dimorphic because of the direction of growth of the ischial tuberosities during adolescent development (Coleman, 1969; Scheuer and Black, 2000). Rapid inferior growth of the ischiopubic ramus and lateral growth of the ischial tuberosities creates the subpubic concavity in females (Figure 2.1, scores 1 and 2). In males the area is more convex (Figure 2.1, scores 4 and 5) due to greater inferior growth of the ischial tuberosities and greater thickness of the ischiopubic ramus possibly due to a robust gracilis muscle attachment (Buikstra and Ubelaker, 1994; Coleman, 1969; Klales, 2012; Scheuer and Black, 2000). In females, the lateral curve of the ischiopubic ramus starts below the inferior margin of the pubic symphysis forming a concavity that is absent in males, however, males often display a pronounced convexity of the inferior pubic ramus (Klales et al., 2012). When left and right hip bones are articulated at the pubic symphysis the left and right ischiopubic rami form the subpubic angle. The degree of the subpubic angle reflects the shape of the pelvic outlet, which is wider in females than in males to accommodate the passage of the fetus during parturition, leading to a greater subpubic angle. The ischiopubic ramus ridge is created by similar growth patterns as the subpubic contour. The ridge is located on the medial aspect of the ischiopubic ramus immediately below the pubic symphysis and "forms a narrow, crest like ridge in females" (Figure 2.1, scores 1 and 2) which is absent in males (Figure 2.1, scores 4 and 5) (Buikstra and Ubelaker, 1994:17).

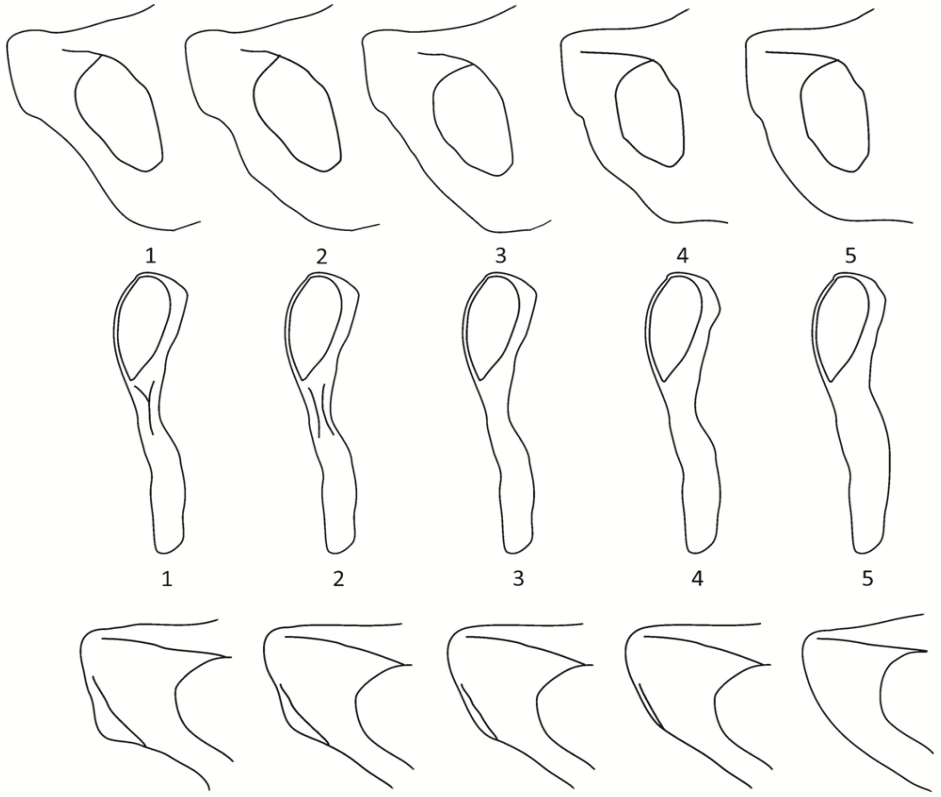

Figure 2.1: Five scale scoring system for the subpubic contour (top), the ischiopubic ramus ridge (middle) and the ventral arc (bottom). Scores 1 and 2 in each image represents typical female morphology, score 3 represents indeterminate morphology, scores 4 and 5 represent male morphology. [Reproduced from Klales et al., 2012:4]

The greater sciatic notch of each specimen was assessed according to the standard observation methods outlined by Buikstra and Ubelaker (1994) and by Walker (2005). The angle of the greater sciatic notch is defined as the arc that is created by following the anterior surface of the dorsal aspect of the hip bone beginning at the posterior inferior point of the preauricular sulcus, inferior to the auricular surface, and terminating at the ischial spine (Walker, 2005). The width of the greater sciatic notch is governed by the direction and amount of growth of the posterior portion of the ilium during adolescence (Coleman, 1969). Males have a more prolonged superior growth of the posterior portion of the ilium creating a narrow notch (Figure 2.2 score 3, 4, and 5) whereas females show

a prolonged lateral growth creating a wider notch (Figure 2.2 score 1) (Coleman, 1969). Score 2 tends to represent indeterminate sex (Walker, 2005). The shape of the greater sciatic notch in females creates a greater posterior component of the true pelvis and the pelvic outlet that contribute to parturition success (Hager, 1996).

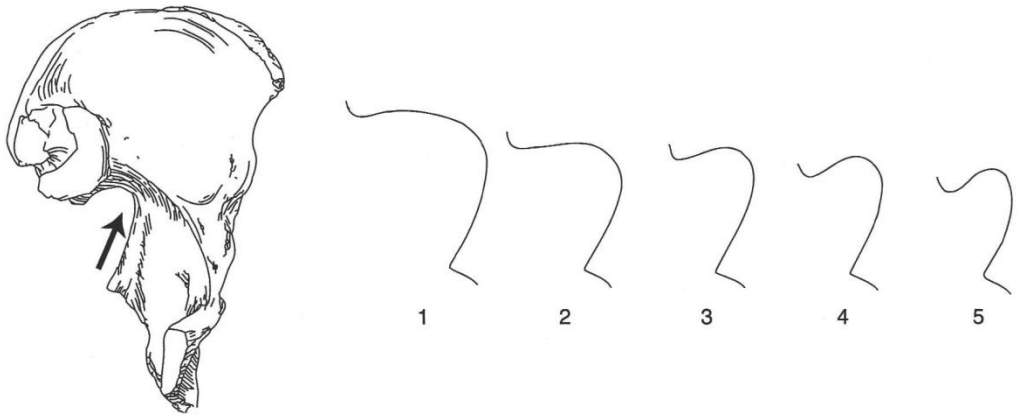

Figure 2.2: Five scale scoring system for the greater sciatic notch. Score 1 represents typical female morphology, score 2 represents indeterminate morphology, scores 3, 4 and 5 represent male morphology. [Reproduced from Buikstra and Ubelaker, 1994:18]

Each specimen was assigned to one of five sex categories based on the mean score of the four non-metric traits. A specimen with a modal score of "1" across all four traits was categorized as female, "2" was categorized as possible female, "3" was considered indeterminate sex, "4" was categorized as possible male, and "5" was categorized as male. However, in practice, it was very rare for a specimen to express all of the characteristics that are expected in one sex category, the majority of the specimens expressed non-metric trait morphologies that are characteristic of two or more sex categories. The mean score in such cases would result in a decimal that would have to be rounded up or down to a whole number representing the sex category. Because the whole

numbers are not ranked, that is "5" is not larger than "1" a typical rounding practice is not appropriate. The decision, whether to round up or down, was made to align the sex estimation with the mode score. For example a specimen with scores resembling 4;2;2;3 received a mean score of 2.75 which would typically be rounded up to 3, as the mean is closer to that value, but the sex estimation is closer to 2, as two traits suggest possible female. In this case, the mean score was rounded to 2 to suggest a possible female. In another example, a specimen with scores resembling 3;3;3;2, which also produced a mean score of 2.75, was rounded up to 3 because more of the non-metric traits suggest an individual of indeterminate sex rather than possible female sex. In instances of bimodal sex estimations, for example 1;1;2;2 or 4;4;5;5 more weight was given to the trait scores that estimated sex more confidently. In the previous case, the mean was rounded to fit the confident sex estimation female (1) and male (5) than to the possible female (2) or possible male (4). In instances where a bimodal score included indeterminate sex, such as 2;2;3;3 or 4;4;3;3 more weight was given to the possible sex category over the indeterminate sex category. For specimens that did not have a mode score to assist in sex categorization, for example 4;3;2;5, the mean value of 3.5 was rounded up to 4 (possible male) because there are more male like non-metric traits (scores 4 and 5) than female like non-metric traits (2).

2.2.2. NextEngine laser scanner

The specimens were scanned using the NextEngine desktop three-dimensional surface scanner (NextEngine, Inc.). The scanner uses normal light and a series of 4 class 1M lasers to capture both the surface colour and surface topography of an object

(NextEngine, Inc. no date). The geometric point resolution was set to capture 310 points per cm^2 for objects in a wide field of view with an accuracy of up to 0.038cm (resolution published as 2.0k points per square inch with an accuracy of 0.015 inch NextEngine, 2009). Each specimen required repositioning at a perpendicular orientation in order to capture as much pelvic topography as possible. The first hip bone position secured the long axis of the pelvis parallel to the vertical arm of the PartGripper (Figure 2.3A). The ischiopubic ramus was oriented in the centre of the PartGripper platform and the ilium was oriented over the ischiopubic ramus so that the anterior superior and posterior superior iliac tuberosities were within the borders of the turntable. The scanner was set to capture the image in 360 degrees with eleven scans in this orientation.

The second scan position had the long axis of the pelvis lying on the PartGripper platform perpendicular to the scanner base in order to capture the superior surface of the iliac crest, inferior surface of the ischiopubic ramus, and the inside of the acetabulum that were missed in the first scan position. The hip bone was oriented to ensure that the ischiopubic ramus and the apex of the ilium would fit inside the turntable boundaries and that the scanner could capture all of the hip bone (Figure 2.3B). The scanner was set to capture the image in 360 degrees with eight scan in this orientation. If these two scans positions did not capture the entire shape of the pelvis, single scans were taken of the missing area(s) to fill in the missing data.

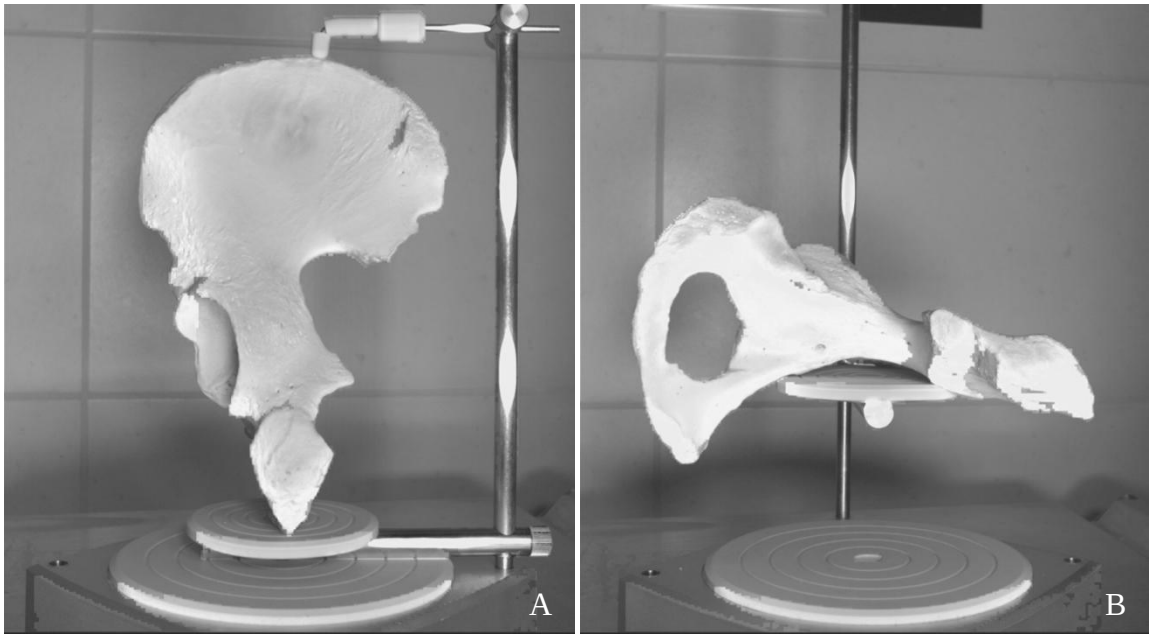

Figure 2.3: Image "A" the first hip bone scan position parallel to the NextEngine PartGripper. Image "B" the second hip bone scan position perpendicular to the PartGripper.

The multiple scans were fused into a single three-dimensional image using ScanStudio software (ScanStudio HD 1.2.0, NextEngine, Inc). The fuse settings were selected for no hole filling and a Resolution Ratio of 0.9 (default setting) to maintain the same mesh triangle size as the original scans (NextEngine, 2009). On three occasions (UBC_50, UBC_51, UBC_53) surface hole filling was required on the iliac crest and the ischiopubic ramus to accommodate landmark placement. The three holes were no more than 5 cm long and 1 cm wide. Because the holes were on a curved surface the fill holes settings were set for a curve to follow the natural outline initiated by the boundaries in the original scan data. This function did not affect the integrity of the landmark data in these areas because the hole filling function served only as a support for the landmark already in contact with original surface data. The surface scans were then exported as .ply files to be imported for landmark placement.

2.2.3. Landmark placement

Bookstein (1991) describes three types of landmarks that are used in GM and used in this research. Type 1 landmarks are discrete juxtapositions, defined in terms of intersecting structures such as between sutures or the branching points of a tree. Type II landmarks are "maxima of curvature or other local morphogenetic processes" (Bookstein, 1991: 64). This category includes locations on an object that experience push or pull forces such as the tips of muscle attachments on bone, or the ranges of a curve such as the "'corner' of the jaw and the 'corners' of the orbital rim" (Bookstein, 1991: 65). Type II landmarks are defined in terms of local features, but they are not surrounded on all sides by structures as in Type I. In contrast, Type III landmarks are extremal points and are defined in terms of locations furthest away far away from another landmark such as "end points." "Fuzzy" landmarks of types I and II are larger than single point landmarks, but are still recognized as areas of biological significance (Bytheway and Ross, 2010). Landmarks should be selected according to how easy they are to locate by inexperienced users and how repeatable the landmarks are on all of the specimens being studied (Bytheway and Ross, 2010; Slice, 2007).

Thirty landmarks, 9 Fuzzy type I, 13 type II, 8 type III, (Table 2.2, Figure 2.4) were selected to represent hip bone shape and sexual dimorphism. The twenty-five landmarks that Bytheway and Ross (2010) found to capture the most significant hip bone sexual dimorphism were selected. Bytheway and Ross selected landmarks based on several criteria including: demonstrated significance in the literature, repeatability among the specimens, representation of object shape, representation of biological importance in

the form of sex differences, and regions that have not been used in metric analysis. Five new landmarks were selected to complete the hip bone shape (Landmark 7, 28, and 30), and to represent the sexually dimorphic qualities identified by Brůžek (2002).

Table 2.2: Landmark types and definitions.

Landmark Type	Hip Bone Region	Landmark
II	Ilium	1. Anterior inferior iliac spine
II	Ischium	2. Ischial spine
II	Ilium	3. Iliac tubercle
II	Ilium	4. Anterior superior iliac spine
II	Ilium	5. Posterior superior iliac spine
"Fuzzy"	Pubis	6. Midpoint of the pubic symphyseal face
II	Ilium	*7. Posterior inferior point of the preauricular sulcus
II	Pubis	8. Pubic tubercle
II	Ilium	9. Point of maximum curvature in the greater sciatic notch
III	Ilium	10. and *11. Two points of the auricular surface that produce the maximum width at the anterior portion
III	Ischium	12. and 13. Two points on the ischium that produce the maximum width of the ischial tuberosity
III	Pubis	14. The most inferior medial point on the obturator foramen rim
III	Ischium	15. The most superior lateral point on the obturator foramen rim
II	Pubis	16. The most anterior inferior point of the lunate surface
III	Pubis	17. Most superior point on the symphyseal face
II	Ischium	18. The most posterior inferior point of the lunate surface
II	Pubis	19. Arcurate (iliopubic) eminence
III	Pubis	20. Ischiopubic ramus at the narrowest point inferior to the pubic symphysis
"Fuzzy"	Ilium	21. Posterior gluteal line
"Fuzzy"	Ischium	22. Most posterior point on the ischial tuberosity
"Fuzzy"	Ischium	23. Most inferior point on the ischial tuberosity
"Fuzzy"	Pubis	24. Most inferior point on the symphyseal face
III	Pubis	*25. Most lateral point of the phallic ridge on the ischiopubic ramus
"Fuzzy"	Ilium	26. Inferior gluteal line
"Fuzzy"	Ilium	27. Anterior gluteal line
"Fuzzy"	Ilium	*28. Maximum arc of the iliac crest
II	Ilium	29. Posterior inferior iliac spine
"Fuzzy"	Ischium	*30. Most superior part of the ischial tuberosity

* Indicate new landmarks created for this research

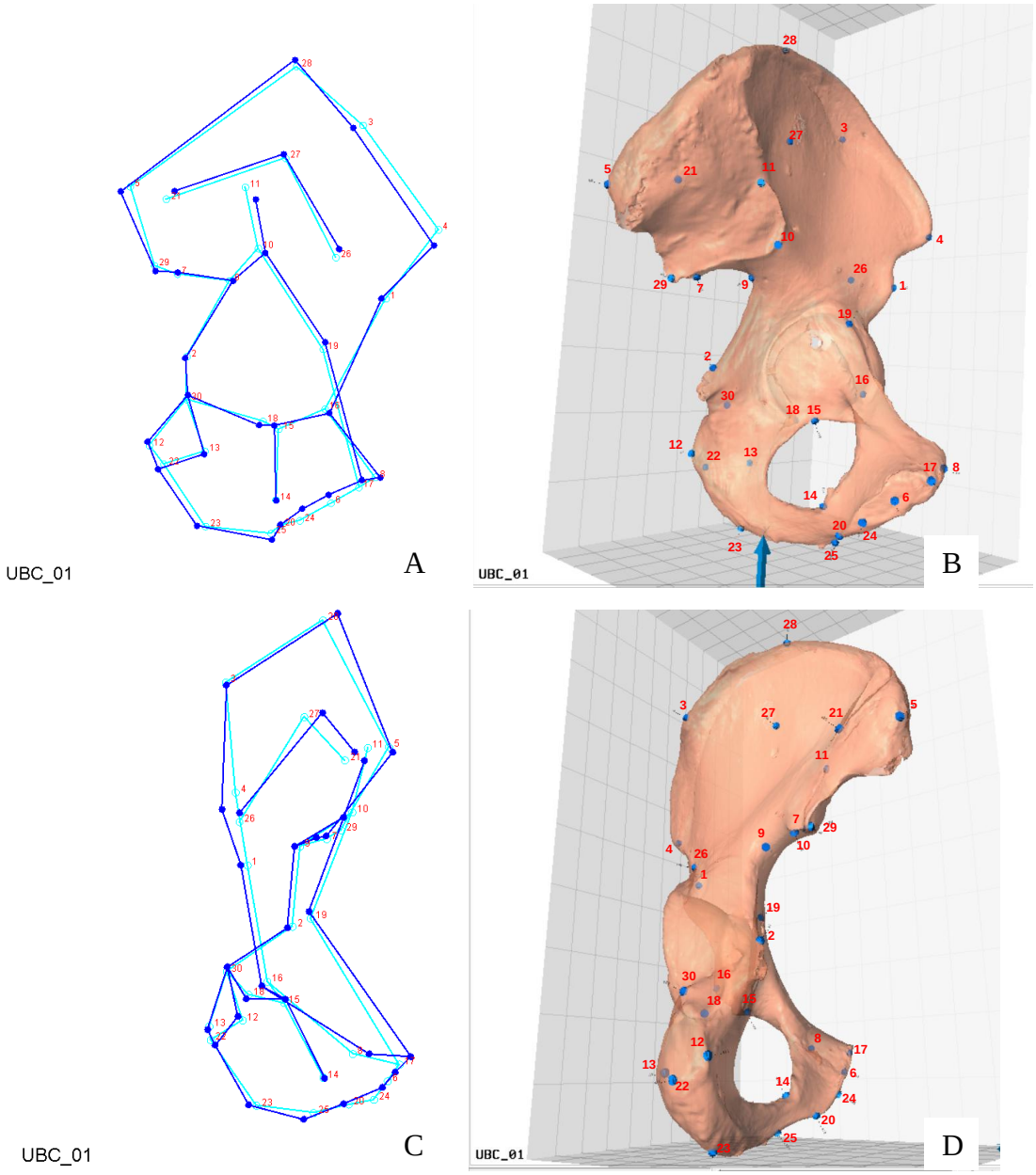

Figure 2.4: Landmark placement and wireframe graph comparison. A: MorphoJ wireframe image Axis 1 vs. 2. B: Landmark ™ opaque image with landmarks; anterior view. C: MorphoJ wireframe image Axis 1 vs. 3. D: Landmark ™ opaque image with landmarks; posterior view.

Brůžek (2002) identified the composite arch and the phallic ridge as two shape features of the pelvis that contribute to sexual dimorphism. The composite arch is comprised of the curvature of the anterior portion of the auricular surface and curvature

of the anterior portion of the sciatic notch. In females, both contours make up two distinct circles with different radii, which form the composite arch. In males, both contours form the circumference of one circle, in which case there is no composite arch. This site of sexual dimorphism was not included as a sex trait to be measured against the geometric morphometric results because it is a metric method of sex estimation rather than an ordinal method. Landmarks 10 and 11 are positioned on the anterior portion of the auricular surface and are included in this study to capture the shape differences of this area that Brůžek (2002) alludes to between males and females in his study. The phallic ridge is a lateral projection of bone on the ischiopubic ramus inferior to the pubic symphyseal face that is morphologically distinct in males with a broad ischiopubic ramus and no ridge (Brůžek, 2002). Landmark 25 was selected to capture the range of shape variation in the location of the most lateral point of the phallic ridge and determine the level of sexual dimorphism in this anatomic feature.

The three-dimensional models were imported into the Landmark 3.6 software (Institute for Data Analysis and Visualization, 2002) as .ply files in order to apply the landmarks (Figures 2.4B and 2.4D) using a semi-automated process. The process consisted of selecting a reference image (UBC_01) and manually placing all of the landmarks on it. The first ten landmarks were manually applied to all subsequent specimens before the remaining landmarks were applied automatically on each model by the software. The ten manually placed landmarks serve as a coordinate reference so the software can judge where to place each remaining landmark. Despite the reference locations, each automatically placed landmark required manual refinement to ensure it was placed correctly (Landmark User Guide, 2007). Landmarks configurations were also

created to represent the shape of the ilium, ischium, and pubis independently (as indicated in Table 2.2, Figure 2.5) and the combined ilium-ischium, ilium-pubis, and ischium-pubis datasets that represent various aspects of fragmented hip bones.

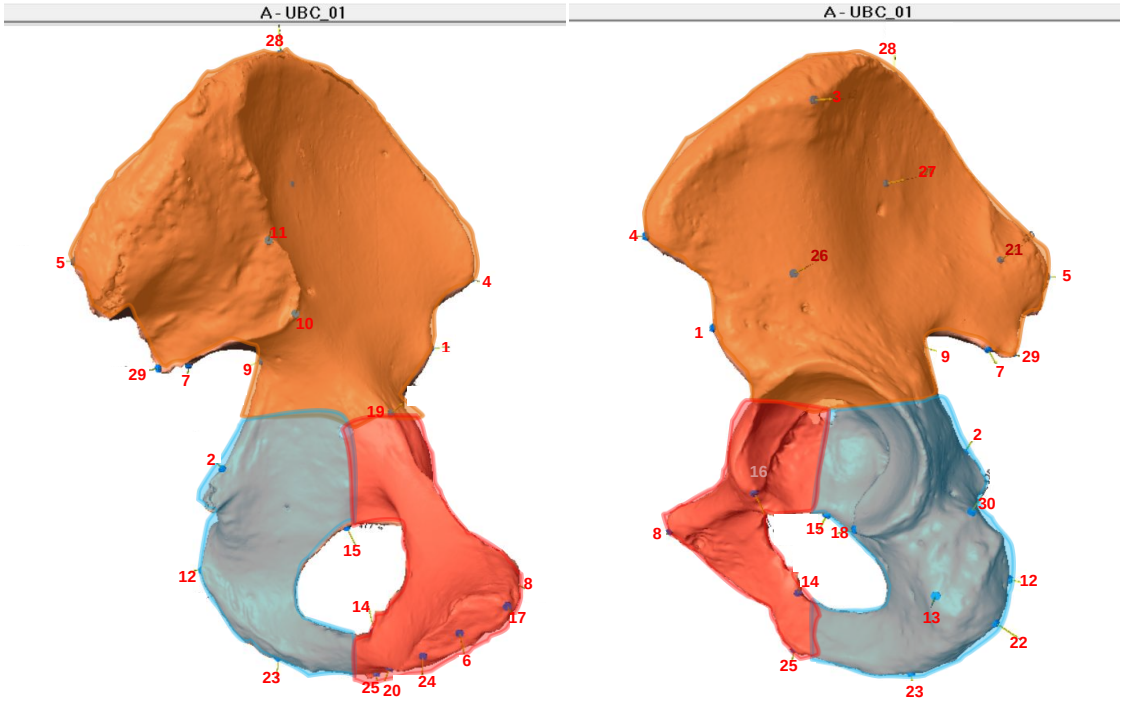

Figure 2.5: Landmarks grouped into hip bone regions, ilium in orange, ischium in blue, and pubis in red.

2.2.4. Geometric morphometric and statistical analysis

Geometric Morphometric analysis was used in this study to quantify hip bone shape variation in whole and partial segments in order to assess the sexual dimorphism of hip bone shape and to determine the relationship between non-metric trait morphology and hip bone shape in whole and partial segments. The process started by aligning the landmark configurations of the 59 specimens into a common size and orientation through Procrustes superimposition using translation, scaling, and rotation. A statistical test of

total variation was performed using a Procrustes analysis of variance (ANOVA) to identify the effect centroid size and hip bone shape had on estimated sex and non-metric trait morphology. The pattern of individual shape variation among the specimens was investigated for each landmark configuration dataset (whole bone, isolated ilium, isolated ischium, isolated pubis, combined ilium-ischium, combined ilium-pubis, and combined ischium-pubis) using principal component analysis (PCA) to locate those areas of the pelvis that are better at isolating sexually dimorphic shapes. A Spearman's ranked correlation was performed to measure the strength of the relationship between sex and shape variation, and non-metric trait morphology and shape variation.

2.2.4.1. Procrustes superimposition

The most widely used analysis of shape variability is through Procrustes superimposition (Mitteroecker and Gunz, 2009; Slice, 2007; Zelditch et al., 2012). This method calculates the best fit among shapes. Meaning landmark configurations are scaled to the same unit centroid size ["the square root of the summed squared distances of each landmark from the centroid of the landmark configuration." (Zelditch et al., 2012:457)], by minimising the sum of the squared distances between corresponding landmarks of two superimposed shapes among landmark configurations, this is also known as squared Procrustes distance (Bookstein, 1991; Mitteroecker and Gunz, 2009; Slice, 2007; Zelditch et al., 2012). The superimposition process involves three steps, translation, scaling, and rotation (Figure 2.6). When the Procrustes superimposition calculates the best fit there is a risk that one or more points could have very large shape differences represented by a large displacement in the location of that coordinate among

the objects, when the rest of the Procrustes coordinates have very few shape differences (Slice, 2005; Zelditch et al., 2012). This local displacement is the "Pinocchio effect," and can cause a disproportionate amount of localized shape difference (Slice, 2005). In order to avoid the Pinocchio effect MorphoJ (Apache License, Version 2.0) overlays all of the landmark configurations onto one another based on the centre point of each landmark configuration, rather than centroid size, thereby placing less emphasis on landmark outliers (Klingenberg, 2008). To find the coordinates of the centre, or origin, of each landmark configuration the centroid position coordinate (the average coordinates among all of the landmark configurations) is subtracted from the corresponding coordinates of each landmark configuration (Zelditch et al., 2012). This first step is called translation because the centroid position has been translated to the origin of the landmark configuration (Zelditch et al., 2012). The second step is to scale the newly translated landmark configurations either to a common size, a mean centroid size, or to an optimized least-squares estimate of scale (Slice, 2005, 2007; Mitteroecker and Gunz 2009). The final step in minimising the Procrustes distance is to rotate the landmark configurations around their centroids so all of the corresponding landmarks are in their closest proximity (Mitteroecker and Gunz, 2009). MorphoJ aligns the objects by principle axes. The result is a set of new landmark coordinates, called Procrustes coordinates, which can be used to evaluate shape difference.

When interpreting shape differences among Procrustes landmarks it is important to discern the biologically significant shape difference from measurement error. The accuracy of GM is dependent on recognizing important sources of observer error and measurement error when placing landmarks (von Cramon-Taubadel et al., 2007). Errors

can occur when landmarks are not precisely positioned on the object or landmarks are selected that do not contain biological relevance to the questions being asked (Bookstein, 1991; Slice, 2005; Zelditch et al., 2012). Tests of intraobserver error by conducting repeat measures of object shape is one way of assessing the overall effect of landmark positioning error on the results of shape analyses, however, it does not test the reproducibility or precision of each individual landmark (von Cramon-Taubadel et al., 2007). In order to assess measurement error between corresponding landmarks the average distance from the mean can be taken as an absolute measure of error (Arnqvist and Mårtesson, 1998).

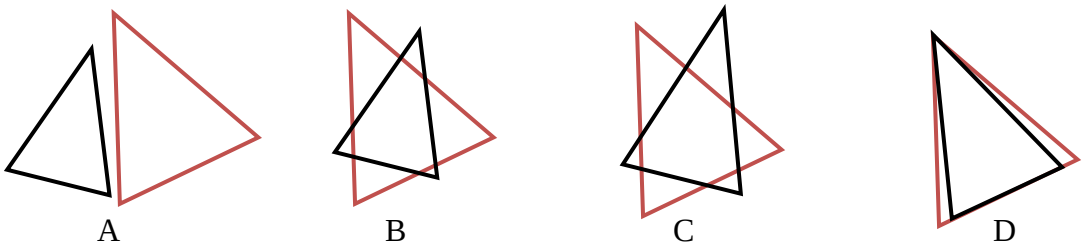

Figure 2.6: Illustration of Procrustes Superimposition. Image "A" raw landmark configurations data. Image "B" centered configurations. Image "C" centered and scaled configurations. Image "D" centered, scaled and rotated configurations.

To ensure the repeatability of the landmarks used in this study, two tests of intra-observer error were applied to the whole bone landmark configuration to see if alterations in landmark position among the samples contribute to specimen shape differences (Klingenberg, 2011). Landmarks were reapplied to the first ten specimens in the data set, and subjected to a full Procrustes fit. Five months separated the time between landmark placement events. The first test assessed the digitizing error, or the precision of placing the landmarks on the three-dimensional model, by comparing the standard deviation of

the Procrustes coordinates along each of the three dimensions between the original episode of landmark placement and the second landmark placement event (Corner et al., 1992; von Cramon-Taubadel et al., 2007). There is no gold standard for measuring digitization error in GM, however, Corner and colleagues (1992) suggest comparing the standard deviations of mean landmark coordinates to negate the measurement error of disproportionate Procrustes distances that arise due to the Pinocchio effect (von Cramon-Taubadel et al., 2007). This method is useful for evaluating the consistency of landmark placement on models within a frame of reference (Corner et al., 1992; von Cramon-Taubadel et al., 2007). The Corner and colleagues (1992) method was revised by von Cramon-Taubadel and colleagues (2007) to accommodate those landmarks that are not in a constant frame of reference. As a result, this new method compares the standard deviations of mean Procrustes coordinates from a partial Procrustes superimposition. The landmarks in MorphoJ us a full Procrustes superimposition, which von Cramon-Taubadel and colleagues (2007) describe will underestimate the measurement error. This will be taken into consideration when evaluating the intra-observer differences between standard deviations.

The second error test determined whether the digitizing error is influencing the mean shape deviations away from the expected measurements of sexual dimorphism. The Procrustes analysis of variance (ANOVA) measures the proportion of total variance derived from the Procrustes distances and Procrustes coordinates between the original and repeated measurements (Aldridge et al., 2005; Klingenberg and McIntyre, 1998). If the mean sum of squares in the second landmark placement event is less than the mean sum of squares in the initial landmark placement event then the placement of landmarks

in the second event did not negate the shape differences identified in the first event (Klingenberg and McIntyre, 1998).

2.2.4.2. Multivariate analyses

A Procrustes ANOVA was also used to measure the amount of size and shape variation within the study sample using centroid size and Procrustes distances (Klingenberg et al, 2002). The Procrustes ANOVA is an extension of the Goodall's F test, which determines the amount of shape variation that is not predicted by size (Klingenberg, 2002; Zelditch et al., 2012). The Procrustes ANOVA tests the null hypothesis at 10,000 randomized permutations of landmark reshuffling to simulate the null hypothesis (Klingenberg et al., 2002). If there is a relationship between shape and object effects, in this case estimated sex and non-metric traits, or size and object effects after 10,000 permutations, the null hypothesis is rejected (Klingenberg et al., 2002). A limitation of the Procrustes ANOVA is that is assumes there is isotropic variation for each landmark (Klingenberg, 2002). Biological variation is not isotropic, therefore, a principal component analysis was used to visualize the individual shape variation for each landmark configuration dataset. However, the Procrustes ANOVA is a useful tool for identifying the general pattern of statistical significance among size, shape, sex, and non-metric traits.

Principal component analysis (PCA) was used to display the patterns of shape differences that make up the significant differences between shape and sex. Principal component analysis is an ordination method of analysis that reduces the dimensionality of the Procrustes coordinate data into a more manageable dataset (Jolliffe, 1986). The

analysis transforms the shape data within a study sample into ranked uncorrelated principal components (PC) according to the amount of shape variation contained within each (Blackith and Reyment, 1971). The PCs from the Procrustes coordinate data were generated from a covariance matrix. The PCs depict the shape changes that contribute to the greatest amount of variation in the study sample as a wireframe graph and as PC scores (Blackith and Reyment, 1971; Klingenberg, 2011). By plotting the PC scores that contain the greatest amount of shape variation against each other, patterns of variation emerge creating groups of individuals that share the same shape (Zelditch et al., 2012). In this study, the PC scores are expected to illustrate the components of shape that distinguish sex categories. This analysis is very useful for investigating the levels of shape variation that separate the five sex categories for each landmark configuration dataset. The Spearman's correlation determined the existence of relationships and the strength of those relationships among the level of shape variation within the sex categories, and between the level of shape variation within those sex categories and non-metric trait morphology.

2.3. Hypotheses

To address the first research question, which is, what are the hip bone shape differences that contribute to sex categorization, shape difference among the specimens, was explored and quantified in GM as mean Procrustes distances. The variance among the mean Procrustes distances, quantified by the PCA, will inform how well GM captures the sex-based shape differences among the specimens and indicate those areas of the hip bone, in whole and fragmented parts, that contribute the most to the shape differences. It

is possible that specimens categorized as possible male and possible female will contain the second greatest level of shape differences. I anticipate that some shape differences exist between male and possible male sex categories and between female and possible female sex categories. Specimens categorized as indeterminate sex could fall close to either the male or the female end of the spectrum, occupy the space in-between males and females, or could stand independent of either sex category.

The Spearman's correlation and the Procrustes ANOVA addressed the second research question, which is, what are the correlations between sex-based shape differences of the hip bone and the non-metric traits used to estimate sex. The Spearman's correlation tested the strength of the relationship between shape and non-metric trait scores while the Procrustes ANOVA tested the statistical significance of the shape differences. The null hypotheses of the ANOVA and the Spearman's correlation are:

> Null Hypothesis 1: There are no shape differences in the whole hip bone that relate to estimated sex.
>
> Null Hypothesis 2: There are no shape differences in the whole hip bone that relate to individual non-metric traits.
>
> Null Hypothesis 3: There are no shape differences in the pubic region of the hip bone that relate to estimated sex.
>
> Null Hypothesis 4: There are no shape differences in the pubic region of the hip bone that relate to individual non-metric traits.
>
> Null Hypothesis 5: There are no shape differences in the ischial region of the hip bone that relate to estimated sex.
>
> Null Hypothesis 6: There are no shape differences in the ischial region of the hip bone that relate to individual non-metric traits.
>
> Null Hypothesis 7: There are no shape differences in the iliac region of the hip bone that relate to estimated sex.

Null Hypothesis 8: There are no shape differences in the iliac region of the hip bone that relate to individual non-metric traits.

Should no shape differences among the individual sex categories are uncovered then it could mean that there is little agreement between the estimated sex of the sample population and the shape analysis. One reason for this disagreement could be because the landmarks confounded or failed to capture morphological differences that distinguish the individual sex categories. If the shape analysis agrees with the assigned sex categories as larger groups, that is males (including males, possible males, and possibly individuals of indeterminate sex) from females (including females, possible females and possibly individuals of indeterminate sex), but no clear pattern of morphology is found between males and possible males or females and possible females, then it could mean that there are no patterns to human variability within the smaller sex categories. Should no shape differences exist between the indeterminate sex category and any of the remaining sex categories it could allude to a way of refining non-metric trait scores to improve sex estimations in the hip bone. Should the individuals categorized as indeterminate sex display shapes that are unique in comparison to those found among male and female groups, it could allude to the presence of "intersexed" hip bone shape and demonstrate a need to develop categorization nomenclature that captures this phenomenon. On the other hand, if all four of the null hypotheses, or only some of the null hypotheses, are rejected, meaning sex differences are revealed that distinguish shape within the female and/or the male sex categories, it could support the argument to consider a five-scale sex categorical system when interpreting sex in human osteology, rather than a binary system. It could also help human osteologists understand the sexual dimorphism of non-

metric traits better and determine which trait has a stronger relationship with the five-sex category system.

If there are no relationships between hip bone shapes and the ventral arc, ischiopubic ramus ridge, subpubic contour, or greater sciatic notch morphology then it could suggest that the factors influencing non-metric trait morphology are independent of the factors that influence hip bone shape. It could also mean that one party in the relationship, either non-metric trait morphology or hip bone shape, is more strongly affected by environmental, genetic, or other factors than the opposing party creating an reaction independent of that party.

Chapter 3 : Results

3.1. Sex Estimation and Non-Metric Trait Scores

The results of the sex estimation and the non-metric trait scores (Table 3.1) indicate the majority of the specimens were estimated as possible males (M?). This majority might have been due to a large amount of "3" scores for the subpubic contour (SPC) and ischiopubic ramus ridge (IPRR) that contribute to a less confident assessment of sex. Confident estimates of female (F) and male (M) specimens are consistent with the amount of "1" and "5" scores for the ventral arc (VA), SPC, IPRR, and greater sciatic notch (GSN). It is interesting that the great number of "5" scores for the GSN did not produce more confident male estimates. These GSN scores could therefore be acting as mitigating "maleness" factors for the SPC and IPRR scores at "3."

Table 3.1: Summary of non-metric trait scores and sex estimation.

Non-Metric Trait	Value Label	Counts	Non-Metric Trait	Value Label	Counts
Ventral Arc	1	6	**SPC**	1	9
	2	4		2	11
	3	9		3	21
	4	29		4	13
	5	11		5	5
IPRR	1	4	**GSN**	1	4
	2	13		2	7
	3	22		3	6
	4	14		4	16
	5	6		5	26
Sex Estimation	F	7	SPC= Subpubic contour		
	F?	5	IPRR=Ischiopubic ramus ridge		
	?	10	GSN=Greater sciatic notch		
	M?	29			
	M	8			

3.2. Intra-Observer Error

Intra-observer error was determined in two ways. The first test measured the precision of each landmark at the x, y, and z coordinates to identify the landmarks and the axis of direction of those landmarks that contribute to digitization error. Because a full Procrustes fit underestimates observer error, a conservative value of 0.5mm or greater was selected to identify the landmarks that are less precise, from the more precise landmarks (von Cramon-Taubadel et al., 2007). This value is less than the cut off suggested by Aldridge and colleagues (2005) for high precision between landmark means, 1mm absolute difference between observations, in order to compensate for the underestimated observer error. The mean Procrustes landmark standard deviations for the first and second landmark placement episodes are presented in Table 3.1. The asterisks indicate mean standard deviation differences that are greater than 0.5mm. The landmarks and the axes of direction of the landmarks containing the greatest differences between mean standard deviations were considered more prone to digitizing error in this study. The landmarks and axes of direction with the most digitizing error include the apex of the auricular surface (landmark 10) in the medial/lateral (x axis) and superior/inferior (y axis) directions, the arcurate eminence (landmark 19) in the superior/inferior direction, and the anterior gluteal line (landmark 27) in the superior/inferior and anterior/posterior (z axis) directions.

Table 3.2: Mean Procrustes landmark standard deviation (mm) for the first and second episodes of landmark placement.

	First Measurement			Second Measurement		
Landmark	**X**	**Y**	**Z**	**X**	**Y**	**Z**
1	0.980	0.720	0.674	1.035	0.779	0.543
2	0.468	0.821	0.910	0.569	0.766	0.850
3	1.247	1.513	2.161	1.354	1.560	1.993
4	1.264	1.056	0.642	1.135	1.259	0.633
5	1.882	1.882	1.055	1.043	2.038	1.192
6	0.924	0.925	0.462	0.892	0.902	0.516
7	0.571	0.524	1.414	0.664	0.862	1.404
8	1.198	0.982	0.603	1.060	1.142	0.556
9	0.507	0.281	0.755	0.456	0.545	0.933
10	0.884	0.805	0.905	*1.380	*1.642	1.086
11	0.472	0.792	0.985	0.605	0.946	1.215
12	0.750	1.267	0.498	0.683	0.827	0.592
13	0.638	0.771	0.703	0.692	0.499	0.533
14	0.616	0.880	0.334	0.889	0.695	0.257
15	0.675	0.899	0.405	0.582	0.836	0.818
16	0.941	0.641	0.537	0.843	0.788	0.701
17	0.988	0.853	0.617	0.743	0.906	0.604
18	0.616	0.976	0.433	0.591	0.946	0.522
19	1.121	1.415	0.514	1.095	*0.729	0.780
20	0.527	1.330	0.603	0.827	1.346	0.511
21	0.763	1.499	1.577	0.566	1.143	1.613
22	0.470	1.261	0.832	0.611	1.128	0.946
23	0.975	1.271	0.707	1.106	1.484	0.798
24	1.004	1.069	0.681	1.104	1.167	0.699
25	0.858	1.381	0.615	1.070	1.478	0.657
26	0.919	1.026	1.167	0.670	0.793	0.681
27	0.979	1.211	0.538	0.904	*1.923	*1.493
28	0.981	0.591	0.692	1.189	0.649	0.794
29	0.569	0.718	1.443	0.807	0.854	1.530
30	0.631	1.196	1.015	0.604	1.230	1.183

* Indicate standard deviation differences that are 0.5mm or greater

The Procrustes ANOVA (Table 3.2) compared the proportion of the total variance of all specimens between the repeated landmark data (Error 1) to the initial landmark data (Individual). The critical component of the Procrustes ANOVA is that the mean sum of squares measurement of Error 1 does not exceed the magnitude of mean sum of squares for the individual data (Klingenberg et al., 2002). The mean sum of squares for the

repeated landmark data was small compared to the individual specimen data suggesting that digitizing error is small (Klingenberg et al., 2002). The parametric *F* statistic, the ratio of between-subject variance to within-subject variance, of the initial landmark data indicates that there is significantly more shape variance among the individual shapes than there are between the two episodes of landmark placement (Aldridge et al., 2005). The results of these two tests suggest that although a few landmarks are less precise in position, the differences in landmark placement are not influencing the overall shape differences of the specimens.

Table 3.3: Procrustes ANOVA calculating measurement error for centroid size and object shape. Bolded values indicate significance at a 0.05 alpha level.

Centroid Size					
Source	**Sum of Squares**	**Mean Squares**	**df**	**F**	**P value**
Individual	6091.5	676.83	9	142.8	**<0.0001**
Error 1	47.397	4.7397	10		
Shape					
Source	**Sum of Squares**	**Mean Squares**	**df**	**F**	**P value**
Individual	0.092	1.238×10^{-4}	747	4.75	**<0.0001**
Error 1	0.022	2.606×10^{-5}	830		

3.3. Procrustes Analysis of Size and Shape

In order to test the significance of size and shape in the study sample, a Procrustes ANOVA was performed on the each dataset. Sex and each non-metric trait were selected as covariates for centroid size and object shape to test the null hypothesis that there is no relationship between shape and sex, or between shape and non-metric trait. The results of the Procrustes ANOVAs (Table 3.3) indicate that centroid size is statistically significant in the isolated ischium and not object shape, meaning the null hypothesis number 3 is

accepted: there is no shape difference in the ischium among sex or non-metric trait categories. However, the remaining three null hypotheses are rejected: there are similarities present between hip bone shape and estimated sex as well as relationships between hip bone shape and non-metric trait categories for the whole hip bone, isolated ilium, isolated pubis, and combined datasets. Size is also a statistically significant component of sex with combined ilium and ischium shape, most likely due to the influence of centroid size on the ischium. Greater sciatic notch scores also demonstrate a statistically significant relationship with centroid size values in respective ilium and ischium datasets as well as their combined dataset. Interestingly, the ventral arc also has a relationship with centroid size in the ischium-pubis dataset, a likely consequence of the relationship between size and the ischium.

Table 3.4: Procrustes ANOVA results for log centroid size and Procrustes distances (shape) grouped by non-metric trait and sex estimation scores for all datasets. Bolded values indicate significance at a 0.05 alpha level.

Whole Bone Dataset								
	Centroid size				Shape			
Individuals	**MS[5]**	**df**	**F**	**P value**	**MS**	**df**	**F**	**P value**
Estimated Sex	215.03	4	0.83	0.514	$2.007x10^{-4}$	332	2.87	**<0.0001**
VA[1]	252.98	4	0.98	0.425	$1.817x10^{-4}$	332	2.55	**<0.0001**
SPC[2]	124.51	4	0.47	0.760	$1.521x10^{-4}$	332	2.07	**<0.0001**
IPRR[3]	129.81	4	0.49	0.745	$1.323x10^{-5}$	332	1.76	**<0.0001**
GSN[4]	411.48	4	1.67	0.169	$1.888x10^{-4}$	332	2.67	**<0.0001**
Ilium Dataset								
	Centroid size				Shape			
Individuals	**MS**	**df**	**F**	**P value**	**MS**	**df**	**F**	**P value**
Estimated Sex	125.24	4	1.23	0.3094	$8.549x10^{-4}$	128	2.38	**<0.0001**
VA	173.06	4	1.76	0.1505	$8.115x10^{-4}$	128	2.24	**<0.0001**
SPC	85.79	4	0.82	0.5190	$6.909x10^{-4}$	128	1.86	**<0.0001**
IPRR	80.44	4	0.76	0.5529	$6.052x10^{-4}$	128	1.60	**<0.0001**
GSN	258.57	4	2.81	**0.0343**	$8.764x10^{-4}$	128	2.45	**<0.0001**
Ischium Dataset								
	Centroid size				Shape			
Individuals	**MS**	**df**	**F**	**P value**	**MS**	**df**	**F**	**P value**

Estimated Sex	103.74	4	7.71	**<0.0001**	$6.639x10^{-4}$	68	0.94	0.6259
VA	79.61	4	5.22	**0.0013**	$1.014x10^{-3}$	68	1.48	0.0083
SPC	70.94	4	4.46	**0.0034**	$7.893x10^{-4}$	68	1.13	0.2317
IPRR	86.94	4	5.91	**0.0005**	$7.416x10^{-4}$	68	1.05	0.3651
GSN	104.02	4	7.74	**<0.0001**	$6.006x10^{-4}$	68	0.84	0.8463
Pubis Dataset								
	Centroid size				Shape			
Individuals	**MS**	**df**	**F**	**P value**	**MS**	**df**	**F**	**P value**
Estimated Sex	25.48	4	0.99	0.4207	$1.811x10^{-3}$	80	4.25	**<0.0001**
VA	54.59	4	2.32	0.0689	$1.351x10^{-3}$	80	2.94	**<0.0001**
SPC	17.38	4	0.66	0.6223	$1.275x10^{-3}$	80	2.74	**<0.0001**
IPRR	32.43	4	1.29	0.2868	$1.257x10^{-3}$	80	2.69	**<0.0001**
GSN	18.91	4	0.72	0.5812	$1.226x10^{-3}$	80	2.91	**<0.0001**
Ilium-Ischium Dataset								
	Centroid size				Shape			
Individuals	**MS**	**df**	**F**	**P value**	**MS**	**df**	**F**	**P value**
Estimated Sex	358.39	4	2.14	**0.0888**	$3.339x10^{-4}$	224	2.81	**<0.0001**
VA	292.45	4	1.69	0.1649	$3.165x10^{-4}$	224	2.63	**<0.0001**
SPC	205.01	4	1.14	0.3456	$2.653x10^{-4}$	224	2.14	**<0.0001**
IPRR	189.05	4	1.05	0.3910	$2.145x10^{-4}$	224	1.68	**<0.0001**
GSN	511.33	4	3.27	**0.0180**	$3.468x10^{-4}$	224	2.94	**<0.0001**
Ilium-Pubis Dataset								
	Centroid size				Shape			
Individuals	**MS**	**df**	**F**	**P value**	**MS**	**df**	**F**	**P value**
Estimated Sex	83.472	4	0.36	0.8391	$2.652x10^{-4}$	236	2.75	**<0.0001**
VA	169.944	4	0.74	0.5662	$2.264x10^{-4}$	236	2.28	**<0.0001**
SPC	50.019	4	0.21	0.9313	$1.963x10^{-4}$	236	1.93	**<0.0001**
IPRR	78.449	4	0.33	0.8542	$1.746x10^{-4}$	236	1.69	**<0.0001**
GSN	240.081	4	1.08	0.3776	$2.440x10^{-4}$	236	2.49	**<0.0001**
Ischium-Pubis Dataset								
	Centroid size				Shape			
Individuals	**MS**	**df**	**F**	**P value**	**MS**	**df**	**F**	**P value**
Estimated Sex	66.824	4	1.14	0.3466	$4.602x10^{-4}$	176	2.93	**<0.0001**
VA	148.31	4	2.83	**0.0335**	$3.912x10^{-4}$	176	2.41	**<0.0001**
SPC	52.58	4	0.88	0.4804	$3.474x10^{-4}$	176	2.10	**<0.0001**
IPRR	38.16	4	0.63	0.6436	$3.609x10^{-4}$	176	2.20	**<0.0001**
GSN	125.88	4	2.33	0.0680	$3.535x10^{-4}$	176	2.14	**<0.0001**

1. VA=Ventral arc; 2. SPC=Subpubic contour; 3. IPRR=Ischiopubic ramus ridge; 4. GSN=Greater Sciatic Notch; 5. MS= Mean squares.

3.4. Principal Component Analysis

In order to investigate the relationships between the datasets and shape in more detail a principal component analysis (PCA) was performed to display the patterns of

shape difference found in the hip bone datasets by the Procrustes ANOVA. The PCA results are presented separately for each dataset representing landmark configurations of the hip bone, isolated ilium, isolated ischium, isolated pubis, combined ilium-ischium, combined ilium-pubis, and combined ischium-pubis. Two wireframe graphs are used to illustrate the shape changes at the positive end of each PC axis (scale 0.1, images labelled "A") and at the negative end of each PC axis (scale -0.1, images labelled "B"). Scatterplots of PCA scores illustrate the individual specimens, coloured by sex category that share common shapes and how different sex-based shapes can be within each dataset (Klingenberg, 2011). The purpose of analysing the hip bone as whole, as isolated segments and as combined segments is to determine which region or regions of the hip bone contribute the most to sex-based shape differences.

Table 3.5: Principal components retained for analysis.

Dataset	Total Variance	PC	Eigenvalues	% Variance	Total %
Whole Bone	0.007	1	0.00119	18.242	18.242
		2	0.00068	10.324	28.566
Ilium	0.013	1	0.00247	19.586	19.586
		2	0.00202	16.026	35.612
		4	0.00110	7.177	42.789
Ischium	0.012	1	0.00200	16.653	16.653
		2	0.00189	15.761	32.413
Pubis	0.012	1	0.00252	24.135	24.135
		2	0.00213	20.380	44.516
		3	0.00106	10.155	54.670
Ilium-Ischium	0.008	1	0.00150	20.037	20.037
		2	0.00090	12.079	32.117
Ilium-Pubis	0.006	1	0.00124	19.496	19.496
		2	0.00078	12.313	31.809
Ischium-Pubis	0.007	1	0.00116	14.830	14.830
		2	0.00096	12.280	27.111

Not all of the principal components generated by the PCA will be relevant to understanding sexual dimorphism (Hallgrimsson et al., 2008; Jolliffe, 1986; Zelditch et al., 2012). The criteria for relevancy in this study consist of two parts: a high percentage of total shape variance and/or a demonstrable strong and statistically significant relationship with sex and non-metric trait scores in order to answer the research questions were retained for analysis. Principal components were retained if only one criterion was met. The Spearman's correlation tests (described in section 3.4) provided insight into identifying those PCs that had a strong relationship with sex and non-metric trait morphology.

3.4.1. Whole bone dataset

The shape variation represented by PC1 (Figure 3.1) include hip bone height, which prompts a change in the height of the inferior and anterior gluteal lines, the iliac tubercle, and the anterior superior iliac spine (ASIS). Relative to individuals with a positive PC1 score, those at the negative end of the axis express a shifting posterior portion of the ilium superiorly, as demarcated by the posterior superior and posterior inferior iliac spines (PIIS). The posterior inferior point of the preauricular sulcus also shifts superiorly with the ilium. Reflected in the movement of the posterior portion of the ilium is the shift in the posterior gluteal line and the anterior portion of the auricular surface in a superior trajectory, and a widening of the GSN. The hip bone narrows at the ischium resulting in a smaller and more anteriorly positioned ischial tuberosity, a shorter ischiopubic ramus, and a more anteriorly positioned posterior border of the ilium between the ischial spine and the point of maximum curvature in the GSN. The pubic bone

lengthens at the pubic symphyseal face causing the arcurate eminence to move inferiorly, and a smaller or more posteriorly positioned pubic tubercle.

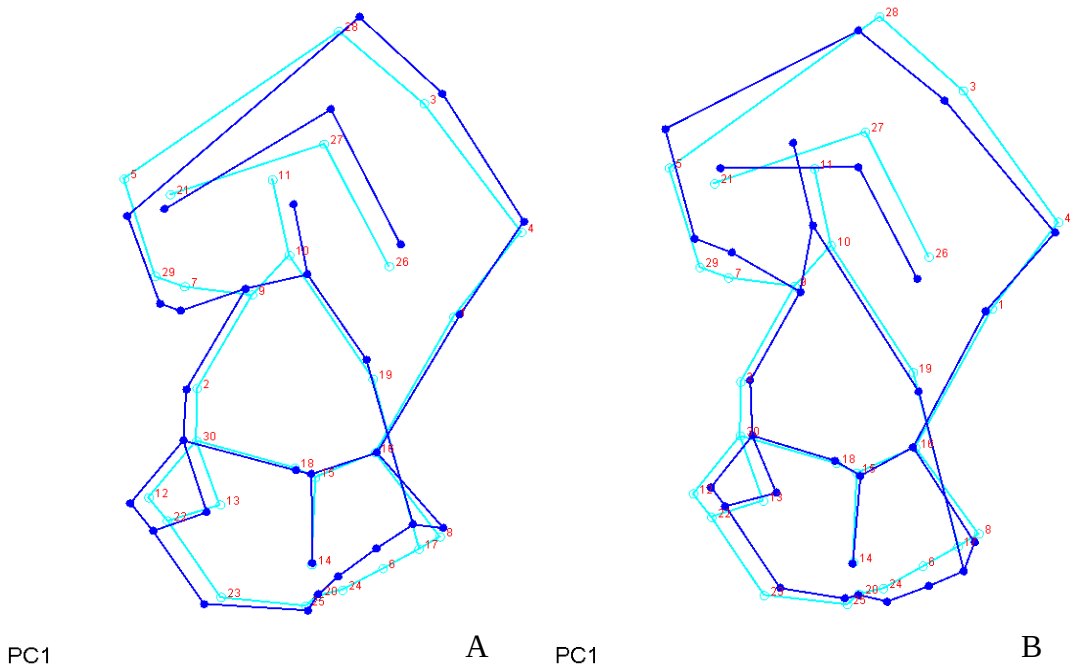

Figure 3.1: Wireframe graphs illustrating the shape changes on the PC1 axis of the whole bone dataset. Dark blue lines represent shape change; light blue lines represent the mean shape. A: the shape at the positive end of the PC1 axis. B: the shape at the negative end of the PC1 axis.

The variation in hip bone shape on the PC2 axis (Figure 3.2) is characterized by an increase in hip bone width at the ilium resulting in a more medially and inferiorly positioned iliac tubercle. A more posteriorly and inferiorly positioned posterior gluteal line, a more medially positioned maximum curvature of the GSN, and a more posteriorly positioned anterior portion of the auricular surface complete the shape variation. The ischium widens at the superior and posterior points of the ischial tuberosity, the pubic tubercle moves anteriorly and medially, the inferior medial point on the obturator foramen rim moves more medially, and the arcurate eminence moves inferiorly.

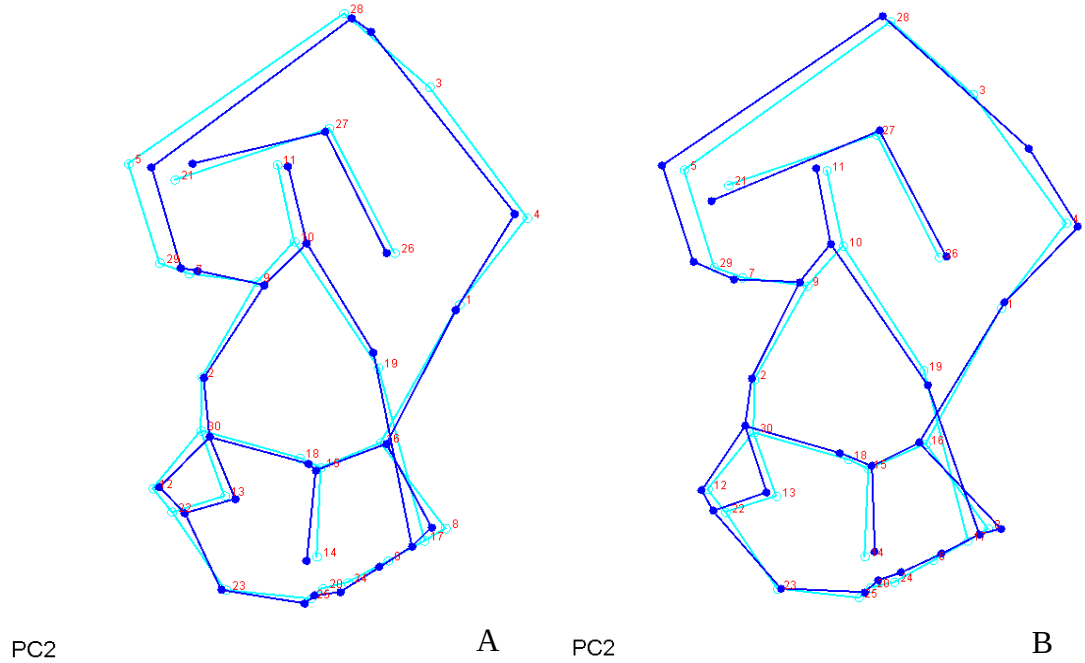

Figure 3.2: Wireframe graphs illustrating the shape changes on the PC2 axis of the whole bone dataset. Dark blue lines represent shape change; light blue lines represent the mean shape. A: the shape at the positive end of the PC2 axis. B: the shape at the negative end of the PC2 axis.

The distributions of specimens on these PCs are presented in Figure 3.3. The specimens categorized as male (blue) and possible male (purple) sex occupy the positive end of the PC1 axis almost exclusively, with the females (yellow) and possible females (green) predominately distributed at the opposite end. This pattern indicates that the males poses whole hip bone shapes with a tall hip bone with a short pubic bone, a long and wide ischium, and a very narrow greater sciatic notch (i.e., the dark blue wireframe in Figure 3.1A), while the females and possible females display the opposite morphology (i.e., Figure 3.1B). The males and possible males dispersed along the PC2 axis indicate variability in ilium width, ilium tubercle height, ischial tuberosity configuration, pubic tubercle location, and arcurate eminence height. Of the three specimens classified as

indeterminate sex (red), two of them occupy the positive end of the PC1 axis, which suggests they have a male shape. One of the specimens of indeterminate sex falls close to a specimen categorized as female, which suggests this specimen has a more female hip bone shape. There is an area of overlap slightly to the negative side of the axis origin (-0.03 to 0.0), where specimens of all five categories fall, which suggests that this is the area of transition between the female and male whole bone shapes. The sexual dimorphism displayed in the hip bone dataset distinguishes well between male and female shapes but does not distinguish between male and possible male or female and possible female.

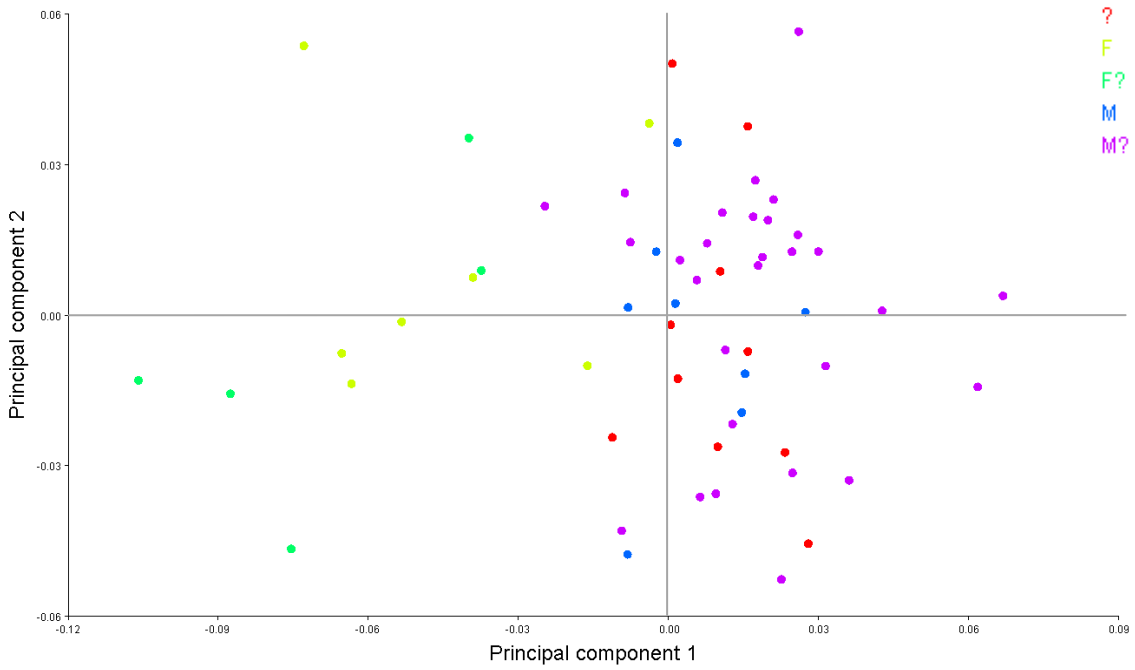

Figure 3.3: Distribution of specimens from the whole hip bone dataset categorized by estimated sex. PC1 and PC2.

3.4.2. Ilium dataset

The shape variation expressed in the isolated ilium dataset is more subtle than the shape variation of the ilium expressed in the whole hip bone, but follows a similar pattern. The pattern of variance contained in PC1 is illustrated by changes in ilium height, which influence the position of the gluteal lines, the anterior portion of the auricular surface, and the superior border of the GSN. Relative to individuals with a positive PC1 score (Figure 3.4A), those at the negative end of the axis (Figure 3.4B) express an increase in ilium height, which corresponds to an increase in the height of the inferior, anterior and posterior gluteal lines. Ilium width decreases at the anterior superior and anterior inferior iliac spines causing the anterior portion of the auricular surface to move laterally. The posterior portion of the ilium moves inferiorly creating a more inferiorly and anteriorly positioned anterior portion of the auricular surface and a narrower superior edge of the GSN.

The change in the shape of the ilium on the PC2 axis (Figure 3.5) are characterized by a medial extension of the posterior superior and PIIS, causing the maximum arc of the iliac crest to also extend in that direction and the posterior gluteal line to extend medially and inferiorly. The iliac tubercle extends inferiorly and laterally while the anterior superior and anterior inferior iliac spines (AIIS) move superiorly. The inferior gluteal line moves superiorly in response to the anterior iliac spines while the anterior gluteal line moves inferiorly following the iliac tubercle. In comparison with the pattern of variance of the iliac region in the whole bone, the width of the iliac blade is a less defined shape pattern in the isolated ilium.

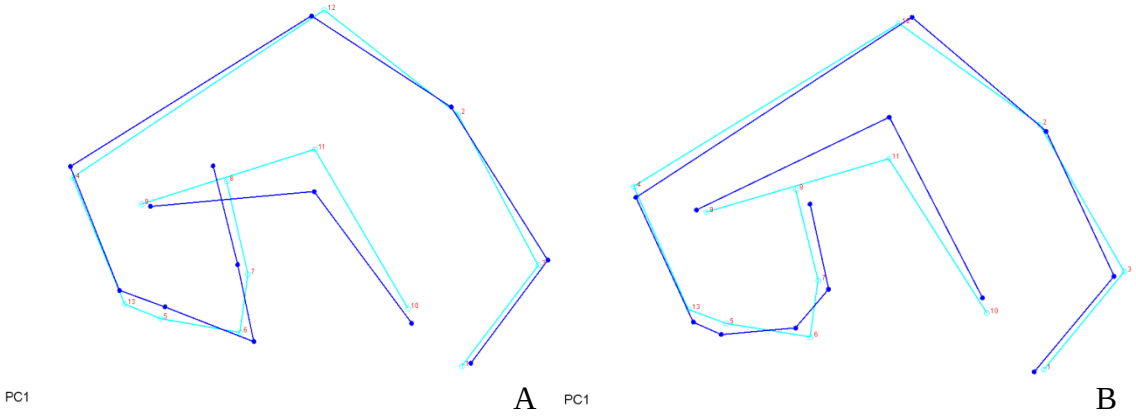

Figure 3.4: Wireframe graphs illustrating the shape changes on the PC1 axis of the ilium dataset. Dark blue lines represent shape change; light blue lines represent the mean shape. A: the shape at the positive end of the PC1 axis. B: the shape at the negative end of the PC1 axis.

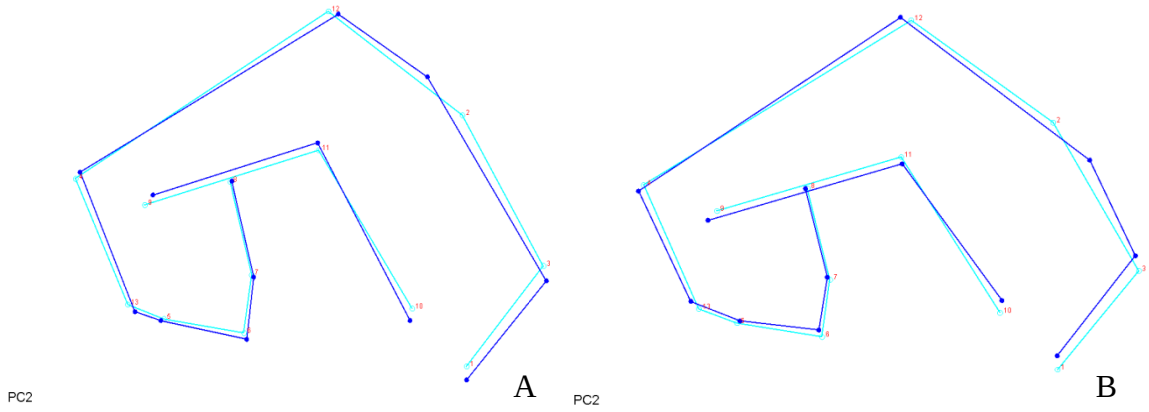

Figure 3.5: Wireframe graphs illustrating the shape changes on the PC2 axis of the ilium dataset. Dark blue lines represent shape change; light blue lines represent the mean shape. A: the shape at the positive end of the PC2 axis. B: the shape at the negative end of the PC2 axis.

In the isolated ilium PC4 was also had a statistical significant correlation with sex, and fits the inclusion criteria outlined in section 3.3. The changes in the ilium on the PC4 axis, relative to the individuals with positive scores (Figure 3.6A), those at the negative end (Figure 3.6B) express a decrease in ilium height at the maximum arc of the iliac crest, the iliac tubercle, the ASIS, and the posterior superior iliac spine (PSIS). The ilium

also widens at the anterior superior and PSIS. Contrary to typical responses seen in the gluteal lines to a decrease in iliac height, the inferior, anterior, and posterior gluteal lines move superiorly. The superior border of the GSN widens in response to a widening of the ilium and the anterior portion of the auricular surface moves posteriorly.

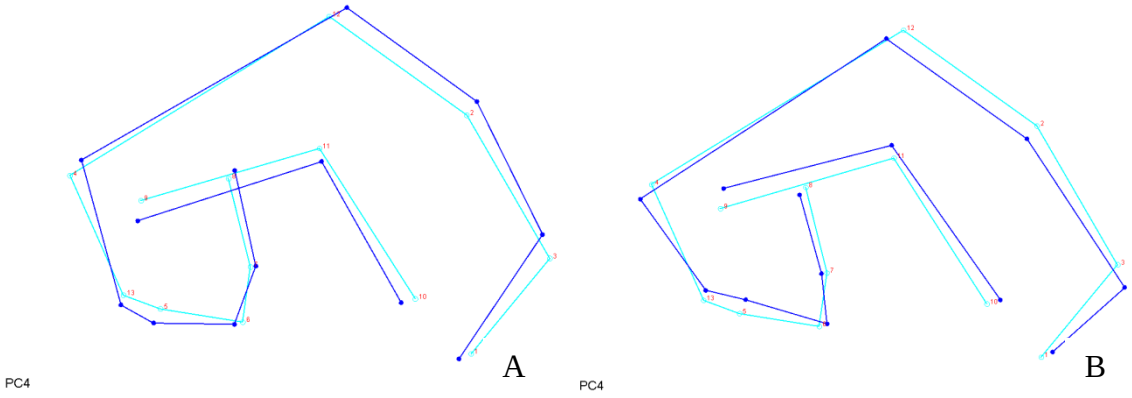

Figure 3.6: Wireframe graphs illustrating the shape changes on the PC4 axis of the ilium dataset. Dark blue lines represent shape change; light blue lines represent the mean shape. A: the shape at the positive end of the PC4 axis. B: the shape at the negative end of the PC4 axis.

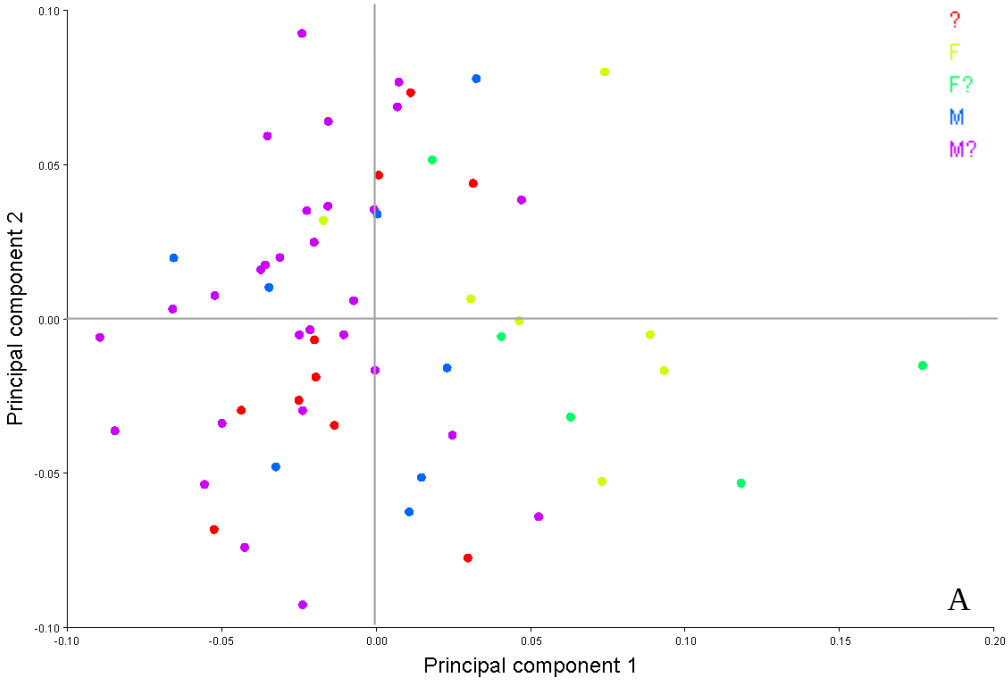

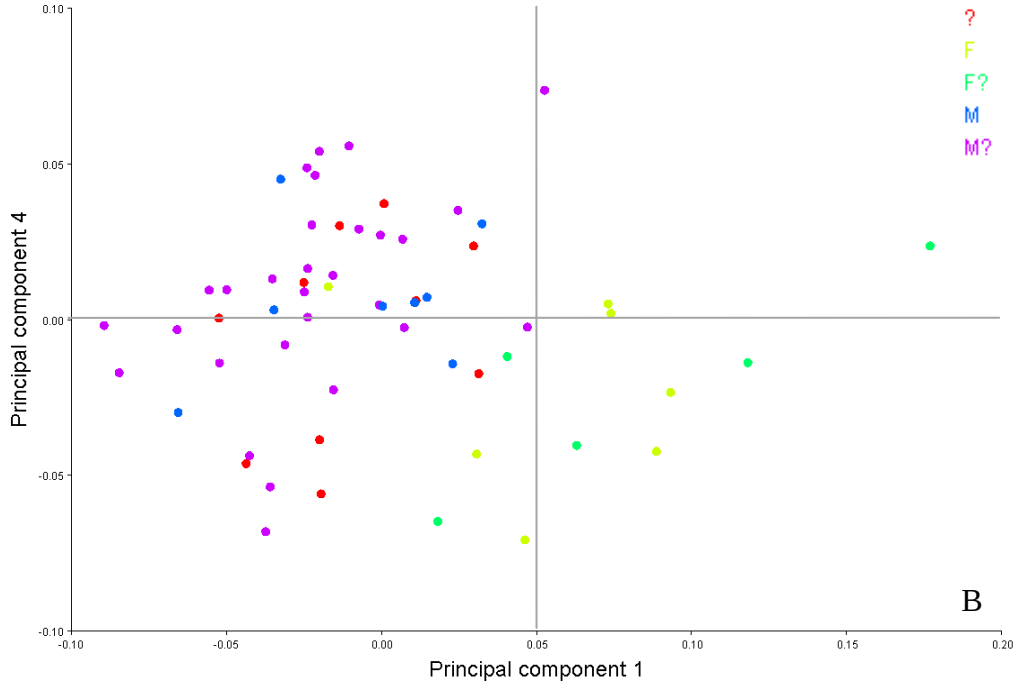

Figure 3.7: Distribution of specimens from the ilium dataset categorized by estimated sex. A: PC1 and PC2. B: PC1 and PC4.

The distribution of specimens along these PCs is presented in Figure 3.7. The specimens categorized as female and possible female specimens tend to cluster at the positive end of the PC1 axis in Figures 3.7A and 3.7B while the specimens categorized as male, possible male and indeterminate sex cluster mainly at the negative end of PC1. There is an area of overlap of all five sex categories towards the positive end of the PC1 axis (-0.03 to 0.05), which is a larger area of overlap than PC1 of the whole hip bone. All sex categories are dispersed along the PC2 axis. In the shapespaces combining PC1 and PC4, the area of overlap appears to concentrate more at the positive end of the PC1 axis (0.02 to 0.05), with the exception of one female individual at the negative end of PC1. The female and possible female individuals cluster more closely to the negative end of PC4. This suggests that most of the females tend to possess shape characteristics

reflecting a short and wide ilium, a superiorly positioned iliac tubercle, a medially positioned anterior portion of the auricular surface, a wider GSN, and a more medially positioned maximum arc of the iliac crest. The position of the gluteal lines on the female individuals is variable. The majority of males, possible males, and individuals of indeterminate sex tend to possess a tall iliac blade with a laterally positioned maximum arc of the iliac crest, a superiorly positioned iliac tubercle, a laterally positioned anterior portion of the auricular surface, and a narrower GSN. The position of the gluteal lines and iliac spines are variable among the males, possible males, and individuals of indeterminate sex.

3.4.3. Ischium dataset

The shape variation captured by PC1 and PC2 of the isolated ischium include ischial tuberosity size, which influences the distance between the most superior part of the ischial tuberosity and the ischial spine, location of the posterior inferior point of the lunate surface, orientation of the most superior lateral point of the obturator foramen rim, and the most inferior point on the ischial tuberosity. Relative to individuals with a positive PC1 (Figure 3.8A), those at the negative end of the axis (Figure 3.8B) express an increase ischial tuberosity height at the superior point with an inferior extension of the ischial ramus, and ischial tuberosity width at the medial edge. The length of the ischium increases at the most inferior point of the ischium.

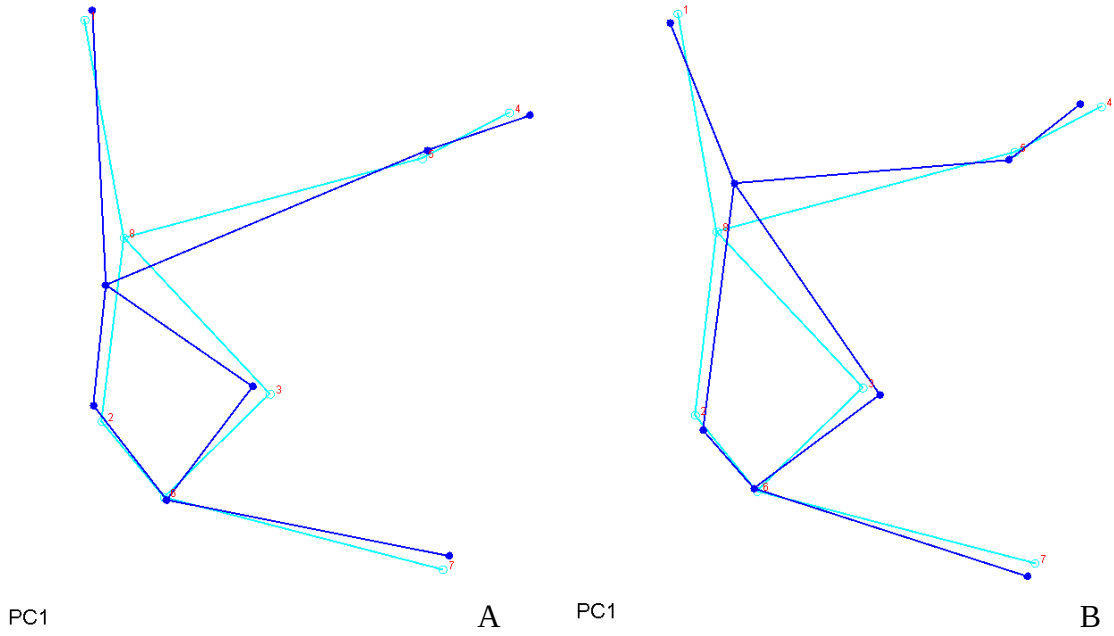

Figure 3.8: Wireframe graphs illustrating the shape changes on the PC1 axis of the ischium dataset. Dark blue lines represent shape change; light blue lines represent the mean shape. A: the shape at the positive end of the PC1 axis. B: the shape at the negative end of the PC1 axis.

The shape variation captured in the ischium by PC2 (Figure 3.9) is characterized by the size of the ischial tuberosity, position of the superior lateral point on the obturator foramen rim, the posterior inferior point of the lunate surface, and the length of the ischial ramus. Relative to the individuals at the positive end of the PC2 axis, the individuals on the negative end express a shortening of the ischial tuberosity at the superior and most posterior points, a widening of the ischial tuberosity at the medial edge, a shorter ischium and more inferiorly located inferior point, and a more superiorly extended superior lateral point of the obturator foramen and posterior inferior point of the lunate surface.

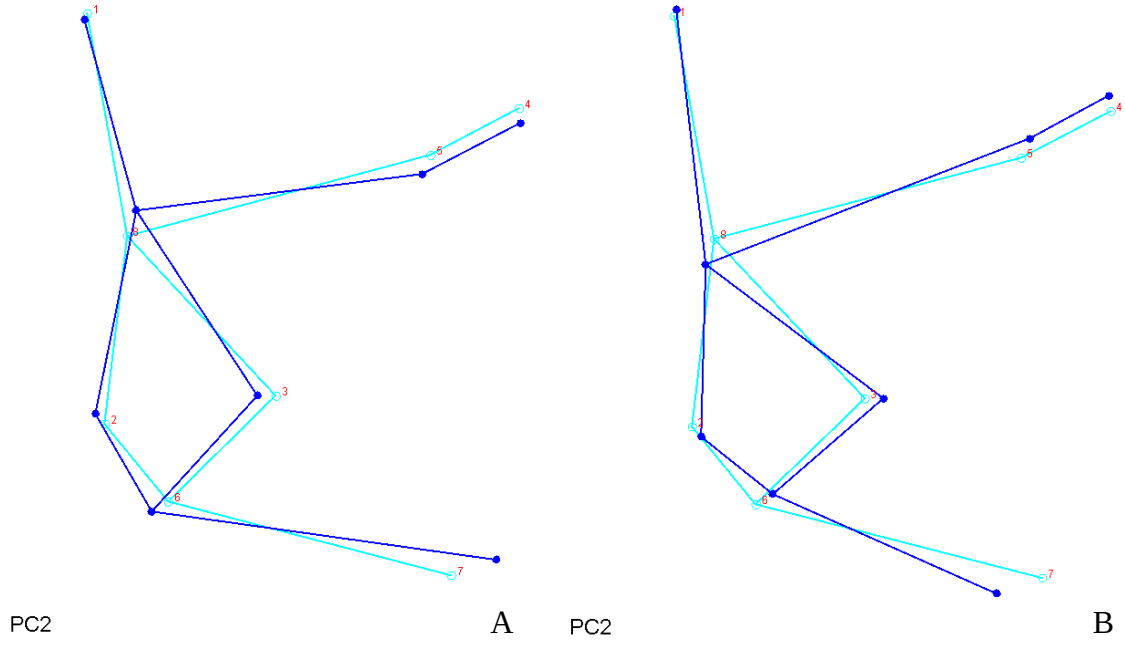

Figure 3.9: Wireframe graphs illustrating the shape changes on the PC2 axis of the ischium dataset. Dark blue lines represent shape change; light blue lines represent the mean shape. A: the shape at the positive end of the PC2 axis. B: the shape at the negative end of the PC2 axis.

The components of shape in the ischium captured by PC1 and PC2 in Figures 3.8 and 3.9 do not distinguish patterns of sexual dimorphism when specimens are distributed in the shapespaces (Figure 3.10). This suggests that ischium shape is not a dominant source of sexual dimorphism. The PCA results complement the results of the Procrustes ANOVA; sexual dimorphism in ischium is related to size differences rather than shape differences.

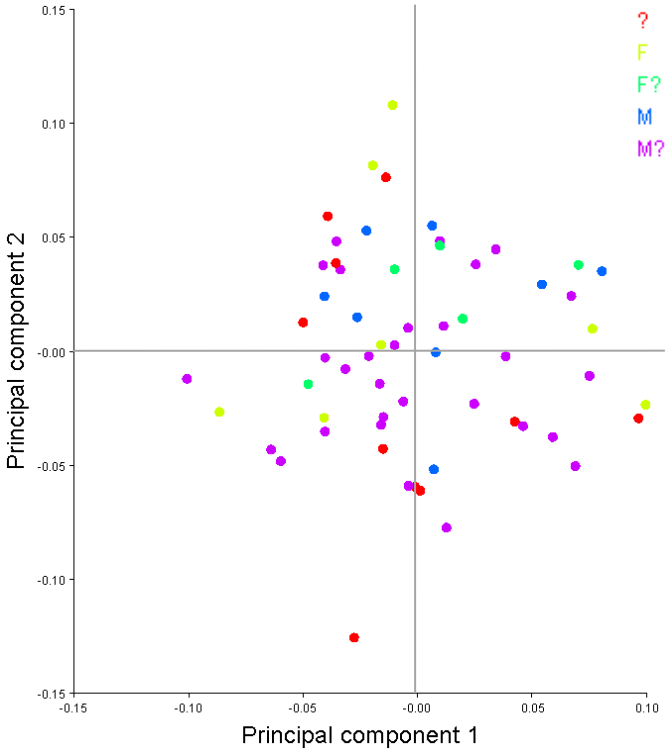

Figure 3.10: Distribution of specimens from the ischium dataset categorized by estimated sex, PC1 and PC2.

3.4.4. Pubis dataset

The shape variation expressed in the isolated pubis is represented by the length and width of the pubic symphyseal face, the orientation of the most inferior point on the symphyseal face, the position of the phallic ridge, the location of the arcurate eminence, the situation of the pubic tubercle, the length of the pubic bone, the movement of the most inferior medial point on the obturator foramen rim, and the orientation of the most anterior inferior point of the lunate surface. The pattern of variance contained in PC1 of the pubis dataset is illustrated by changes in the arcurate eminence, the pubic tubercle, the width of the pubic symphyseal face, the phallic ridge, and the most anterior inferior point of the lunate surface. Relative to individuals with a positive PC1 score (Figure 3.11A),

those at the negative end of the axis (Figure 3.11B) express a more superiorly positioned arcurate eminence, a more inferiorly positioned pubic tubercle, a narrower symphyseal face, a posterior medial movement of the most lateral point of the phallic ridge on the ischiopubic ramus, and an inferior movement of the most anterior inferior point of the lunate surface.

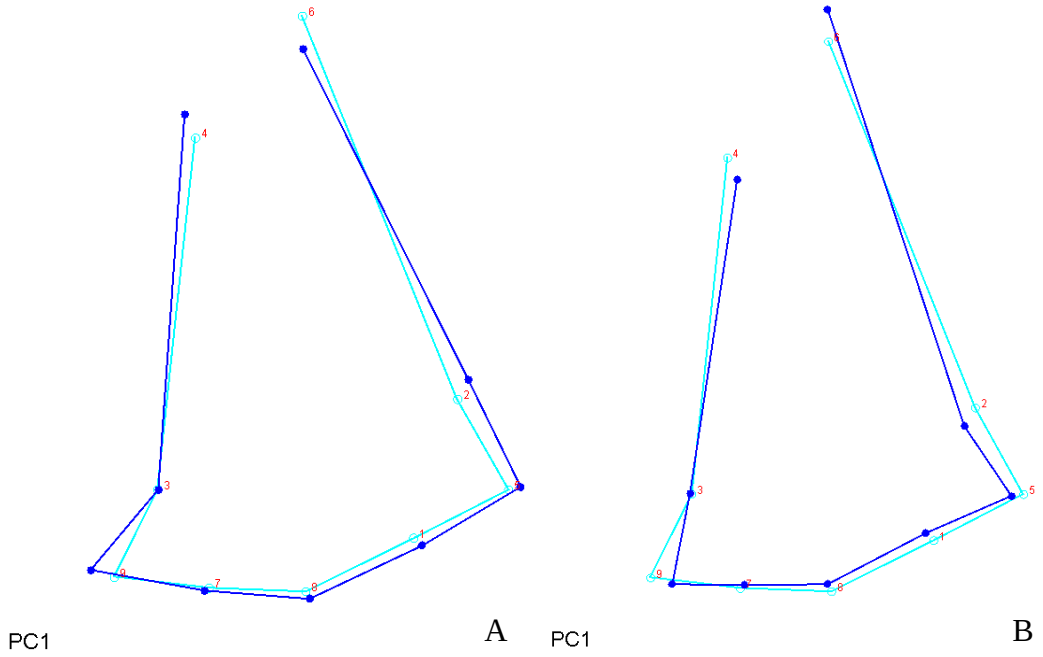

Figure 3.11: Wireframe graphs illustrating the shape changes on the PC1 axis of the pubis dataset. Dark blue lines represent shape change; light blue lines represent the mean shape. A: the shape at the positive end of the PC1 axis. B: the shape at the negative end of the PC1 axis.

The change in the shape of the pubis on the PC2 axis (Figure 3.12) are characterized by a narrowing of the pubis at the arcurate eminence, the pubic tubercle, and at the superior point of the symphyseal face. Other shape changes include a lengthening pubic bone at the symphyseal face, and a more anterior and medially positioned phallic ridge and ischiopubic ramus ridge. The most inferior medial point of

the obturator foramen moves superior lateral, and the most anterior inferior point of the lunate surface moves superior medial.

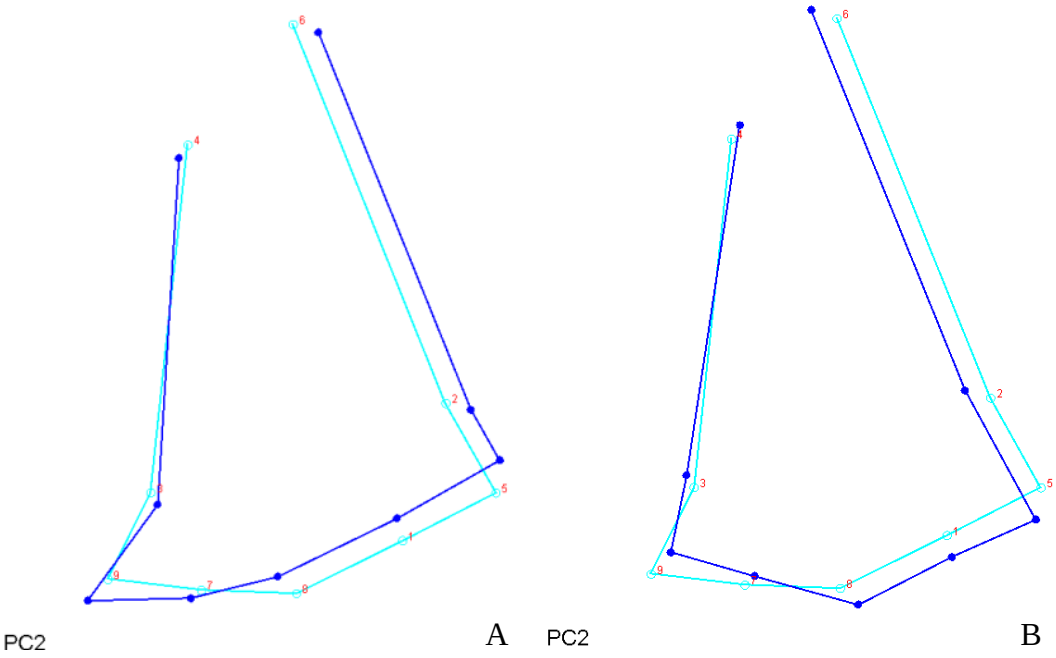

Figure 3.12: Wireframe graphs illustrating the shape changes on the PC2 axis of the pubis dataset. Dark blue lines represent shape change; light blue lines represent the mean shape. A: the shape at the positive end of the PC1 axis. B: the shape at the negative end of the PC1 axis.

The changes in the ilium on the PC3 axis, relative to the individuals with positive scores (Figure 3.13A), those at the negative end of the axis (Figure 3.13B) express a more anteriorly positioned arcurate eminence, a more lateral position of the pubic tubercle, a shortening of the symphyseal face, a movement of the ischiopubic ramus and the phallic ridge in a medial and inferior direction, a lateral movement of the most inferior medial point on the obturator foramen, and a more superiorly positioned anterior inferior point of the lunate surface.

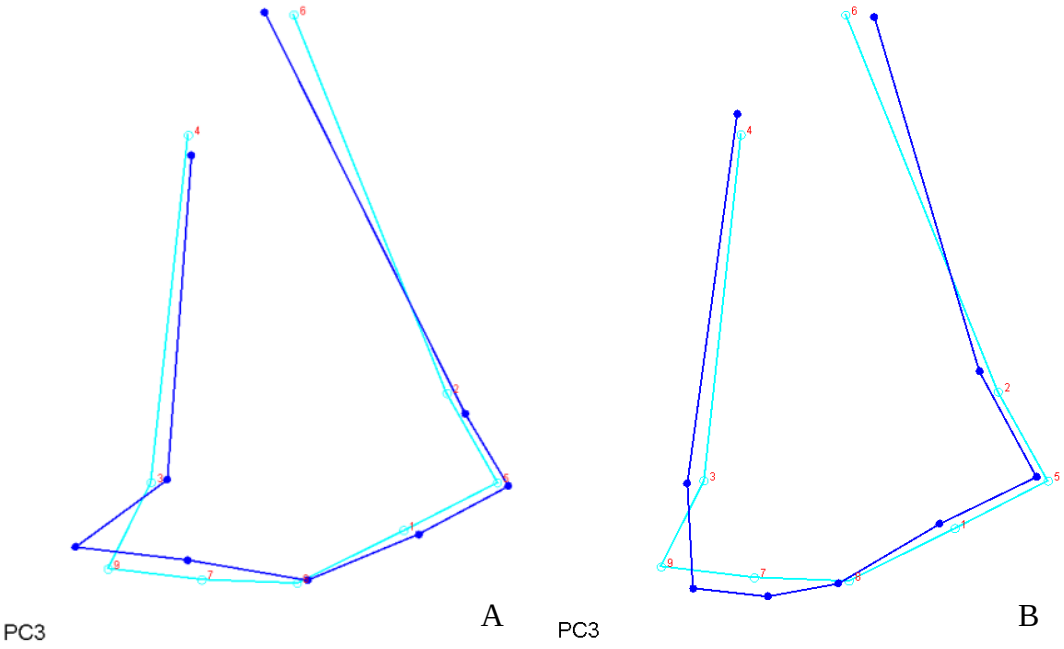

Figure 3.13: Wireframe graphs illustrating the shape changes on the PC3 axis of the pubis dataset. Dark blue lines represent shape change; light blue lines represent the mean shape. A: the shape at the positive end of the PC3 axis. B: the shape at the negative end of the PC3 axis.

The distributions of specimens along these PCs are presented in Figure 3.14. The specimens do not group clearly along PC1, however, there is a clearer separation of specimens along PC2 (Figure 3.14A). The majority of male, possible male and individuals of indeterminate sex tend to cluster at the positive end of PC2 while the female and possible female specimens cluster at the negative end of PC2. The area of overlapping specimens occurs mostly toward the negative end of the PC2 origin with a possible female specimen outlier at roughly 0.02. The shape characteristics that largely distinguish males from females are a longer and a narrow pubic bone. The presence of some males in the negative axis of PC2 suggest that some males poses female like pubic bone shapes or there are confounding factors of shape from some of the other landmarks such as the inferior medial aspect of the obturator foramen, the most anterior inferior

point of the lunate surface, or the arcurate eminence. The possible female outlier on PC2 (UBC_29) possesses a wider pubic bone, which is pulling the individual toward the positive side of PC2.

The shape variance represented by PC2 of the pubis dataset is similar to the shape variance of the pubis region represented by PC1 of the whole hip bone dataset and both shapes variances represent strong sexually dimorphic patterns, however, when PC2 is plotted against PC3 (Figure 3.14B) an interesting pattern emerges among the sex categories. After the specimens group along the PC2 axis, there appears to be a further separation of specimens along the PC3 axis of female specimens from the rest of the group. There is some overlap between female and possible female specimens at the origin of PC3, and between male and possible male specimens toward the origin of PC2, however, the majority of the specimens identified as female occupy the PC2 negative and PC3 positive quadrant of the shapespaces. The pubis characteristics that are expressed in this quadrant include a laterally placed phallic ridge and ischiopubic ramus, and posteriorly positioned arcurate eminence. Unfortunately, the shape changes in PC3 could not discriminate between specimens estimated as indeterminate sex, possible male sex or male sex. Although, the specimens estimated as indeterminate sex reside close to the other males in the scatterplot indicating the pubis shape distinguishes them as males.

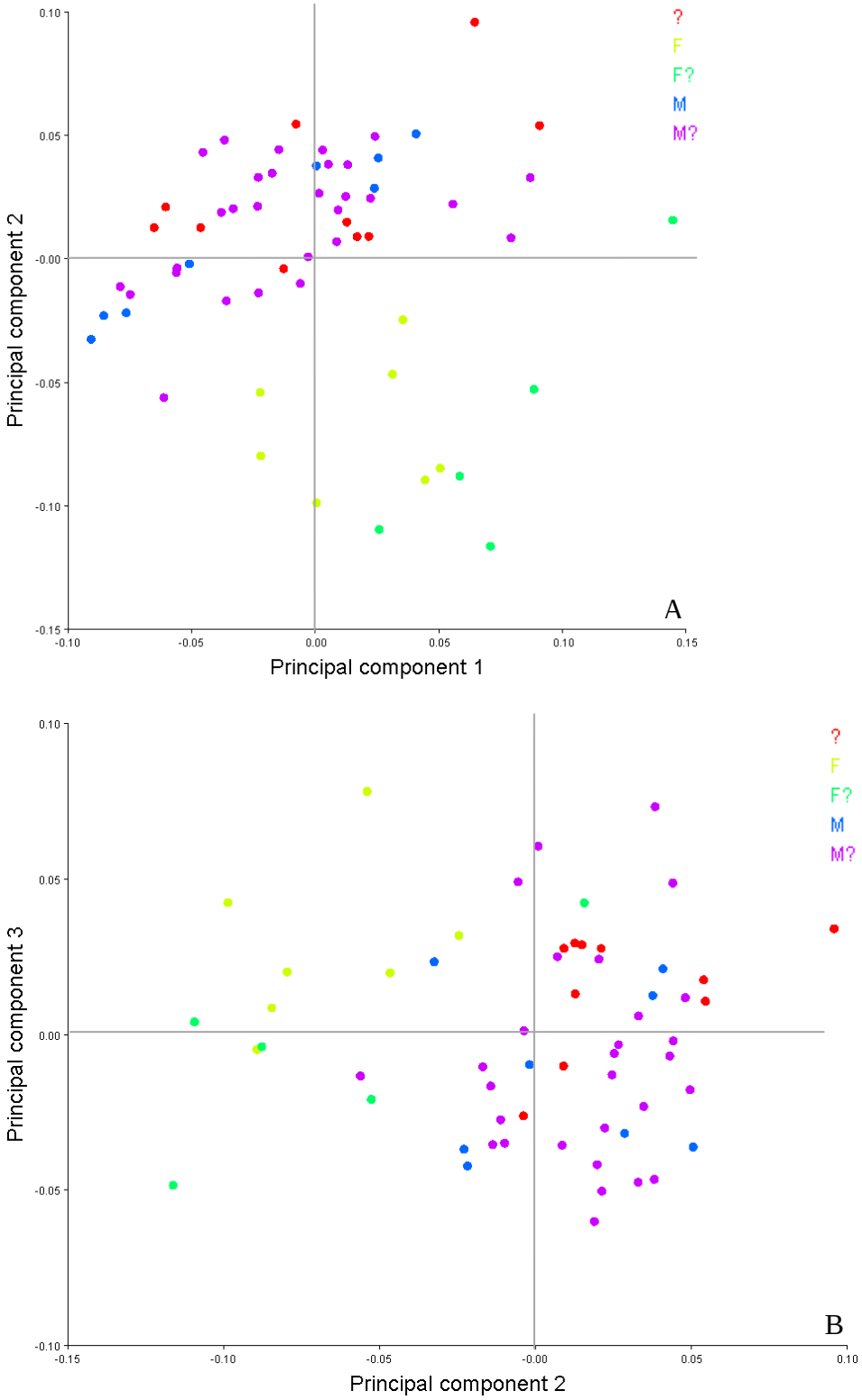

Figure 3.14: Distribution of specimens from the pubis dataset categorized by estimated sex. A: PC1 and PC2. B: PC2 and PC3.

3.4.5. Ilium-ischium dataset

The pattern of variance contained in PC1 and PC2 of the ilium-ischium dataset is illustrated by changes in hip bone height, width of the iliac blade, width of the ischial body, the angle of the GSN, the position of the anterior portion of the auricular surface, location of the posterior portion of the ilium and the iliac tubercle, and the location of the ischial tuberosity. The pattern of variance of the ilium-ischium is virtually identical to the pattern of variance seen in the whole hip bone dataset, (section 3.3.1). The only difference between the two patterns is that there is less change in the anterior portion of the auricular surface in PC2 of the ilium-ischium dataset then there is in the whole bone dataset.

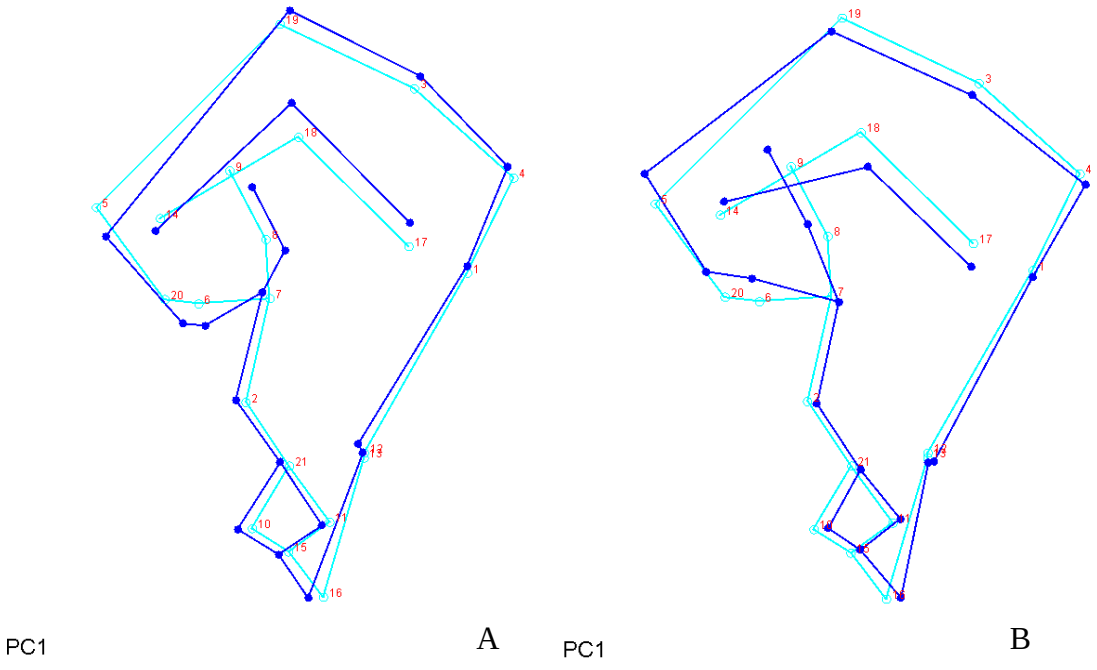

Figure 3.15: Wireframe graphs illustrating the shape changes on the PC1 axis of the ilium-ischium dataset. Dark blue lines represent shape change; light blue lines represent the mean shape. A: the shape at the positive end of the PC1 axis. B: the shape at the negative end of the PC1 axis.

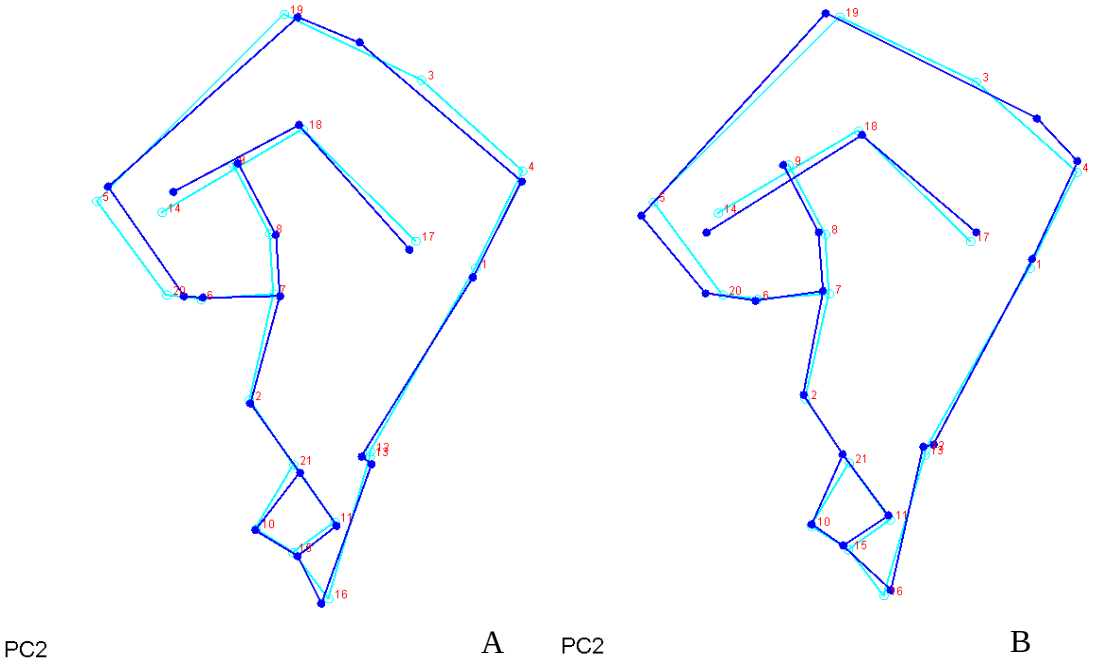

Figure 3.16: Wireframe graphs illustrating the shape changes on the PC2 axis of the ilium-ischium dataset. Dark blue lines represent shape change; light blue lines represent the mean shape. A: the shape at the positive end of the PC2 axis. B: the shape at the negative end of the PC2 axis.

The distribution of specimens on these PCs is presented in Figure 3.17, which is also similar to the distribution of the whole bone dataset with a few exceptions. There is an outlier specimen, classified possible male (UBC_21), at the negative end of the PC1 axis that widens the area of overlap among the specimens (-0.04 to 0.0). This specimen was given a greater sciatic notch score of 3, which is drawing the individual shape into the negative end of the PC1 axis. As in the whole bone dataset, the sexual dimorphism displayed in the ilium-ischium dataset distinguishes between male and female shapes but does not distinguish between specimens of possible female and female sex or possible male and male sex.

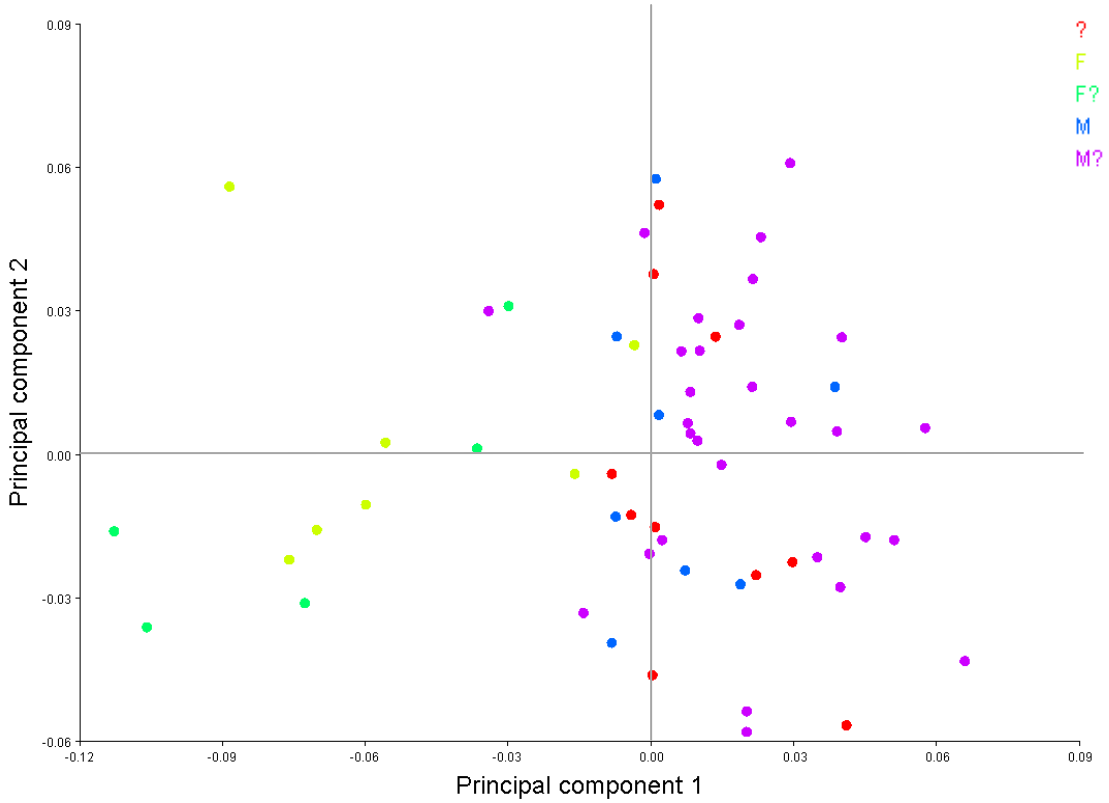

Figure 3.17: Distribution of specimens from the ilium-ischium dataset categorized by estimated sex, PC1 and PC2.

3.4.6. Ilium-pubis dataset

The shape variation expressed the ilium-pubis dataset is also similar to the patterns of shape illustrated by the whole bone data set. Hip bone height, width of the iliac blade, location of the anterior portion of the auricular surface, position of the iliac tubercle, pubic bone length, width of the symphyseal face, and the position of the arcurate eminence represent the patterns of variance contained in PC1 and PC2 of the ilium-pubis dataset (Figure 3.18). Refer to section 3.3.1 for a description of the pattern of shape variance in the ilium and the pubis seen on PC1 and PC2 of the whole bone dataset.

A slight difference in the pattern of shape between the two datasets is that the iliac tubercle is slightly more superiorly located along the PC2 axis of the ilium-pubis dataset.

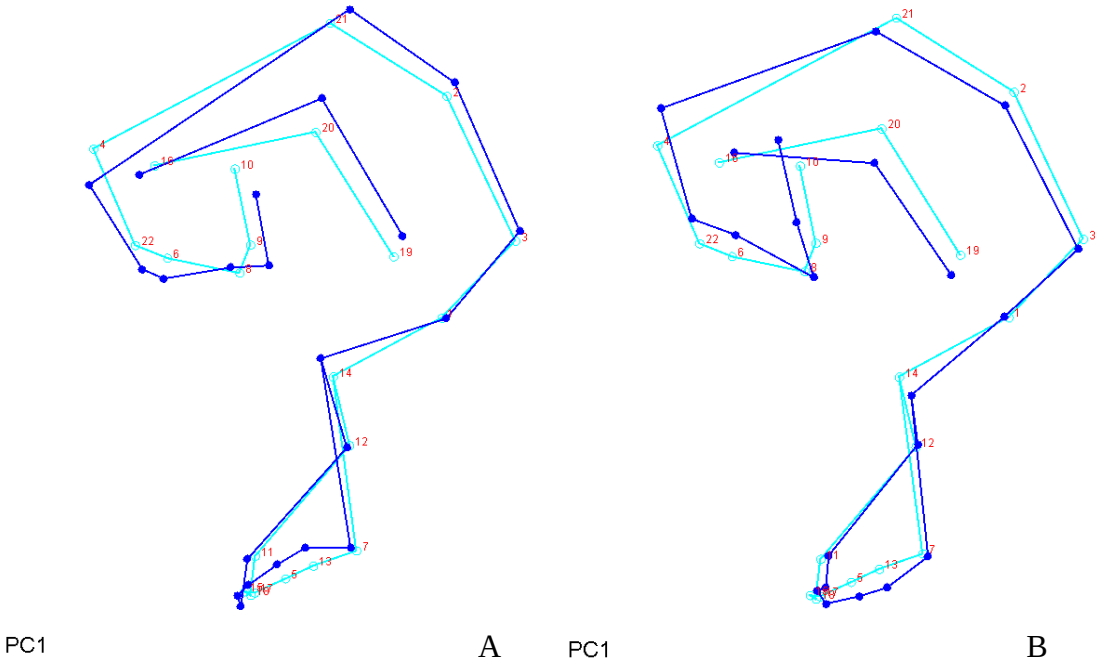

Figure 3.18: Wireframe graphs illustrating the shape changes on the PC1 axis of the ilium-pubis dataset. Dark blue lines represent shape change; light blue lines represent the mean shape. A: the shape at the positive end of the PC1 axis. B: the shape at the negative end of the PC1 axis.

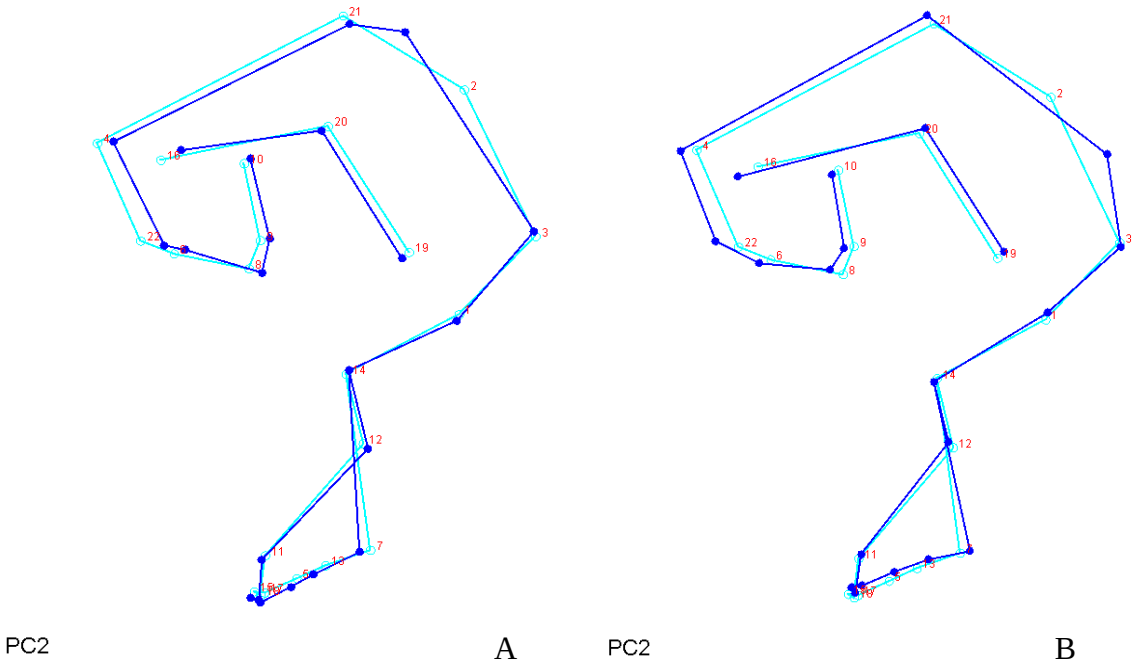

Figure 3.19: Wireframe graphs illustrating the shape changes on the PC2 axis of the ilium-pubis dataset. Dark blue lines represent shape change; light blue lines represent the mean shape. A: the shape at the positive end of the PC2 axis. B: the shape at the negative end of the PC2 axis.

The distribution of specimens on these PCs is presented in Figure 3.20 and is similar to the distributions of specimens of both the whole bone dataset and the ilium-ischium dataset. The area of overlap among all specimens is as large in the ilium-pubis dataset (-0.03 to 0.01) as it was in the ilium-ischium dataset. One specimen identified as female (UBC_15) lies toward the positive end of PC1 because of a superiorly positioned iliac tubercle and gluteal lines. The ilium-pubis dataset distinguishes between male and female shapes, but does not distinguish between males and possible male or female and possible female shapes.

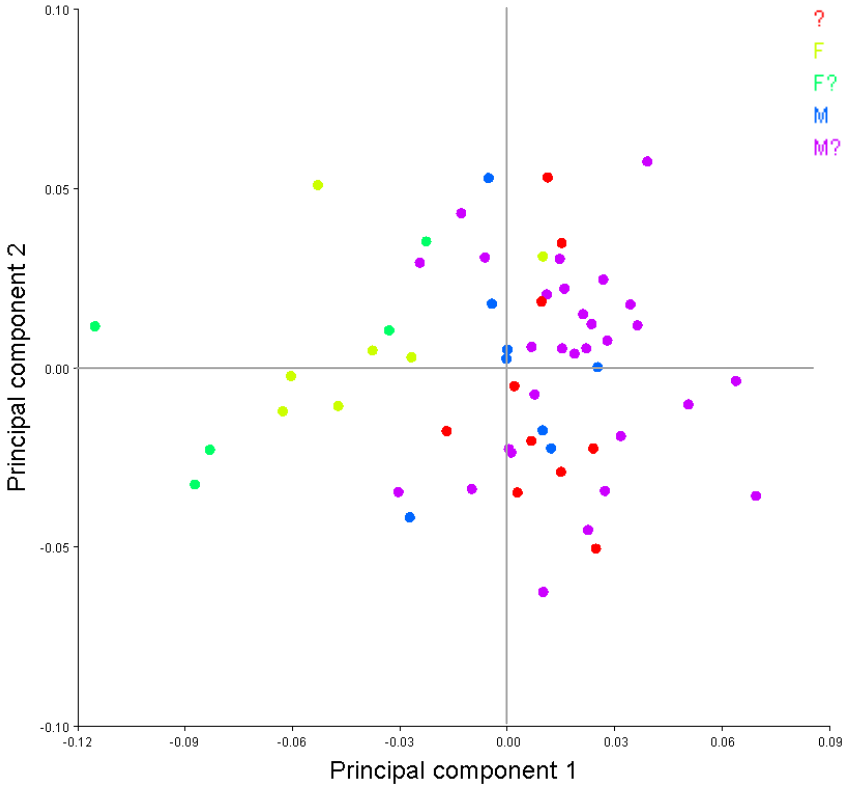

Figure 3.20: Distribution of specimens from the ilium-pubis dataset categorized by estimated sex. PC1 and PC2.

3.4.7. Ischium-pubis dataset

The pattern of variance contained in PC1 and PC2 of the ischium-pubis dataset is characterized by changes in the length of the pubic bone, the height and width of the ischial tuberosity, the position of the arcurate eminence, the orientation of the pubic tubercle, the height of the ischial spine, the location of most inferior point on the ischium, the position of the inferior points of the lunate surface, and the positions of the points on the obturator foramen rim. Relative to individuals with a positive PC1 score (Figure 3.21A), those at the negative end of the axis (Figure 3.21B) express a shortening of the pubic bone at the symphyseal face, a widening of the ischiopubic ramus in the inferior direction at the phallic ridge, the most inferior point of the ischium and the most posterior

point of the ischial tuberosity, and the most posterior portion of the ischial tuberosity. A superior anterior movement of the ischial spine persuading an anterior movement of posterior inferior point of the lunate surface, the most superior lateral point on the obturator foramen rim, the anterior inferior point of the lunate surface, and a superior anterior movement of the arcurate eminence. The differences between the shape patterns of this dataset and the whole bone dataset on PC1 is greater variation in the location of the most anterior inferior point on the lunate surface and a superior/inferior change in ischial spine position. The ends of the PC1 axis that contain the ischium-pubis shape differences are also opposite to those in the whole bone dataset.

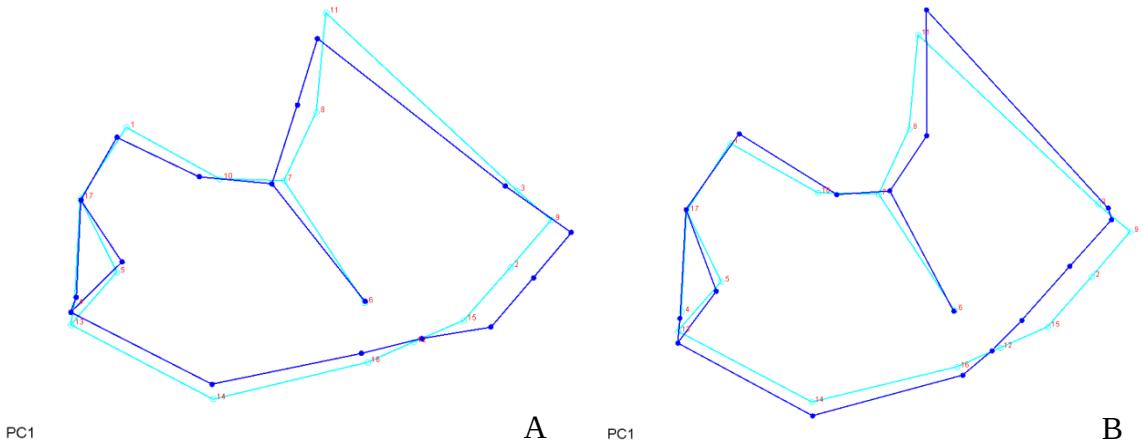

Figure 3.21: Wireframe graphs illustrating the shape changes on the PC1 axis of the ischium-pubis dataset. Dark blue lines represent shape change; light blue lines represent the mean shape. A: the shape at the positive end of the PC1 axis. B: the shape at the negative end of the PC1 axis.

The variation in the shape of the ischium-pubis dataset on the PC2 axis (Figure 3.22) is characterized by a lengthening and narrowing of the pubic bone at the symphyseal face, a posterior movement of the pubic tubercle, a superior posterior movement of the arcurate eminence, a shortening and widening of the ischial tuberosity, a superior anterior movement of the ischial spine and the most posterior inferior point on

the lunate surface, and a posterior movement of the most inferior medial point of the obturator foramen. Unlike on the PC1 axis, there is very little difference in the shape variation between the whole bone dataset and the ischium-pubis dataset.

When compared to the components of shape in the pubis dataset, PC1 of the ischium-pubis dataset comprised of shape variations from PC2 and PC3 of the pubis dataset. Principal component two of the ischium-pubis dataset comprised of shape variations from PC1 and PC2 of the pubis dataset.

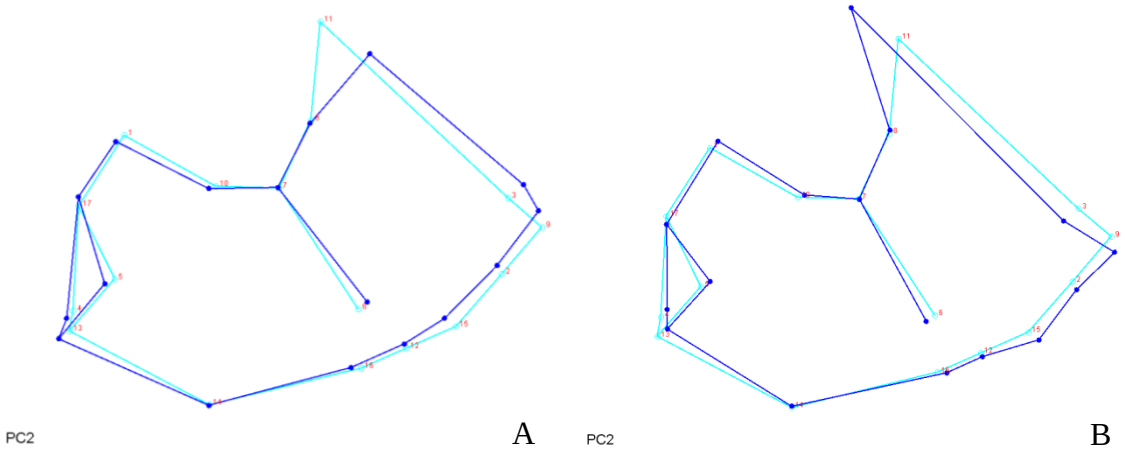

Figure 3.22: Wireframe graphs illustrating the shape changes on the PC2 axis of the ischium-pubis dataset. Dark blue lines represent shape change; light blue lines represent the mean shape. A: the shape at the positive end of the PC2 axis. B: the shape at the negative end of the PC2 axis.

The distribution of specimens on the PCs (Figure 3.23) separate males and females clearly with little overlap. The specimens categorized as female and possible female occupy the positive end of the PC1 axis, and the majority of specimens categorized as male, possible male, and indeterminate sex tend to occupy the negative end of the PC1 axis. Principal component two also largely distinguishes female (toward

the positive end) from possible female (toward the negative end), though with a few overlapping individuals.

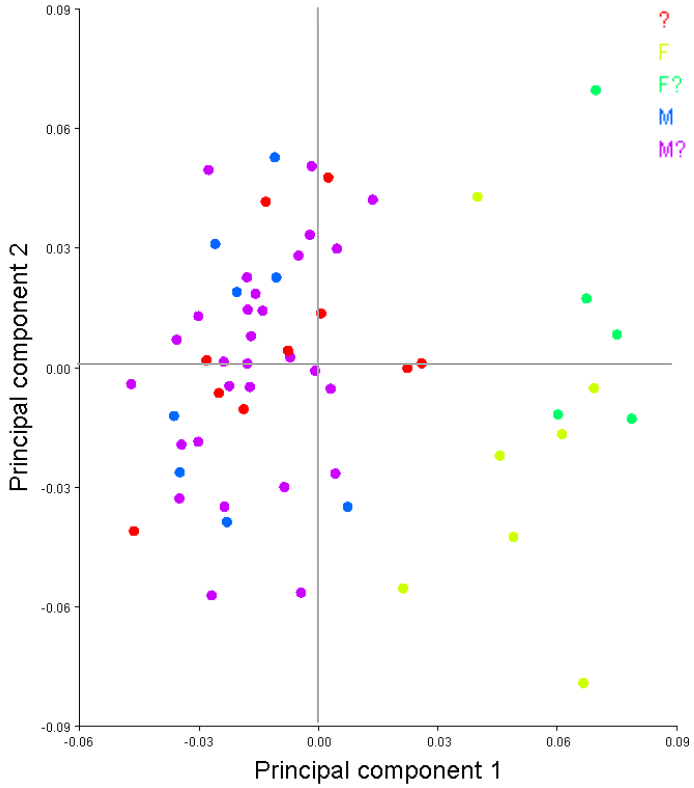

Figure 3.23: Distribution of specimens from the ischium-pubis dataset categorized by estimated sex, PC1 and PC2.

3.4.8. Summary of PCA results

The PCA results address the first research question regarding the aspects of hip bone shape that contribute the most to the categorization of sex. They also allude to the shape within portions of the hip bone that are strong indicators of sex. The isolated pubis and combined ischium-pubis datasets more clearly distinguish between specimens categorized as male and female and specifically between those specimens categorized as

female and possible female than the other datasets. Unfortunately, none of the datasets could distinguish between male and possible male hip bone shapes. The whole hip bone, isolated ilium, combined ilium-ischium, and combined ilium-pubis datasets performed moderately well at distinguishing between male and female sex categories with little to moderate overlap. The isolated ischium dataset did not perform well at distinguishing sex-based shapes among the specimens because it is more sexual dimorphic in size.

3.5. Spearman's Correlation

The Spearman's correlation (Table 3.5) examined the relationships between the components of hip bone shape and estimated sex categories, and between the components of shape and non-metric trait score (see Appendixes J-P for a complete list of PCs and their relationship with sex and non-metric trait morphology) in order to address the second research question. The correlation between components of shape and sex categories mirror the patterns distinguished in the principal component plots, emphasizing those components that differentiate to some degree the sex categories. Consequently, we can consider how the pattern of non-metric trait morphology contributes to the pattern of sex-based shape differences of each dataset of hip bone shape.

Table 3.6: Spearman correlation testing the significance of non-metric trait score and estimated sex on selected principal components. Italicised values indicate a significant correlation at a 0.05 alpha level. Bolded values indicate a significant correlation at a 0.01 alpha level.

Whole Bone Dataset						
PC[1]		Sex	VA[2]	SPC[3]	IPRR[4]	GSN[5]
1	r	**0.476**	*0.322*	**0.460**	*0.316*	**0.737**
	p-value	**0.000**	*0.013*	**0.000**	*0.015*	**0.000**
2	r	0.017	-0.058	0.031	0.045	-0.057
	p-value	0.900	0.662	0.817	0.733	0.668
Ilium Dataset						
PC		Sex	VA	SPC	IPRR	GSN
1	r	**-0.444**	*-0.319*	**-0.385**	*-0.330*	**-0.641**
	p-value	**0.000**	*0.014*	**0.003**	*0.011*	**0.000**
2	r	0.043	0.061	0.012	0.114	-0.074
	p-value	0.745	0.648	0.929	0.390	0.575
4	r	*0.301*	0.137	0.198	0.205	**0.340**
	p-value	*0.020*	0.300	0.132	0.120	**0.008**
Ischium Dataset						
PC		Sex	VA	SPC	IPRR	GSN
1	r	0.047	0.076	-0.052	0.013	0.015
	p-value	0.723	0.568	0.697	0.924	0.908
2	r	-0.009	0.034	-0.047	-0.053	*-0.285*
	p-value	0.948	0.801	0.721	0.692	*0.029*
Pubis Dataset						
PC		Sex	VA	SPC	IPRR	GSN
1	r	**-0.385**	-0.183	-0.204	-0.246	*-0.289*
	p-value	**0.003**	0.166	0.121	0.060	*0.026*
2	r	**0.415**	**0.472**	**0.498**	**0.367**	**0.389**
	p-value	**0.001**	**0.000**	**0.000**	**0.004**	**0.002**
3	r	**-0.369**	-0.112	-0.178	**-0.569**	**-0.407**
	p-value	**0.004**	0.398	0.176	**0.000**	**0.001**
Ilium-Ischium Dataset						
PC		Sex	VA	SPC	IPRR	GSN
1	r	**0.478**	*0.285*	**0.425**	**0.402**	**0.778**
	p-value	**0.000**	*0.028*	**0.001**	**0.002**	**0.000**
2	r	0.070	0.073	0.044	0.104	-0.077
	p-value	0.598	0.582	0.742	0.435	0.560
Ilium-Pubis Dataset						
PC		Sex	VA	SPC	IPRR	GSN
1	r	**0.413**	0.221	**0.447**	*0.310*	**0.673**
	p-value	**0.001**	0.092	**0.000**	*0.017*	**0.000**
2	r	-0.019	-0.026	-0.038	0.005	-0.149
	p-value	0.884	0.848	0.774	0.969	0.260
Ischium-Pubis Dataset						
PC		Sex	VA	SPC	IPRR	GSN
1	r	**-0.596**	**-0.439**	**-0.404**	**-0.534**	**-0.404**
	p-value	**0.000**	**0.001**	**0.002**	**0.000**	**0.002**
2	r	0.118	*0.291*	0.190	0.164	0.146
	p-value	0.372	*0.025*	0.150	0.215	0.270

1. PC= Principal Component; 2. VA=Ventral arc; 3. SPC=Subpubic contour;
4. IPRR=Ischiopubic ramus ridge; 5. GSN=Greater Sciatic Notch

The GSN is more consistently related to the pattern of sex-based shape in the hip bone because there are morphological shifts in the posterior portion of the ilium associated with GSN shape and a great distinction between male and female GSN morphologies. The components of hip bone shape incorporating the ilium illustrate that on PC1, which contains the highest r value and statistical significance for GSN scores, female hip bone shape is associated with a wide GSN include more superiorly positioned PSIS and PIIS, preauricular sulcus and the posterior gluteal line. The anterior portion of the auricular surface is more posterior with a wider GSN. Other, related changes in the ilium corresponding with a wider GSN are a more inferiorly positioned maximum arc of the iliac crest, iliac tubercle, ASIS, anterior gluteal line, and inferior gluteal line. A wide GSN is also associated with a more medially positioned arcurate eminence depicted in the shape components of the whole bone and the ilium-pubis datasets. The corresponding hip bone shape for a narrow GSN (male shape) would be opposite to the descriptions formerly given. In the whole bone and ilium-ischium datasets, a wide GSN is also associated with a more anteriorly positioned ischial spine and ischial tuberosity with a shorter ischial ramus. A shorter ischium ramus is also depicted in PC2 of the ischium dataset where the Pearson's correlation uncovered a relationship with GNS score.

Those PCs that display statistically significant relationships with sex also tend to show relationships with GSN, subpubic contour (SPC), ischiopubic ramus ridge (IPRR) and ventral arc (VA). The female hip bone shapes closely associated with a SPC and IPRR are a long pubic bone, a laterally positioned ischiopubic ramus and a laterally positioned phallic ridge demonstrated in the components of shape for the pubis and combined ischium-pubis. In PC3 of the pubis dataset IPRR was correlated with the shape

component and SPC was not. The ischiopubic ramus was lateral at the positive end of the PC3 axis of the pubis and medial at the negative end of the axis, which correlated with IPRR morphology. The phallic ridge, a landmark of SPC, was also lateral at the positive axis of PC3 and more medial at the negative axis of this shape component, which suggests the shape change in the phallic ridge should also have correlated with SPC. However, the length of the pubic bone was static in PC3 of the pubis dataset, which suggests that pubic bone length has more of an effect on SPC morphology than ischiopubic ramus and phallic ridge location. A long pubic bone was also associated with a more posteriorly positioned end point of the lunate surface and a shorter ischial ramus, evident in the shape components of the ischium-pubis dataset. The ventral arc is correlated to the shape components depicting a wide symphyseal face among male individuals and a narrow symphyseal face among female individuals, as seen in the ischium-pubis dataset.

The majority of the non-metric traits had significant relationships with hip bone shape variations that discriminate between males and females. The components of shape that differentiated females from possible females in the hip bone included a posteriorly and superiorly positioned arcurate eminence, a narrower pubic symphyseal face, a phallic ridge that extended laterally, and a more laterally situated ischiopubic ramus. Possible females possess the opposite orientation of these features. The non-metric traits that are associated with these differentiating components of shape are the greater sciatic notch, the ischiopubic ramus ridge, and the ventral arc.

3.6. Summary of Results

All of the hip bone configurations, except the ischium, contained shape variation that differentiated specimens into larger male and female estimated sex categories, however, there was a relationship between centroid size and isolated ischium. The majority of the non-metric traits are linearly correlated with high statistical significance with the components of shape that discriminate between males and females. The components of hip bone shape that distinguish males from females include a taller but narrower iliac blade, a shorter pubic bone with a broader pubic symphyseal face, a more posteriorly and medially positioned phallic ridge, and a more posteriorly oriented ischium. The components of shape that distinguished between female and possible female included a more medially positioned arcurate eminence, a narrower pubic symphyseal face, a more laterally oriented ischiopubic ramus, and a laterally oriented phallic ridge. The effect the pubis shape had on grouping female sex categories was strong enough to be seen when the pubis was combined with the ischium. These components of shape distinguish the sexes in whole and partial hip bone regions. The non-metric traits with the strongest relationship with sex were the greater sciatic notch, subpubic contour, ischiopubic ramus ridge, and the ventral arc. All of these non-metric traits also had strong and statistically significant linear relationships to the shape components of the pubis and ischium-pubis that distinguished between female and possible female sex.

Chapter 4 : Discussion

The research questions of this study addressed the shape differences that contribute to the categorization of sex, and the relationships between the components of hip bone shape and the ordinal traits used to estimate sex in whole and partial hip bone regions. The majority of the components of hip bone shape distinguished between males and females well. The shape components correlated, in ranked order, with the greater sciatic notch, the subpubic contour, the ischiopubic ramus ridge, and the ventral arc. When the hip bone is segmented into the various shapes, the isolated pubis and combined ischium-pubis generated the best grouping by sex. The shape differences that characterized male and female sex differences were the height and width of the iliac blade, the length and breadth of the pubic bone, and the orientation of the ischium. Pubic length and width, position of the arcurate eminence, ischiopubic ramus shape, and orientation of the phallic ridge were the shape components that distinguished between female and possible female specimens but not with males, possible males nor with individuals of indeterminate sex. All of the non-metric traits had significant correlations with the components of shape that distinguished female and possible female individuals. The region of hip bone that did not display sexual dimorphic properties in the hip bone was the shape of the ischium.

4.1. The Ischium

The ischium posed interesting results. According to the Procrustes ANOVA results, the shape of the ischium was not sexually dimorphic but size was. This is

consistent with the findings of Bilfeld and colleagues (2012) who found the ischium to be the least accurate (60%) in a geometric morphometric (GM) study of sexually dimorphic differences in the hip bone. This is also consistent with Coleman's (1969) findings, that no significant difference in the total amount of growth in the ischial tuberosity distinguished males and females. Coleman did note, however, that some females showed greater growth at the medial border of the ischium and greater growth at the inferior margin of the ischial tuberosity in some males.

This pattern of male and female difference in ischium growth, although not a significant component of sex differences, is demonstrable in the components of shape in the whole bone, the ilium-ischium, and the ischium-pubis. When the ischium is combined with other, more sexually dimorphic regions of the hip bone (the ilium and pubis), its sexually dimorphic properties emerge in the principal component analysis (PCA). Bilfeld and colleagues (2012) produced similar results, also using PCA, when the ischium was combined to ilium and pubis shape. Bytheway and Ross (2010) also noted considerable sexually dimorphic differences in the ischium in their study of sex differences in the whole hip bone using GM. When Bilfeld and colleagues combined the ilium and pubis with the ischium, the sex identifying power of the ilium (as the ilio-ischial complex) and the pubis (as the ischiopubic complex) improved by as much as 10% relative to the ilium and pubis alone. The PCA brings out the sexually dimorphic components of the ischium when combined with the respective ilium and pubis shapes, however, in the whole hip bone shape, sexually dimorphic components remain similar to that of the ilium-ischium shape and there is improvement in sex estimation (Bilfeld et al., 2012).

The sexually dimorphic shape qualities of the ischium, seen only in relationship with other more sexually dimorphic areas of the hip bone, is reminiscent of the technique used in ordinal and metric sex estimation methods where sex estimation outcomes can improve by combining many different sexually dimorphic traits or measurements in the analysis (Brůžek, 2002; Buikstra and Ubelaker, 1994; Rogers and Saunders, 1994). This phenomenon also contributes an understanding as to which sex traits are more reliable than others for improving sex estimation. The pubis is considered the most sexually dimorphic region of the hip bone, if not the entire skeleton (Bilfeld et al, 2012; Brůžek, 2002; González, et all, 2007; Phenice, 1969; Rogers and Saunders, 1994). However when the two great sex estimating regions, the ilium and the pubis, are combined as the ilium-pubis shape the separation in the specimen distribution graph do not group individuals by sex better than the ischium-pubis shape. This is also consistent with the specimen distribution graph Bilfeld and colleagues (2012). The ischiopubic complex of Bilfeld and colleagues' GM study separated males from females better than their iliopubic or ilio-ischial complex.

In Bilfeld and colleagues' (2012) study the ischiopubic complex correctly assigned sex in over 92% of cases, second only marginally to their "modified pubis" (the pubic bone and the ischiopubic ramus). The authors do not attempt to explain why the ischiopubic complex was more sexually dimorphic than the other complexes only that the ischium obstructed the sex estimating capacity of the pubis and that the other complexes "have not previously been described as sexually dimorphic" (2012:586). One possible reason why the ischiopubic complex in Bilfeld and colleagues' study and the ischium-pubis shape in this study are more sexually dimorphic than an ilium-pubis shape, could

be due to greater individual variability within GSN shape of the ilium that is confounding the distribution of shape by sex. Walker (2005) describes male GSN shape (scores 3, 4 and 5) as more variable in relation to female GSN shape (scores 1 and 2), because growth of the male hip bone is more variable among individuals. Contrarily, there is greater individual variability of female pubis shape (Arsuaga and Carretero, 1994). These two areas of the hip bone, the ilium and pubis, contain individualizing factors of the opposing sex, so instead of assisting the components of shape to identify sex based shape components, the regions are confounding sex based shape differences in the PCA. The shape of the ischium is less sexually dimorphic than the GSN so the sexual dimorphic components of the pubic bone outweigh the individualizing components of ischium shape, and consequently pulled the sexually dimorphic size components out of the ischium in the PCA.

4.2. The Ilium

Adolescent growth of the hip bone follows different trajectories between males and females, which produces the sexual dimorphic shape (Coleman, 1969). Coleman (1969) describes the growth pattern that produces characteristic male and female hip bone shapes. Iliac height, defined by Coleman as the position of the maximum arch of the iliac crest and ASIS, grows in a superior lateral direction. In males, the iliac crest grows laterally in early adolescence followed by strong growth superiorly (Coleman, 1969). In females, the iliac crest grows superiorly in early adolescence and continues in a lateral direction (Coleman, 1969). The position of the maximum arc of the iliac crest, the iliac tubercle, and the anterior superior iliac spine in the study sample reflects the sexually

dimorphic growth trajectories by being more superiorly positioned in males and more inferiorly positioned in females. Coleman (1969) also noted the PSIS grows in a more superior direction in females than in males creating the characteristic female shape in the posterior portion of the ilium.

The current study also demonstrated the components of sex-based shape in the ilium noted by Coleman (1969). A shorter and more posteriorly positioned maximum arc of the iliac spine, and a wider ilium at the anterior superior and posterior superior iliac spines characterizes females. The female ilium , which included females and possible females, also exhibits a more superiorly positioned AIIS and PIIS, a more posteriorly positioned anterior portion of the auricular surface, and a wide superior portion of the greater sciatic notch represented by the point of maximum curvature in the greater sciatic notch and the posterior inferior point of the preauricular sulcus. Males, possible males and indeterminate sex specimens tend to display more superior and anteriorly positioned maximum arc of the iliac crest and iliac tubercle, a more superiorly positioned inferior, anterior and posterior gluteal lines. The larger male group also exhibit a narrower ilium with more superiorly positioned anterior superior and PSIS, a more inferiorly positioned AIIS and PIIS, and a more anteriorly positioned anterior portion of the auricular surface. The shape representation of the auricular surface in this study is also similar to the dimorphic shapes of the auricular surface uncovered by Anastasiou and Chamberlain (2013) using GM.

Coleman (1969) observed in his study that the ischial spine, PIIS and the maximum curvature of the greater sciatic notch produce sexually dimorphic trends when these three landmarks are considered together and individualizing trends when these three

landmarks are considered separately. Coleman also states that in some cases the individual growth of the greater sciatic notch could produce a sciatic notch shape in males that is more like the female shape. In my study, the greater sciatic notch had a very significant relationship with sex. The components of shape of the greater sciatic notch (PIIS, the posterior inferior point of the preauricular sulcus, the point of maximum curvature in the greater sciatic notch, and the ischial spine) were part of the shapes that identified the specimens of indeterminate sex as part of the larger male group (of males and possible males), grouped the male and possible male specimens together, and grouped the female and possible female specimens well. Other studies also found significant sexual dimorphism in the GSN using GM by applying semi-landmarks a two-dimensional GSN shape and in three-dimensional analyses of the whole hip bone (Bilfeld et al., 2012; Bytheway and Ross, 2010; Gómez-Valdés et al., 2012; González et al., 2009) while others did not (Steyn et al., 2004). Older studies on GSN shape using ordinal methods (MacLaughlin and Bruce, 1986; Rogers and Saunders, 1994; Walker, 2005) have noted the individual variation in the shape of the GSN observed by Coleman (1969).

4.3. The Pubis

As the posterior portion of the hip bone moves superiorly, the pubis widens and lengthens (Coleman, 1969). The largest amount of growth measured in the pubis is at the inferior border of the pubic symphysis for both sexes, however, the superior border of the pubic symphysis had significant sexual differences according to Coleman (1969). Coleman describes more female growth at the superior pubic ramus, identified in this study sample by a more superiorly positioned arcurate eminence in females, and a wider

ischiopubic ramus in the inferior direction, and a longer pubic symphysis in males in the superior direction. In this and in other studies, female pubic bone shape is characterized by a long narrow pubic bone, a more laterally placed ischiopubic ramus, a more superiorly positioned anterior inferior point of the lunate surface, a more posteriorly and superiorly positioned arcurate eminence, and a pubic tubercle that is more lateral and inferiorly positioned (Anderson, 1990; Brůžek, 2002; Bytheway and Ross, 2010; Rogers and Saunders, 1994). Male pubic bone shapes are characterized by a shorter and wider pubic bone, and a more inferiorly positioned anterior inferior point of the lunate surface, a more anteriorly positioned arcurate eminence, and medially positioned pubic tubercle.

This, and other studies, show that female hip bone shape is more variable than male hip bone shape (Arsuaga and Carretero, 1994). The shape differences that group female specimens is a more superiorly positioned arcurate eminence, a more posteriorly positioned pubic tubercle, and a more laterally positioned ischiopubic ramus at the inferior point of the pubic symphysis. The shape differences that group the possible female specimens are a more inferiorly positioned arcurate eminence, a more anteriorly positioned pubic tubercle, and a more medially positioned ischiopubic ramus at the inferior point of the pubic symphysis. The pubic bone shape responsible for grouping possible female from female specimens are similar to the shape differences Sitek and colleagues (2012) found between female-to-male transsexuals (FtM) and the female control group. In their study, Sitek and colleagues found that FtM transsexuals differed from the female control group in the subpubic angle, the height of the pubic symphysis, and the breadth of the pubic symphysis. The differences in pubic bone shape between the female and possible female individuals for this study also involved the subpubic angle.

The possible female specimens had a more medially positioned ischiopubic ramus, which narrows the SPC. The pubic symphysis was longer in possible females, and the pubic tubercle was positioned superiorly and laterally, which could illustrate a wider pubic symphysis. The separation between female and possible female shape in the isolated pubic bone may suggest that there are more distinguishing features in the pubic bone, such as the position of the arcurate eminence, position of the ischiopubic ramus ridge and the projection of the pubic tubercle that contribute to female shape variation.

4.4. Non-Metric Traits and Hip Bone shape

The GSN and the SPC have the highest correlation to the components of shape that group males and females in the current study. This finding is consistent with Arsuaga and Carretero's (1994) study of hip bone morphology and multivariate analysis of an undocumented skeletal sample. The authors found that female hip bones varied in shape and non-metric trait scores associated with pelvic inlet size (a longer pubic bone, a more posteriorly positioned auricular surface, and SPC) and possessed a wider GSN. Although Arsuaga and Carretero did not perform a correlation of PCA and non-metric trait scores, their relationship is based on the multivariate analysis of measurements that captured these non-metric trait morphologies. Arsuaga and Carretero (1994) also found that the female hip bone is more variable in non-metric trait morphology than the male hip bone, which is what can be derived from the current study. Variability in the female pelvic inlet and outlet shape that incorporate the GSN, SPC and pubic bone length have also been detected in different populations (Kurki, 2013; Ridgeway et al., 2011). The likely explanation for population differences in obstetric capacity is adaptation to

extrinsic factors such as environment (Kurki, 2013). Other extrinsic factors such as nutritional availability and activity level are also possible contributors to shape variation, however, more research is needed in these fields to determine their direct influence on the female hip bone.

Another possible factor influencing female hip bone shape variation is individual rates of adolescent growth in females. The timing of growth that influence the shape of the GSN and the SPC in females occur very close together if not simultaneously (Coleman, 1969). The posterior portion of the ilium grows more superiorly while the pelvic outlet grows laterally to permit parity Coleman (1969). The IPRR, SPC, and VA are influenced by the trajectory and rate of growth on the pubis during adolescence. The variation in these trajectories and rates of growth could be influenced in part by genetic factors that control endocrine secretions that influence the duration and direction of hip bone growth, as seen in the hip bone shape among female to male transsexual (Blecher and Erickson, 2007; Sitek et al., 2012). Female to male transsexuals had significant differences in SPC shape, pubic bone shape, and ischium height compared to the female control group. As a result of possible differences in adolescent growth, the shape of the SPC, IPRR and VA distinguished female and possible female specimens in the current study.

Genetic control of the timing of endocrine secretions levels produced at puberty influence the length of time secondary sex characteristics have to form and the degree to which they form and could also have been a factor in the individualizing features of male hip bone shape in the current study (Coleman, 1969; Greulich and Thoms, 1944). Walker (2005) suggests that male greater sciatic notch is more variable in shape due to

individualizing levels of growth hormone secreted during adolescence and controlled by sex determining factors (Blecher and Erickson, 2007). Because males have a prolonged adolescent growth phase compared to females, there is a prolonged exposure of growth hormone in males, which results in larger body size, larger hip bone size compared to females (Coleman, 1969). However, a deficiency in growth hormone or other growth factors could influence the amount of hip bone growth achieved in males (Cameron, 1991).

Genetic factors that cause variations in the amount and duration of sex hormone exposure during adolescence should be taken into account along with extrinsic factors of shape variation when comparing skeletal sex between populations because differences in phenotypic expressions of skeletal sex could be reflecting factors such as nutritional access rather than population affinity (Vercellotti et al., 2011; Zakrzewski, 2003). Environmental factors that could influence amount and duration of sex hormone exposure, such as decreased nutritional content, suggests that modern populations would not necessarily be good proxies for developing sex estimation techniques that will be applied to past populations (MacLaughlin and Bruce, 1986; Pinhasi et al., 2005). To account for phenotypic differences in skeletal sex across time and between individuals brought on by genetic or environmental influences, ranges in sex estimation should be used in order to capture the greatest amount of shape variation in the hip bone.

Chapter 5 : Conclusions and Future Research

The general pattern discerned from the geometric morphometric analysis of the hip bone is that the pubic region and combined ischium-pubis shape contain the most shape variation that discriminates males from females, and females from possible females. The non-metric traits that respond to the shape differences in the pubic bone and the combined ischium-pubis are the subpubic contour, ischiopubic ramus ridge and ventral arc. The greater sciatic notch shape also contributed to grouping sex into males, females and possible females because it is more discriminating toward the female shape then toward the male shape. The PCA discerned the sexually dimorphic size variation in the ischium from the individualizing shape morphology when combined with the pubis. The sexually dimorphic components of shape changed very little among the isolated ilium, the combined ilium-ischium, the combined ilium-pubis, and the whole hip bone. The greater sciatic notch and subpubic contour are highly correlated with classifying individuals into males and females because the shape of these non-metric traits is the result of the dimorphic requirement of the female pelvis of parturition.

The patterns of sex-based shape uncovered by this research have illuminated an interesting perspective on the theory sex categorization in the future. Sex does not need to be divorced from biology in order to demonstrate its dynamic properties. The hip bone has been subjected to changes due to evolutionary adaptation and is currently being subjected to intrinsic and extrinsic forces that influence its shape. The current study also alludes to the possible benefits of categorizing sex on a five-point scale for the purposes of capturing morphological variation not just between the sexes but also within sex.

Geometric morphometrics can be used to further the debate in favour of categorizing skeletal sex on a scale of morphological variation.

Geometric morphometrics also has the potential to be useful in developing standardized sex estimation technique based on three-dimensional models of whole or fragmented hip bones to advance the current ordinal method of sex estimation in the greater sciatic notch, ischiopubic ramus ridge, subpubic contour and ventral arc. Understanding the components of shape among these non-metric traits that discriminate males from possible males could add valuable insight into how these sex traits relate to sexual dimorphism.

Authors who have proposed new techniques in sex estimation stress the importance of accounting for population affinity as a variable in sex estimation (MacLaughlin and Bruce, 1986; Rosenberg, 2002; Washburn 1948). However, I believe that creating a universal model of sex categorization that focuses on capturing all possible morphological variation displayed by population groups could not only benefit studies of skeletal sex between populations, but also studies of skeletal sex in which population affinity is unknown or is not contemporary with modern populations or populations of the recent past. Forensic analysis, archaeological excavations, and paleoanthropological studies all come into contact with human hip bones of unknown population affinity and require a confident and reliable method of sex estimation. Therefore, it is very important to develop a reliable, reproducible, and universal method of estimating sex along a scale of morphological differences to document, interpret, and compare skeletons.

References Cited

Adams DC, Rohlf FJ, Slice DE. 2004. Geometric morphometrics: ten years of progress following the 'revolution'. Ital J Zool. 71:5-16.

Agarwal SC. 2012. The past of sex, gender, and health: bioarchaeology of the aging skeleton. American Anthropologist 114(2):322-335.

Albanese J. 2003. A metric method for sex determination using the hipbone and the femur. J Forensic Sci. 48(2):1-11.

Anastasiou E, Chamberlain AT. 2013. The sexual dimorphism of the sacro-iliac joint: an investigation using geometric morphometric techniques. J Forensic Sci. 58(S1):S126-S134.

Anderson BE. 1990. Ventral arc of the os pubis: anatomical and developmental considerations. American Journal of Physical Anthropology. 83: 449-458.

Arnqvist G, Mårtesson T. 1998. Measurement error in geometric morphometrics: empirical strategies to assess and reduce its impact on measures of shape. Acta Zoological Academiae Scientiarum Hungaricae. 44(1-2):73-96.

Arsuaga JL, Carretero JM. 1994. Multivariate analysis of the sexual dimorphism of the hip bone in a modern human population and in early hominids. American Journal of Physical Anthropology. 93:241-257.

Arun M, Nagesh RK, Kumar P. 2012. Estimation of sex from fragments of os coxa by metric analysis. Australian Journal of Forensic Sciences. 44(2):145-153.

Baab KL, McNulty KP, Rohlf FJ. 2012. The shape of human evolution: a geometric morphometric perspective. Evolutionary Anthropology. 21:151-165.

Badyaev AV. 2002. Growing apart: an ontogenetic perspective on the evolution of sexual size dimorphism. Trends in Ecology and Evolution. 17(8):369-378.

Betti L, von Cramon-Taubadel N, Manica A, Lycett SJ. 2013. Global geometric morphometric analyses of the human pelvis reveal substantial neutral population history effects, even across sexes. PLoS One. 8(2):1-10.

Bigoni L, Velemínská J, Brůžek J. 2010. Three-dimensional geometric morphometric analysis of cranio-facial sexual dimorphism in a Central European sample of known sex. HOMO Journal of Comparative Human Biology. 61:16-32.

Bilfeld MF, Dedouit F, Rousseau H, Sans N, Braga J, Rougé D, Telmon N. 2012. Human coxal bone sexual dimorphism and multislice computed tomography: geometric morphometric analysis of 65 adults. J Forensic Sci. 57(3): 578-588.

Biwasaka H, Aoki Y, Sato K, Tanijiri T, Fujita S, Dewa K, Yoshioka K, Tomabechi M. 2012. Analyses of sexual dimorphism of reconstructive pelvic computed tomography images of contemporary Japanese using curvature of the greater sciatic notch, pubic arch and greater pelvis. Forensic Science International. 219:288e1-288e8.

Blackith RE, Reyment RA. 1971. Multivariate Morphometrics. New York: Academic Press.

Blackless M, Charuvastra A, Derryck A, Fausto-Sterling A, Lauzanne K, Lee E. 2000. How sexually dimorphic are we? Review and synthesis. American Journal of Human Biology. 12:151-166.

Blecher SR, Erickson RP. 2007. Genetics of sexual development: a new paradigm. American Journal of Medical Genetics Part A. 143A: 3054-3068.

Bookstein FL. 1991. Morphometric Tools for Landmark Data, Geometry and Biology. New York: Cambridge University Press.

Brown KA. 1998. Gender and sex: distinguishing the difference with ancient DNA. In: Whitehouse RD, editor. Gender and Italian Archaeology: Challenging the Stereotypes. London: Accordia. pp 35-44.

Bruner E. 2004. Geometric morphometrics and paleoneurology: brain shape evolution in the genus *Homo*. Journal of Human Evolution. 47:279-303.

Brůžek J. 2002. A method for visual determination of sex, using the human hip bone. American Journal of Physical Anthropology. 117:157-168.

Buikstra J, Ubelaker D. 1994. Standards for Data Collection from Human Skeletal Remains. Research Series 44. Fayetteville: Arkansas Archaeological Survey.

Butler J. 1993. Bodies That Matter: On the Discursive Limits of "Sex." New York: Routledge.

Byers SN. 2002. Introduction to Forensic Anthropology: A Textbook. Toronto: Allyn and Bacon.

Bytheway JA, Ross AH. 2010. A geometric morphometric approach to sex determination of the human adult os coxa. J Forensic Sci. 55(4):859-864.

Cameron N. 1991. Human growth, nutrition, and health status in sub-Saharan Africa. Yearbook of Physical Anthropology. 34:211-250.

Coleman WH. 1969. Sex differences in the growth of the human bony pelvis. American Journal of Physical Anthropology. 31:125-152.

Corner BD, Lele S, Richtsmeier JT. 1992. Measuring precision of three-dimensional landmark data. Journal of Quantitative Anthropology. 3: 347-359.

Cox M, Mays S. 2000. Human Osteology in Archaeology and Forensic Science. New York: Cambridge University Press.

Đurić M, Rakočević Z, Đonić D. 2005. The reliability of sex determination of skeletons from forensic context in the Balkans. Forensic Science International. 147:159-164.

Fausto-Sterling A. 2000. Sexing the Body: Gender Politics and the Construction of Sexuality. New York: Basic Books.

Geller PL. 2005. Skeletal analysis and theoretical complications. World Archaeology 37(4):597-609.

Gilchrist R. 1999. Gender and Archaeology: Contesting the Past. New York: Routledge.

Gluckman PD, Hanson MA. 2006. Evolution, development and timing of puberty. Trends in Endocrinology and Metabolism. 17(1): 7-12.

Gómez-Valdés JA, Quinto-Sánchez M, Garmendia AM, Veleminska J, Sánchez-Mejorada G, Brůžek J. 2012. Comparison of methods to determine sex by evaluating the greater sciatic notch: visual, angular and geometric morphometrics. Forensic Science International. 221:156.e1-156.e7.

González PN, Bernal V, Perez SI. 2009. Geometric morphometric approach to sex estimation of human pelvis. Forensic Science International. 189:68-74.

González PN, Bernal V, Perez SI. 2011. Analysis of sexual dimorphism of craniofacial traits using geometric morphometric techniques. International Journal of Osteoarchaeology. 21:82-91.

Grabowski MW, Polk JD, Roseman CC. 2011. Divergent patterns of integration and reduced constraint in the human hip and the origins of bipedalism. Evolution. 65(5):1336-1356.

Greulich WW, Thoms H. 1944. The growth and development of the pelvis of individual girls before, during, and after puberty. Yale Journal of Biology and Medicine. 17(1):91-105.

Gustafsson A, Lindenfors P. 2004. Human size evolution: no evolutionary allometric relationship between male and female stature. Journal of Human Evolution. 47:253-266.

Hager LD. 1996. Sex differences in the sciatic notch of great apes and modern humans. American Journal of Physical Anthropology. 99:287-300.

Hallgrimsson B, Zelditch ML, Parsons TE, Kristensen E, Young NM, Boyd SK. 2008. Morphometrics and biological anthropology in the postgenomic age. In: Katzenberg MA and Saunders SR, editors. Biological Anthropology of the Human Skeleton, second edition. New Jersey: Wiley-Liss. pp 207-236.

Hollimon SE. 2011. Sex and gender in bioarchaeological research: theory, method, and interpretation. In: Agarwal SC and Glencross BA editors. Social bioarchaeology. Malden: Wiley-Blackwell. pp 149-182.

Iguchi T, Fukazawa Y, Bern HA. 1995. Effects of sex hormones on oncogene expression in the vagina and on development of sexual dimorphism of the pelvis and anococcygeus muscle in the mouse. Environmental Health Perspectives. 103(7):79-82.

Institute for Data Analysis and Visualization. 2007. User Guide 3.6. Davis: IDAV, University of California.

Jolliffe IT. 1986. Principal Component Analysis. New York: Springer-Verlag.

Kimmerle EH, Ross A, Slice D. 2008. Sexual dimorphism in America: geometric morphometric analysis of the craniofacial region. J Forensic Sci. 53(1):54-57.

Kjellström A. 2004. Evaluations of sex assessment using weighted traits on incomplete skeletal remains. Int J Osteoarchaeol. 14: 360-373.

Klales AR, Ousley SD, Vollner JM. 2012. A revised method of sexing the human innominate using Phenice's nonmetric traits and statistical method. American Journal of Physical Anthropology. 149:104-114.

Klingenberg CP. 2011. MorphoJ: an integrated software package for geometric morphometrics. Molecular Ecology Resources. 11:353-357.

Klingenberg CP, Barluenga M, Meyer A. 2002. Shape analysis of symmetric structures: quantifying variation among individuals and asymmetry. Evolution. 56(10):1909-1920.

Klingenberg CP, McIntyre GS. 1998. Geometric morphometrics of developmental instability: analyzing patterns of fluctuating asymmetry with Procrustes methods. Evolution. 52(5):1363-1375.

Kurki HK. 2007. Protection of obstetric dimensions in a small-bodied human sample. American Journal of Physical Anthropology. 133:1152-1165.

Kurki HK. 2011. Pelvic dimorphism in relation to body size and body size dimorphism in humans. Journal of Human Evolution. 61:631-643.

Kurki HK. 2013. Bony pelvic canal size and shape in relation to body proportionality in humans. American Journal of Physical Anthropology. 151:88-101.

Lewis ME. The Bioarchaeology of Children: Perspectives from Biological and Forensic Anthropology. New York: Cambridge University Press.

Listi GA. 2010. The impact of racial metric variation in the os coxae on the morphological assessment of sex. J Forensic Sci. 55(5):1157-1161.

Lovejoy CO. 2005. The natural history of human gait and posture: part 1 spine and pelvis. Gait and Posture. 21:95-112.

Lorber J. 1996. Beyond the binaries: depolarizing the categories of sex, sexuality, and gender. Sociological Inquiry. 66(2): 143-159.

Lorentz K. From bodies to bones and back: theory and human bioarchaeology. In: Schutkowski H, editor. Between Biology and Culture. New York: Cambridge University Press. pp 273-303.

Luo YC. 1995. Sex determination from the pubis by discriminant function analysis. Forensic Science International. 74:89-98.

Lycett SJ, von Cramon-Taubadel N. 2013. Understanding the comparative catarrhine context of human pelvic form: a 3D geometric morphometric analysis. Journal of Human Evolution 64:300-310.

MacLaughlin SM, Bruce MF. 1986. Population variation in sexual dimorphism in the human innominate. Human Evolution. 1(3):221-231.

Manzi G, Saracino B, Bruner E, Passarello P. 2000. Geometric morphometric analysis of mid-sagittal cranial profiles in Neandertals, modern humans and their ancestors. Rivista di Anthropologia. 78:193-204.

Mays S. 2010. The archaeology of human bones: second edition. New York: Routledge.

Mitteroecker P, Gunz P. 2009. Advances in geometric morphometrics. Evol Biol. 36:235-247.

Milne N. 1990. Sexing of human hip bones. J Anat. 172:221-226.

Nettle D. 2002a. Height and reproductive success in a cohort of British men. Human Nature. 13(4):473-491.

Nettle D. 2002b. Women's height, reproductive success and the evolution of sexual dimorphism in modern humans. Proc R Soc Lond. 269:1919-1923.

NextEngine, Inc. (US). NextEngine [Internet]. Santa Monica: NextEngine, Inc. [cited 2013 February 15]. Available from: http://www.nextengine.com/products/scanner/specs.

Nordbladh J, Yates T. 1990. This perfect body, this virgin text: between sex and gender in archaeology. In: Bapty I and Yates T, editors. Archaeology After Structuralism. New York: Routledge. pp 222-237.

Patriquin ML, Loth SR, Steyn M. 2003. Sexually dimorphic pelvic morphology in South African whites and blacks. Homo. 53(3):255-262.

Patriquin ML, Steyn M, Loth SR. 2005. Metric analysis of sex differences in South African black and white pelves. Forensic Science International. 147:119-127.

Phenice T. 1969. A newly developed visual method of sexing in the os pubis. American Journal of Physical Anthropology. 30:297-301.

Pinhasi R, Teschler-Nicola M, Knaus A, Shaw P. 2005. Cross-population analysis of the growth of long bones and the os coxae of three early medieval Austrian populations. American Journal of Human Biology. 17: 470-488.

Plavcan JM. 2011. Understanding dimorphism as a function of changes in male and female traits. Evolutionary Anthropology. 20:143-155.

Pretorius E, Steyn M, Scholtz Y. 2006. Investigation into the usability of geometric morphometric analysis in assessment of sexual dimorphism. American Journal of Physical Anthropology. 129:64-70.

Richtsmeier JT, Deleon, VB, Lele SR. 2002. The promise of geometric morphometrics. Yearbook of Physical Anthropology. 45:63-91.

Ridgeway R, Arias BE, Barber MD. 2011. The relationship between anthropometric measurements and the bony pelvis in African American and European American women. Int Urogynecol J. 22:1019-1024.

Rogers T, Saunders S. 1994. Accuracy of sex determination using morphological traits of the human pelvis. J Forensic Sci. 39(4):1047-1056.

Rosas A, Bastir M. 2002. Thin-plate spline analysis of allometry and sexual dimorphism in the human craniofacial complex. American Journal of Physical Anthropology. 117:236-245.

Rosenberg K. 2002. A late Pleistocene human skeleton from Liujiang, China suggests regional population variation in sexual dimorphism in the human pelvis. Variability and Evolution. 10:5-17.

Ruff C. 1991. Climate and body shape in hominid evolution. Journal of Human Evolution. 21: 81-105.

Ruff C. 2002. Variation in human body size and shape. Annu Rev Anthropol. 31:211-232.

Scheuer L, Black S. 2000. Developmental Juvenile Osteology. San Francisco: Elsevier Academic Press.

Schutz H, Donovan ER, Hayes JP. 2009. Effects of parity on pelvic size and shape dimorphism in *Mus*. Journal of Morphology. 270:834-842.

Šedý J, Naňka O, Špačkavá J, Jarolím L. 2008. Clinical implications of a close vicinity of nervus dorsalis penis/clitoridis and os pubis. J Sex Med. 5:1572-1581.

Sholts SB, Flores L, Walker PL, Wärmländer SKTS. 2011. Comparison of coordinate measurement precision of different landmark types on human crania using a 3D laser scanner and a 3D digitizer: implications for applications of digital morphometrics. International Journal of Osteoarchaeology. 21:535-543.

Sibley LM, Armelagos GJ, van Gerven DP. 1992. Obstetric dimensions of the true pelvis in a medieval population from Sudanese Nubia. American Journal of Physical Anthropology. 89:421-430.

Singh S, Potturi BR. 1978. Greater sciatic notch in sex determination. J Anat. 125(3): 619-624.

Sitek A, Fijałkawska M, Żądzińska E, Antoszewski B. 2012. Biometric characteristics of the pelvis in female-to-male transsexuals. Arch Sex Behav. 41:1303-1313.

Slice DE. 2005. Modern Morphometrics in Physical Anthropology. New York: Kluwer Academic/Plenum Publishers.

Slice DE. 2007. Geometric morphometrics. Annu Rev Anthropol. 36:261-281.

Sofaer JR. 2006. The Body as Material Culture: A Theoretical Osteoarchaeology. New York: Cambridge University Press.

Sørensen MLS. 2000. Gender Archaeology. Cambridge: Polity Press.

SPSS Inc. 2008. SPSS Statistics for Windows, Version 17.0. Chicago: SPSS Inc.

Stone AC. 2008. DNA analysis of archaeological remains. In: Katzenberg MA and Saunders SR, editors. Biological Anthropology of the Human Skeleton. New Jersey: Wiley-Liss. pp 461-483.

Tague RG. 2000. Do bid females have big pelves? American Journal of Physical Anthropology. 112:377-393.

Tague RG. 2005. Big-bodied males help us to recognize that females have big pelves. American Journal of Physical Anthropology. 1127:392-405.

Ubelaker D. 2008. Forensic anthropology: method and diversity of applications. In: Katzenberg MA and Saunders SR, editors. Biological Anthropology of the Human Skeleton. New Jersey: Wiley-Liss. pp 41-69.

Uesugi Y, Taguchi O, Noumura T, Iguchi T. 1992. Effects of sex steroids on the development of sexual dimorphism in mouse innominate bone. Anat Rec. 234(4):541-548.

Vercellotti G, Stout SD, Boano R, Sciulli PW. 2011. Intrapopulation variation in stature and body proportions: social status and sex differences in an Italian medieval population (Trino Vercellese, VC). American Journal of Physical Anthropology. 145: 203-214.

Viðarsdóttir US, O'Higgins P, Stringer C. 2002. A geometric morphometric study of regional differences in the ontogeny of the modern human facial skeleton. J Anat. 201:211-229.

von Cramon-Taubadel N, Frazier BC, Mirazón Lahr M. 2007. The problem of assessing landmark error in geometric morphometrics: theory, methods, and modifications. American Journal of Physical Anthropology. 13:24-35

Walker PL. 2005. Greater sciatic notch morphology: sex, age, and population differences. American Journal of Physical Anthropology. 127:385-301.

Washburn SL. 1948. Sex differences in the pubic bone. American Journal of Physical Anthropology. 6(2):199-207.

White TD. 2000. Human Osteology. Second edition. San Diego: Academic Press.

Wilson JD, George FW, Griffin JE. 1981. The hormonal control of sexual development. Science. 211:1278-1284.

Wilson LAB, Cardoso HFV, Humphrey LT. 2011. On the reliability of a geometric morphometric approach to sex determination: a blind test of six criteria of the juvenile ilium. Forensic Science International. 206:35-42.

Zakrzewski SR. 2003. Variation in ancient Egyptian stature and body proportions. American Journal of Physical Anthropology. 121:219-229.

Zelditch ML, Swiderski DL, Sheets HD, Fink WL. 2004. Geometric Morphometrics for Biologists: A Primer. San Francisco: Elsevier Academic Press.

Zeng Y, Wang Y, Zhu Z, Tang T, Dai K, Qiu S. 2012. Differences in acetabular morphology related to side and sex in a Chinese population. J Anat. 220:256-262.

Appendix A:
Specimens and non-metric trait evaluation, raw data

ID	Ventral Arc	Subpubic Contour	Ischiopubic Ramus Ridge	Greater Sciatic Notch	Mean Score	Estimated Sex
UBC_01	4	4	2	4	3.5	M?
UBC_02	4	4	4	4	4	M?
UBC_03	4	4	3	5	4	M?
UBC_04	3	3	5	5	4	M
UBC_05	4	2	3	3	3	?
UBC_06	4	3	3	4	3.5	M?
UBC_07	4	4	3	5	4	M?
UBC_08	4	2	3	4	3.25	M?
UBC_09	3	2	3	4	3	?
UBC_10	4	3	3	4	3.5	M?
UBC_11	4	3	4	5	4	M?
UBC_12	4	3	4	5	4	M?
UBC_13	3	3	5	5	4	M?
UBC_14	1	1	1	2	1.25	F
UBC_15	1	1	2	2	1.5	F
UBC_16	2	2	1	1	1.5	F
UBC_17	1	1	1	2	1.25	F
UBC_18	5	5	4	5	4.75	M
UBC_19	5	3	4	4	4	M?
UBC_20	4	3	4	3	3.5	M?
UBC_21	5	3	3	5	4	M?
UBC_22	3	3	3	5	3.5	?
UBC_23	5	4	3	5	4.25	M
UBC_24	4	3	4	5	4	M?
UBC_25	4	3	3	5	3.75	?
UBC_26	2	2	2	1	1.75	F?
UBC_27	4	3	4	5	4	M?
UBC_28	1	1	3	3	2	F?
UBC_29	4	2	2	2	2.5	F?
UBC_30	3	3	5	5	4	M?
UBC_31	4	5	5	4	4.5	M
UBC_32	4	3	4	5	4	M?
UBC_33	4	5	5	4	4.5	M
UBC_34	3	2	3	3	2.75	?
UBC_35	4	2	2	4	3	?
UBC_36	2	1	2	2	1.75	F?
UBC_37	2	1	2	1	1.5	F

UBC_38	1	1	2	2	1.5	F
UBC_39	5	4	2	4	3.75	M?
UBC_40	5	4	3	5	4.25	M
UBC_41	4	4	3	5	4	M?
UBC_42	5	4	3	3	3.75	?
UBC_43	4	3	3	5	3.75	?
UBC_44	4	3	2	4	3.25	M?
UBC_45	5	4	4	4	4.25	M?
UBC_46	4	4	1	5	3.5	M?
UBC_47	3	2	3	5	3.25	?
UBC_48	3	3	3	2	2.75	?
UBC_49	5	2	3	5	3.75	M
UBC_50	3	4	4	5	4	M?
UBC_51	4	4	4	4	4	M?
UBC_52	5	5	5	5	5	M
UBC_53	1	1	2	1	1.25	F
UBC_54	4	2	2	3	2.75	F?
UBC_55	4	5	3	4	4	M?
UBC_56	4	3	2	5	3.5	M?
UBC_57	5	2	4	5	4	M
UBC_58	4	3	3	4	3.5	M?
UBC_59	4	3	4	5	4	M?

Appendix B:
Principal Component Analysis, Whole bone, Procrustes Coordinates

PC	Eigenvalues	Variance%	Cum.%
1.	0.00119538	18.242	18.242
2.	0.00067649	10.324	28.566
3.	0.00045841	6.996	35.561
4.	0.00042411	6.472	42.033
5.	0.00036554	5.578	47.612
6.	0.00034131	5.209	52.820
7.	0.00026103	3.983	56.804
8.	0.00024570	3.749	60.553
9.	0.00022186	3.386	63.939
10.	0.00019182	2.927	66.866
11.	0.00017106	2.610	69.477
12.	0.00016732	2.553	72.030
13.	0.00016193	2.471	74.501
14.	0.00013819	2.109	76.610
15.	0.00012966	1.979	78.589
16.	0.00012124	1.850	80.439
17.	0.00011649	1.778	82.217
18.	0.00010161	1.551	83.767
19.	0.00009472	1.445	85.213
20.	0.00008410	1.283	86.496
21.	0.00007565	1.154	87.650
22.	0.00007430	1.134	88.784
23.	0.00006315	0.964	89.748
24.	0.00005724	0.874	90.621
25.	0.00005292	0.808	91.429
26.	0.00005054	0.771	92.200
27.	0.00004641	0.708	92.909
28.	0.00004357	0.665	93.574
29.	0.00003796	0.579	94.153
30.	0.00003687	0.563	94.716
31.	0.00003083	0.471	95.186
32.	0.00003036	0.463	95.649
33.	0.00002549	0.389	96.038
34.	0.00002472	0.377	96.416
35.	0.00002360	0.360	96.776
36.	0.00002130	0.325	97.101
37.	0.00001976	0.301	97.402
38.	0.00001872	0.286	97.688
39.	0.00001778	0.271	97.960
40.	0.00001731	0.264	98.224
41.	0.00001408	0.215	98.439
42.	0.00001277	0.195	98.633
43.	0.00001215	0.185	98.819
44.	0.00001128	0.172	98.991
45.	0.00000920	0.140	99.131
46.	0.00000898	0.137	99.268
47.	0.00000841	0.128	99.397
48.	0.00000668	0.102	99.499
49.	0.00000554	0.084	99.583
50.	0.00000527	0.080	99.663
51.	0.00000435	0.066	99.730
52.	0.00000396	0.060	99.790
53.	0.00000330	0.050	99.841
54.	0.00000323	0.049	99.890
55.	0.00000264	0.040	99.930
56.	0.00000233	0.036	99.966
57.	0.00000115	0.018	99.983
58.	0.00000109	0.017	100.000

Total variance: 0.006552

Appendix C:
Principal Component Analysis, Ilium, Procrustes Coordinates

PC	Eigenvalues	Variance%	Cum.%
1.	0.00246940	19.586	19.586
2.	0.00202051	16.026	35.612
3.	0.00116989	9.279	44.891
4.	0.00107094	8.494	53.385
5.	0.00090482	7.177	60.562
6.	0.00064750	5.136	65.697
7.	0.00053950	4.279	69.977
8.	0.00047998	3.807	73.784
9.	0.00043804	3.474	77.258
10.	0.00039358	3.122	80.380
11.	0.00035505	2.816	83.196
12.	0.00034273	2.718	85.914
13.	0.00026307	2.087	88.001
14.	0.00024245	1.923	89.924
15.	0.00018261	1.448	91.372
16.	0.00017016	1.350	92.722
17.	0.00015105	1.198	93.920
18.	0.00012257	0.972	94.892
19.	0.00011475	0.910	95.802
20.	0.00009500	0.753	96.556
21.	0.00008577	0.680	97.236
22.	0.00007050	0.559	97.795
23.	0.00006292	0.499	98.294
24.	0.00004772	0.378	98.673
25.	0.00004103	0.325	98.998
26.	0.00003228	0.256	99.254
27.	0.00002687	0.213	99.467
28.	0.00001879	0.149	99.616
29.	0.00001653	0.131	99.747
30.	0.00001339	0.106	99.854
31.	0.00001035	0.082	99.936
32.	0.00000810	0.064	100.000

Total variance: 0.01260787

Appendix D:
Principal Component Analysis, Ischium, Procrustes Coordinates

PC	Eigenvalues	Variance%	Cum.%
1.	0.00200048	16.653	16.653
2.	0.00189327	15.761	32.413
3.	0.00147900	12.312	44.725
4.	0.00129765	10.802	55.528
5.	0.00103069	8.580	64.108
6.	0.00077426	6.445	70.553
7.	0.00073467	6.116	76.669
8.	0.00050974	4.243	80.912
9.	0.00047511	3.955	84.867
10.	0.00043354	3.609	88.476
11.	0.00035903	2.989	91.465
12.	0.00032722	2.724	94.189
13.	0.00024330	2.025	96.214
14.	0.00016622	1.384	97.598
15.	0.00013145	1.094	98.692
16.	0.00010835	0.902	99.594
17.	0.00004876	0.406	100.000

Total variance: 0.01201275

Appendix E:
Principal Component Analysis, Pubis, Procrustes Coordinates

PC	Eigenvalues	Variance%	Cum.%
1.	0.00251620	24.135	24.135
2.	0.00212475	20.380	44.516
3.	0.00105866	10.155	54.670
4.	0.00098450	9.443	64.113
5.	0.00065683	6.300	70.414
6.	0.00059639	5.721	76.134
7.	0.00048226	4.626	80.760
8.	0.00038518	3.695	84.455
9.	0.00033797	3.242	87.696
10.	0.00029743	2.853	90.549
11.	0.00023558	2.260	92.809
12.	0.00017826	1.710	94.519
13.	0.00015162	1.454	95.973
14.	0.00011396	1.093	97.066
15.	0.00007970	0.764	97.831
16.	0.00007673	0.736	98.567
17.	0.00005366	0.515	99.081
18.	0.00004100	0.393	99.475
19.	0.00003438	0.330	99.804
20.	0.00002039	0.196	100.000

Total variance: 0.01201275

Appendix F:
Principal Component Analysis, Ilium-Ischium, Procrustes Coordinates

PC	Eigenvalues	Variance%	Cum.%
1.	0.00150097	20.037	20.037
2.	0.00090486	12.079	32.117
3.	0.00058809	7.851	39.968
4.	0.00051660	6.896	46.864
5.	0.00039005	5.207	52.071
6.	0.00035320	4.715	56.786
7.	0.00031782	4.243	61.029
8.	0.00029582	3.949	64.978
9.	0.00025008	3.338	68.317
10.	0.00023536	3.142	71.459
11.	0.00020332	2.714	74.173
12.	0.00019594	2.616	76.789
13.	0.00017364	2.318	79.107
14.	0.00016429	2.193	81.300
15.	0.00013894	1.855	83.155
16.	0.00012497	1.668	84.823
17.	0.00012292	1.641	86.464
18.	0.00010404	1.389	87.853
19.	0.00010113	1.350	89.203
20.	0.00008149	1.088	90.291
21.	0.00007275	0.971	91.262
22.	0.00006711	0.896	92.158
23.	0.00006559	0.876	93.033
24.	0.00006116	0.816	93.850
25.	0.00005329	0.711	94.561
26.	0.00004544	0.607	95.168
27.	0.00004176	0.557	95.725
28.	0.00003807	0.508	96.233
29.	0.00003478	0.464	96.698
30.	0.00002978	0.398	97.095
31.	0.00002697	0.360	97.455
32.	0.00002400	0.320	97.776
33.	0.00002071	0.276	98.052
34.	0.00002036	0.272	98.324
35.	0.00001721	0.230	98.554
36.	0.00001592	0.213	98.766
37.	0.00001388	0.185	98.952
38.	0.00001297	0.173	99.125
39.	0.00001105	0.147	99.272
40.	0.00001061	0.142	99.414
41.	0.00000858	0.115	99.528
42.	0.00000721	0.096	99.625
43.	0.00000609	0.081	99.706
44.	0.00000472	0.063	99.769
45.	0.00000460	0.061	99.830
46.	0.00000362	0.048	99.879
47.	0.00000209	0.028	99.907
48.	0.00000186	0.025	99.931
49.	0.00000158	0.021	99.952
50.	0.00000121	0.016	99.969
51.	0.00000088	0.012	99.980
52.	0.00000054	0.007	99.988
53.	0.00000043	0.006	99.993
54.	0.00000025	0.003	99.997
55.	0.00000022	0.003	100.000
56.	0.00000003	0.000	100.000

Total variance: 0.00749085

Appendix G:
Principal Component Analysis, Ilium-Pubis, Procrustes Coordinates

PC	Eigenvalues	Variance%	Cum.%
1.	0.00124340	19.496	19.496
2.	0.00078526	12.313	31.809
3.	0.00054100	8.483	40.292
4.	0.00040686	6.379	46.671
5.	0.00038949	6.107	52.778
6.	0.00034252	5.371	58.149
7.	0.00030398	4.766	62.915
8.	0.00022961	3.600	66.516
9.	0.00020797	3.261	69.777
10.	0.00018127	2.842	72.619
11.	0.00016458	2.581	75.200
12.	0.00015226	2.387	77.587
13.	0.00014202	2.227	79.814
14.	0.00013753	2.157	81.970
15.	0.00012116	1.900	83.870
16.	0.00010626	1.666	85.536
17.	0.00009916	1.555	87.091
18.	0.00008065	1.265	88.356
19.	0.00007377	1.157	89.512
20.	0.00007029	1.102	90.614
21.	0.00005855	0.918	91.532
22.	0.00005238	0.821	92.354
23.	0.00005146	0.807	93.161
24.	0.00004518	0.708	93.869
25.	0.00004003	0.628	94.497
26.	0.00003797	0.595	95.092
27.	0.00003383	0.530	95.622
28.	0.00003200	0.502	96.124
29.	0.00002965	0.465	96.589
30.	0.00002558	0.401	96.990
31.	0.00002352	0.369	97.359
32.	0.00002229	0.349	97.708
33.	0.00001874	0.294	98.002
34.	0.00001737	0.272	98.275
35.	0.00001617	0.254	98.528
36.	0.00001335	0.209	98.738
37.	0.00001270	0.199	98.937
38.	0.00001122	0.176	99.113
39.	0.00000968	0.152	99.264
40.	0.00000821	0.129	99.393
41.	0.00000684	0.107	99.500
42.	0.00000548	0.086	99.586
43.	0.00000468	0.073	99.660
44.	0.00000415	0.065	99.725
45.	0.00000329	0.052	99.776
46.	0.00000281	0.044	99.821
47.	0.00000239	0.037	99.858
48.	0.00000231	0.036	99.894
49.	0.00000203	0.032	99.926
50.	0.00000131	0.021	99.946
51.	0.00000108	0.017	99.963
52.	0.00000088	0.014	99.977
53.	0.00000069	0.011	99.988
54.	0.00000031	0.005	99.993
55.	0.00000028	0.004	99.997
56.	0.00000009	0.001	99.999
57.	0.00000007	0.001	100.000
58.	0.00000002	0.000	100.000

Total variance: 0.00637762

Appendix H:
Principal Component Analysis, Ischium-Pubis, Procrustes Coordinates

PC	Eigenvalues	Variance%	Cum.%
1.	0.00116129	14.830	14.830
2.	0.00096160	12.280	27.111
3.	0.00061797	7.892	35.002
4.	0.00055574	7.097	42.099
5.	0.00048110	6.144	48.243
6.	0.00046065	5.883	54.126
7.	0.00040154	5.128	59.254
8.	0.00034337	4.385	63.639
9.	0.00032338	4.130	67.769
10.	0.00030539	3.900	71.669
11.	0.00026207	3.347	75.016
12.	0.00024110	3.079	78.095
13.	0.00019031	2.430	80.525
14.	0.00017683	2.258	82.783
15.	0.00016393	2.093	84.877
16.	0.00014811	1.891	86.768
17.	0.00011547	1.475	88.243
18.	0.00010714	1.368	89.611
19.	0.00010085	1.288	90.899
20.	0.00009719	1.241	92.140
21.	0.00008034	1.026	93.166
22.	0.00006724	0.859	94.025
23.	0.00005640	0.720	94.745
24.	0.00005543	0.708	95.453
25.	0.00004922	0.629	96.081
26.	0.00004349	0.555	96.637
27.	0.00003926	0.501	97.138
28.	0.00003646	0.466	97.604
29.	0.00002931	0.374	97.978
30.	0.00002766	0.353	98.331
31.	0.00002354	0.301	98.632
32.	0.00002276	0.291	98.923
33.	0.00001965	0.251	99.174
34.	0.00001336	0.171	99.344
35.	0.00001228	0.157	99.501
36.	0.00000938	0.120	99.621
37.	0.00000766	0.098	99.719
38.	0.00000697	0.089	99.808
39.	0.00000483	0.062	99.869
40.	0.00000428	0.055	99.924
41.	0.00000269	0.034	99.958
42.	0.00000147	0.019	99.977
43.	0.00000110	0.014	99.991
44.	0.00000071	0.009	100.000

Total variance: 0.0078304

Appendix I:
Spearman's Correlation for the Whole Bone Dataset

		Sex Estimation	VA	SPC	IPRR	GSN
PC1	r	**0.476	*0.322	**0.460	*0.316	**0.737
	p-value	0.000	0.013	0.000	0.015	0.000
PC2	r	0.017	-0.058	0.031	0.045	-0.057
	p-value	0.900	0.662	0.817	0.733	0.668
PC3	r	*0.260	**0.370	0.132	0.229	0.082
	p-value	0.047	0.004	0.318	0.082	0.538
PC4	r	*-0.272	-0.180	-0.146	-0.172	-0.116
	p-value	0.037	0.173	0.269	0.194	0.382
PC5	r	-0.075	0.012	-0.111	-0.210	-0.246
	p-value	0.574	0.930	0.404	0.110	0.060
PC6	r	-0.035	.0050	-0.049	0.126	-0.005
	p-value	0.791	.0709	0.714	0.343	0.972
PC7	r	0.001	.0081	0.039	0.161	-0.173
	p-value	0.994	.0540	0.772	0.224	0.191
PC8	r	0.244	*0.307	*0.294	0.082	-0.064
	p-value	0.063	0.018	0.024	0.538	0.630
PC9	r	0.059	0.065	-0.003	-0.115	-0.037
	p-value	0.659	0.624	0.982	0.385	0.781
PC10	r	0.080	0.143	0.237	-0.010	-0.031
	p-value	0.549	0.280	0.070	0.938	0.815
PC11	r	0.121	0.144	0.111	-0.090	0.189
	p-value	0.360	0.275	0.405	0.498	0.151
PC12	r	0.051	0.157	0.087	-0.018	0.072
	p-value	0.699	0.234	0.513	0.889	0.589
PC13	r	*-0.280	0.041	-0.074	**-0.394	-0.090
	p-value	0.031	0.758	0.578	0.002	0.498
PC14	r	0.059	-0.005	-0.006	0.092	-0.031
	p-value	0.655	0.968	0.965	0.487	0.813
PC15	r	0.022	0.097	0.189	0.013	-0.006
	p-value	0.871	0.466	0.151	0.924	0.963
PC16	r	0.027	0.017	-0.042	0.157	-0.144
	p-value	0.842	0.901	0.753	0.236	0.277
PC17	r	0.249	0.106	0.085	0.191	0.076
	p-value	0.058	0.426	0.520	0.146	0.565
PC18	r	0.109	0.191	0.103	-0.023	-0.066
	p-value	0.409	0.147	0.438	0.865	0.620

PC19	r	-0.069	0.031	-0.068	-0.231	-0.182
	p-value	0.606	0.813	0.611	0.079	0.167
PC20	r	0.142	0.133	0.077	0.086	0.028
	p-value	0.282	0.314	0.564	0.518	0.833
PC21	r	0.072	0.086	-0.077	0.073	0.071
	p-value	0.586	0.516	0.561	0.583	0.591
PC22	r	0.022	0.124	-0.023	0.109	0.007
	p-value	0.871	0.351	0.865	0.412	0.957
PC23	r	-0.009	-0.045	-0.098	-0.018	0.053
	p-value	0.871	0.737	0.459	0.892	0.691
PC24	r	-0.050	-0.127	-0.072	-0.040	-0.193
	p-value	0.705	0.338	0.589	0.765	0.143
PC25	r	-0.016	-0.001	-0.021	-0.023	0.075
	p-value	0.903	0.996	0.877	0.860	0.571
PC26	r	-0.098	0.086	-0.243	0.059	0.009
	p-value	0.682	0.516	0.063	0.657	0.945
PC27	r	0.070	-0.094	-0.138	-0.127	-0.049
	p-value	0.598	0.481	0.298	0.337	0.710
PC28	r	0.056	0.176	0.085	-0.096	0.149
	p-value	0.676	0.182	0.521	0.470	0.260
PC29	r	-0.046	0.167	-0.060	0.139	0.072
	p-value	0.730	0.207	0.649	0.295	0.589
PC30	r	-0.059	-0.050	0.090	0.146	-0.095
	p-value	0.657	0.709	0.500	0.269	0.475
PC31	r	0.010	0.067	0.010	-0.047	-0.006
	p-value	0.941	0.612	0.938	0.722	0.964
PC32	r	0.036	0.070	0.191	-0.042	-0.118
	p-value	0.788	0.600	0.148	0.753	0.374
PC33	r	0.200	0.160	0.103	-0.027	0.058
	p-value	0.129	0.227	0.438	0.841	0.662
PC34	r	-0.099	-0.069	0.044	0.018	-0.075
	p-value	0.456	0.604	0.739	0.893	0.572
PC35	r	-0.048	0.033	-0.080	-0.093	0.020
	p-value	0.716	0.805	0.548	0.485	0.878
PC36	r	-0.008	0.048	0.031	0.067	0.065
	p-value	0.952	0.719	0.818	0.613	0.627
PC37	r	-0.095	-0.036	-0.189	-0.116	-0.024
	p-value	0.474	0.786	0.152	0.382	0.857
PC38	r	0.060	0.026	0.138	0.011	0.064
	p-value	0.650	0.846	0.297	0.937	0.630
PC39	r	-0.081	-0.148	-0.027	-0.105	-0.139
	p-value	0.543	0.262	0.837	0.427	0.293
PC40	r	-0.041	0.145	0.066	-0.045	0.040

	p-value	0.760	0.274	0.617	0.734	0.764
PC41	r	-0.006	-0.150	-0.066	0.189	0.075
	p-value	0.964	0.257	0.619	0.151	0.572
PC42	r	-0.174	-0.057	-0.115	-0.075	-0.101
	p-value	0.187	0.670	0.385	0.571	0.445
PC43	r	-0.037	-0.108	-0.048	0.071	-0.043
	p-value	0.783	0.414	0.717	0.593	0.749
PC44	r	-0.162	-0.251	-0.052	0.116	0.046
	p-value	0.219	0.055	0.696	0.383	0.727
PC45	r	0.102	0.027	0.042	0.045	0.017
	p-value	0.443	0.841	0.750	0.736	0.895
PC46	r	0.085	0.038	-0.004	-0.019	0.116
	p-value	0.523	0.773	0.977	0.885	0.382
PC47	r	0.004	0.086	0.019	0.032	0.008
	p-value	0.976	0.516	0.884	0.810	0.950
PC48	r	-0.020	0.056	-0.113	-0.066	-0.102
	p-value	0.880	0.671	0.392	0.618	0.441
PC49	r	-0.014	-0.025	-0.141	-0.021	-0.015
	p-value	0.913	0.850	0.288	0.873	0.913
PC50	r	-0.077	-0.102	-0.079	0.015	-0.083
	p-value	0.562	0.444	0.550	0.912	0.531
PC51	r	-0.169	-0.152	-0.184	-0.146	-0.040
	p-value	0.202	0.252	0.164	0.270	0.762
PC52	r	-0.035	0.142	0.058	0.002	-0.056
	p-value	0.795	0.284	0.660	0.988	0.674
PC53	r	0.064	-0.024	-0.018	0.072	0.024
	p-value	0.631	0.855	0.895	0.586	0.856
PC54	r	-0.062	0.060	-0.006	-0.186	-0.018
	p-value	0.641	0.650	0.963	0.158	0.895
PC55	r	0.021	0.014	0.046	0.163	-0.009
	p-value	0.873	0.919	0.728	0.218	0.947
PC56	r	0.055	-0.049	0.067	0.027	0.049
	p-value	0.679	0.715	0.614	0.842	0.711
PC57	r	0.045	0.048	-0.162	0.020	0.008
	p-value	0.734	0.720	0.220	0.881	0.954
PC58	r	0.086	0.005	-0.125	0.086	0.043
	p-value	0.517	0.969	0.344	0.515	0.745

Appendix J:
Spearman's Correlation for Ilium Dataset

		Sex Estimation	VA	SCP	IPRR	GSN
PC1	r	**-0.444	*-0.319	**-0.385	*-0.330	**-0.641
	p-value	0.000	0.014	0.003	0.011	0.000
PC2	r	-0.043	0.061	0.012	0.114	-0.074
	p-value	0.745	0.648	0.929	0.390	0.575
PC3	r	-0.061	0.057	-0.141	-0.158	-0.084
	p-value	0.647	0.665	0.287	0.232	0.529
PC4	r	*0.301	0.137	0.198	0.205	**0.340
	p-value	0.020	0.300	0.132	0.120	0.008
PC5	r	-0.086	0.006	-0.090	0.126	0.013
	p-value	0.516	0.965	0.499	0.342	0.925
PC6	r	-0.099	-0.018	-0.153	-0.140	-0.030
	p-value	0.458	0.892	0.248	0.292	0.823
PC7	r	-0.050	-0.251	-0.139	0.032	-0.077
	p-value	0.708	0.055	0.295	0.808	0.562
PC8	r	-0.208	-0.174	-0.216	-0.076	-0.072
	p-value	0.113	0.188	0.101	0.567	0.587
PC9	r	-0.027	*0.272	0.162	-0.026	-0.150
	p-value	0.837	0.037	0.221	0.847	0.257
PC10	r	0.206	0.199	0.085	0.179	0.105
	p-value	0.118	0.131	0.522	0.176	0.429
PC11	r	0.109	0.084	0.168	0.115	0.202
	p-value	0.409	0.529	0.202	0.388	0.125
PC12	r	0.105	0.087	0.112	0.018	-0.012
	p-value	0.428	0.513	0.398	0.894	0.929
PC13	r	0.043	0.017	0.078	0.136	0.093
	p-value	0.746	0.897	0.555	0.303	0.484
PC14	r	0.046	0.000	0.014	-0.003	0.151
	p-value	0.727	0.997	0.916	0.980	0.255
PC15	r	-0.107	-0.057	-0.109	0.000	-0.147
	p-value	0.420	0.666	0.413	0.999	0.268
PC16	r	0.006	-0.031	0.034	-0.177	0.167
	p-value	0.963	0.814	0.801	0.181	0.207
PC17	r	-0.039	-0.198	-0.120	0.031	-0.158
	p-value	0.769	0.132	0.367	0.818	0.231
PC18	r	0.030	-0.010	*0.288	-0.106	-0.053
	p-value	0.823	0.940	0.027	0.425	0.690

PC19	r	-0.016	-0.014	-0.049	-0.133	-0.106
	p-value	0.903	0.917	0.710	0.316	0.422
PC20	r	-0.014	0.024	-0.035	-0.108	0.072
	p-value	0.916	0.856	0.790	0.415	0.588
PC21	r	-0.168	-0.033	-0.110	*-0.279	-0.041
	p-value	0.203	0.804	0.406	0.033	0.760
PC22	r	-0.029	-0.186	0.081	0.231	0.036
	p-value	0.828	0.158	0.542	0.078	0.789
PC23	r	-0.047	-0.171	-0.090	-0.065	-0.062
	p-value	0.721	0.197	0.498	0.622	0.641
PC24	r	-0.082	-0.120	-0.080	-0.150	-0.013
	p-value	0.539	0.364	0.545	0.256	0.921
PC25	r	-0.029	-0.012	0.106	0.133	0.058
	p-value	0.827	0.925	0.424	0.316	0.662
PC26	r	0.088	0.057	0.104	0.138	-0.120
	p-value	0.506	0.667	0.431	0.297	0.365
PC27	r	0.078	-0.007	0.143	-0.133	-0.111
	p-value	0.557	0.961	0.281	0.316	0.403
PC28	r	-0.022	0.026	0.036	-0.050	0.072
	p-value	0.867	0.844	0.784	0.706	0.590
PC29	r	-0.022	0.049	0.062	0.055	0.040
	p-value	0.867	0.712	0.639	0.679	0.761
PC30	r	-0.199	-0.104	-0.057	-0.067	-0.121
	p-value	0.131	0.432	0.669	0.613	0.362
PC31	r	0.046	-0.026	0.010	0.188	0.040
	p-value	0.727	0.848	0.937	0.154	0.765
PC32	r	0.017	-0.022	0.125	0.039	0.147
	p-value	0.898	0.870	0.344	0.769	0.266

Appendix K:
Spearman's Correlation for the Ischium Dataset

		Sex Estimation	VA	SPC	IPRR	GSN
PC1	r	0.047	0.076	-0.052	0.013	0.015
	p-value	0.723	0.568	0.697	0.924	0.908
PC2	r	-0.009	0.034	-0.047	-0.053	*-0.285
	p-value	0.948	0.801	0.721	0.692	0.029
PC3	r	0.035	-0.155	-0.080	0.210	0.074
	p-value	0.794	0.242	0.549	0.110	0.576
PC4	r	-0.179	-0.100	*-0.282	-0.092	-0.035
	p-value	0.174	0.452	0.030	0.491	0.795
PC5	r	-0.026	-0.114	-0.034	-0.081	-0.087
	p-value	0.845	0.391	0.800	0.544	0.514
PC6	r	-0.066	0.156	-0.154	-0.193	-0.199
	p-value	0.617	0.237	0.243	0.143	0.131
PC7	r	0.061	0.070	0.009	0.092	0.144
	p-value	0.645	0.598	0.945	0.486	0.276
PC8	r	0.064	0.110	0.001	-0.110	0.037
	p-value	0.628	0.405	0.995	0.405	0.779
PC9	r	*0.305	*0.306	0.175	0.102	0.183
	p-value	0.019	0.019	0.185	0.441	0.165
PC10	r	0.094	0.038	0.095	0.058	0.082
	p-value	0.479	0.773	0.472	0.663	0.539
PC11	r	-0.008	0.117	0.135	-0.196	0.104
	p-value	0.950	0.376	0.307	0.138	0.433
PC12	r	0.122	0.027	-0.023	0.083	0.007
	p-value	0.358	0.838	0.861	0.533	0.957
PC13	r	0.044	0.081	0.043	0.025	-0.154
	p-value	0.743	0.541	0.746	0.851	0.244
PC14	r	**-0.334	*-0.310	**-0.340	*-0.300	-0.202
	p-value	0.010	0.017	0.008	0.021	0.125
PC15	r	-0.154	-0.038	0.044	0.053	0.038
	p-value	0.244	0.777	0.741	0.693	0.777
PC16	r	*-0.283	-0.169	*-0.279	-0.246	-0.232
	p-value	0.030	0.201	0.032	0.060	0.077
PC17	r	-0.020	-0.135	-0.204	-0.005	-0.159
	p-value	0.881	0.307	0.121	0.972	0.229

Appendix L:
Spearman's Correlation for the Pubis Dataset

		Sex Estimation	VA	SPC	IPRR	GSN
PC1	r	**-0.385	-0.183	-0.204	-0.246	*-0.289
	p-value	0.003	0.166	0.121	0.060	0.026
PC2	r	**0.415	**0.472	**0.498	**0.367	**0.389
	p-value	0.001	0.000	0.000	0.004	0.002
PC3	r	**-0.369	-0.112	-0.178	**-0.569	**-0.407
	p-value	0.004	0.398	0.176	0.000	0.001
PC4	r	0.047	-0.004	0.077	0.240	-0.049
	p-value	0.725	0.978	0.561	0.067	0.714
PC5	r	0.042	0.097	-0.135	-0.053	0.020
	p-value	0.753	0.463	0.307	0.691	0.879
PC6	r	0.153	0.110	0.000	0.108	0.096
	p-value	0.247	0.407	0.999	0.417	0.472
PC7	r	-0.068	-0.178	-0.055	-0.034	-0.170
	p-value	0.609	0.177	0.679	0.796	0.198
PC8	r	0.103	-0.031	0.143	0.204	-0.103
	p-value	0.435	0.813	0.282	0.122	0.436
PC9	r	-0.047	-0.007	-0.117	0.096	-0.059
	p-value	0.725	0.960	0.380	0.469	0.659
PC10	r	-0.212	-0.112	*-0.311	0.068	-0.010
	p-value	0.107	0.397	0.017	0.607	0.939
PC11	r	-0.138	-0.114	-0.075	0.017	-0.053
	p-value	0.299	0.388	0.571	0.898	0.690
PC12	r	-0.163	-0.111	-0.090	0.040	0.068
	p-value	0.217	0.401	0.500	0.762	0.611
PC13	r	-0.057	-0.014	-0.217	-0.061	-0.166
	p-value	0.670	0.917	0.099	0.646	0.208
PC14	r	0.122	0.079	0.131	0.040	*0.268
	p-value	0.356	0.552	0.323	0.766	0.040
PC15	r	-0.003	-0.154	-0.033	0.180	0.023
	p-value	0.982	0.243	0.804	0.173	0.860
PC16	r	0.038	*0.295	0.030	-0.012	0.061
	p-value	0.778	0.023	0.823	0.930	0.648
PC17	r	0.185	0.092	0.066	0.039	0.015
	p-value	0.160	0.487	0.619	0.767	0.908
PC18	r	0.189	*0.302	0.138	-0.019	0.009
	p-value	0.152	0.020	0.298	0.887	0.949

PC19	r	0.043	*0.263	0.133	-0.140	0.137
	p-value	0.744	0.044	0.316	0.291	0.300
PC20	r	0.046	0.116	0.081	0.039	0.083
	p-value	0.731	0.383	0.540	0.767	0.531

Appendix M:
Spearman's Correlation of Ilium-Ischium Dataset

		Sex Estimation	VA	SPC	IPRR	GSN
PC1	r	**0.478	*0.285	**0.425	**0.402	**0.778
	p-value	0.000	0.028	0.001	0.002	0.000
PC2	r	0.070	0.073	0.044	0.104	-0.077
	p-value	0.598	0.582	0.742	0.435	0.560
PC3	r	0.115	-0.015	0.103	0.153	00.121
	p-value	0.385	0.911	0.436	0.247	0.361
PC4	r	-0.228	-0.229	-0.106	0.003	-0.124
	p-value	0.082	0.081	0.425	0.981	0.349
PC5	r	-0.127	-0.066	-0.143	0.141	-0.047
	p-value	0.337	0.621	0.281	0.287	0.726
PC6	r	-0.080	-0.130	-0.161	-0.098	0.081
	p-value	0.546	0.327	0.223	0.461	0.542
PC7	r	-0.121	-0.209	-0.155	0.034	0.155
	p-value	0.361	0.112	0.240	0.799	0.240
PC8	r	-0.074	0.153	0.099	0.078	-0.100
	p-value	0.580	0.247	0.457	0.555	0.452
PC9	r	0.055	-0.199	-0.045	0.091	-0.049
	p-value	0.677	0.131	0.733	0.493	0.711
PC10	r	-0.191	-0.148	-0.157	-0.093	-0.139
	p-value	0.148	0.264	0.235	0.484	0.292
PC11	r	-0.004	0.041	0.058	-0.033	0.021
	p-value	0.975	0.755	0.663	0.803	0.874
PC12	r	0.148	0.134	0.203	0.046	0.153
	p-value	0.264	0.311	0.123	0.731	0.247
PC13	r	0.080	-0.066	-0.150	0.139	-0.035
	p-value	0.544	0.620	0.256	0.293	0.790
PC14	r	0.077	-0.082	-0.032	0.028	0.144
	p-value	0.564	0.538	0.811	0.835	0.276
PC15	r	-0.098	-0.143	0.030	-0.182	0.126
	p-value	0.459	0.279	0.823	0.168	0.341
PC16	r	0.096	0.126	0.068	0.043	-0.037
	p-value	0.469	0.343	0.611	0.745	0.779
PC17	r	-0.193	-0.086	-0.121	-0.070	-0.056
	p-value	0.143	0.520	0.361	0.596	0.674
PC18	r	0.097	0.083	0.084	*0.310	0.152
	p-value	0.463	0.534	0.528	0.017	0.249

PC19	r	-0.044	-0.010	0.037	0.047	-0.143
	p-value	0.744	0.937	0.782	0.723	0.280
PC20	r	-0.046	0.078	-0.004	-0.061	0.159
	p-value	0.731	0.558	0.978	0.644	0.231
PC21	r	0.092	0.100	-0.141	0.116	0.111
	p-value	0.490	0.449	0.285	0.381	0.401
PC22	r	-0.083	-0.028	0.127	0.160	0.079
	p-value	0.534	0.831	0.338	0.227	0.552
PC23	r	0.044	0.208	0.075	-0.037	0.070
	p-value	0.742	0.115	0.573	0.784	0.597
PC24	r	-0.007	-0.008	0.004	-0.001	0.001
	p-value	0.961	0.952	0.974	0.993	0.993
PC25	r	-0.011	0.058	0.034	0.009	-0.037
	p-value	0.936	0.663	0.796	0.943	0.782
PC26	r	0.198	-0.010	0.131	**0.356	0.039
	p-value	0.132	0.940	0.323	0.006	0.772
PC27	r	-0.035	-0.001	0.058	0.110	0.021
	p-value	0.790	0.992	0.663	0.406	0.875
PC28	r	0.062	0.157	-0.059	-0.023	0.007
	p-value	0.642	0.234	0.658	0.866	0.956
PC29	r	0.072	-0.071	0.149	0.130	-0.012
	p-value	0.588	0.591	0.259	0.327	0.930
PC30	r	0.038	0.147	0.103	0.102	-0.075
	p-value	0.777	0.266	0.439	0.444	0.571
PC31	r	0.130	0.230	0.199	-0.016	0.114
	p-value	0.327	0.080	0.132	0.902	0.388
PC32	r	0.120	0.133	0.244	-0.109	0.037
	p-value	0.364	0.315	0.063	0.411	0.782
PC33	r	-0.159	-0.046	-0.154	-0.108	-0.092
	p-value	0.229	0.729	0.243	0.416	0.491
PC34	r	0.067	0.025	0.021	0.132	0.025
	p-value	0.613	0.849	0.875	0.320	0.850
PC35	r	-0.071	0.036	0.008	0.204	0.093
	p-value	0.595	0.784	0.950	0.121	0.484
PC36	r	-0.147	-0.188	-0.166	-0.084	-0.041
	p-value	0.268	0.154	0.208	0.525	0.757
PC37	r	-0.026	0.014	-0.105	-0.050	-0.060
	p-value	0.842	0.918	0.428	0.708	0.652
PC38	r	0.159	0.241	0.030	-0.144	0.010
	p-value	0.228	0.066	0.821	0.278	0.940
PC39	r	-0.115	-0.027	-0.019	-0.153	0.001
	p-value	0.385	0.842	0.885	0.247	0.997
PC40	r					

	p-value	-0.094	-0.028	-0.066	-0.066	0.064
		0.478	0.832	0.619	0.618	0.632
PC41	r	-0.003	0.093	-0.024	-0.031	-0.078
	p-value	0.982	0.483	0.855	0.818	0.556
PC42	r	-0.061	-0.039	-0.079	-0.047	-0.037
	p-value	0.644	0.772	0.554	0.727	0.779
PC43	r	0.104	-0.019	0.145	0.152	0.082
	p-value	0.435	0.888	0.273	0.252	0.536
PC44	r	0.094	0.066	0.000	0.100	0.100
	p-value	0.478	0.618	0.999	0.451	0.449
PC45	r	0.055	-0.028	0.103	-0.076	-0.046
	p-value	0.677	0.833	0.440	0.570	0.731
PC46	r	-0.096	-0.084	-0.088	-0.053	-0.158
	p-value	0.469	0.526	0.506	0.690	0.232
PC47	r	-0.049	-0.042	-0.072	-0.053	0.042
	p-value	0.714	0.750	0.589	0.690	0.755
PC48	r	-0.017	-0.034	0.001	-0.017	-0.090
	p-value	0.896	0.798	0.992	0.898	0.498
PC49	r	0.045	0.040	-0.033	-0.115	0.081
	p-value	0.737	0.766	0.804	0.387	0.543
PC50	r	-0.134	-0.194	0.041	0.061	-0.073
	p-value	0.311	0.142	0.760	0.645	0.582
PC51	r	0.066	-0.032	0.026	0.071	0.047
	p-value	0.621	0.809	0.845	0.591	0.723
PC52	r	0.150	0.132	0.171	0.128	0.075
	p-value	0.256	0.320	0.195	0.334	0.575
PC53	r	-0.007	0.026	-0.117	0.173	0.014
	p-value	0.956	0.843	0.378	0.189	0.915
PC54	r	0.176	0.224	0.127	0.086	0.092
	p-value	0.182	0.088	0.336	0.515	0.487
PC55	r	-0.138	-0.145	-0.078	-0.096	-0.104
	p-value	0.296	0.274	0.557	0.470	0.432
PC56	r	-0.006	-0.117	0.168	-0.006	0.067
	p-value	0.962	0.378	0.203	0.962	0.617

Appendix N:
Spearman's Correlation of the Ilium-Pubis Dataset

		Sex Estimation	VA	SPC	IPRR	GSN
PC1	r	**0.413	0.221	**0.447	*0.310	**0.673
	p-value	0.001	0.092	0.000	0.017	0.000
PC2	r	-0.019	-0.026	-0.038	0.005	-0.149
	p-value	0.884	0.848	0.774	0.969	0.260
PC3	r	0.096	*0.257	0.057	0.063	0.015
	p-value	0.469	0.049	0.670	0.635	0.912
PC4	r	0.176	0.022	0.069	0.105	0.250
	p-value	0.182	0.870	0.604	0.429	0.056
PC5	r	0.203	0.072	0.051	0.007	0.137
	p-value	0.124	0.589	0.699	0.961	0.299
PC6	r	0.174	0.248	0.147	**0.336	0.219
	p-value	0.186	0.059	0.265	0.009	0.095
PC7	r	0.194	0.179	0.226	-0.012	0.106
	p-value	0.141	0.176	0.086	0.929	0.423
PC8	r	*-0.258	*-0.289	-0.210	-0.176	-0.076
	p-value	0.048	0.026	0.110	0.182	0.569
PC9	r	0.005	0.101	0.187	-0.011	-0.025
	p-value	0.971	0.449	0.156	0.935	0.853
PC10	r	-0.151	0.121	-0.033	-0.234	-0.079
	p-value	0.254	0.360	0.803	0.075	0.550
PC11	r	0.192	0.175	0.180	0.056	0.021
	p-value	0.145	0.184	0.172	0.675	0.877
PC12	r	-0.146	-0.071	-0.002	-0.180	0.021
	p-value	0.270	0.594	0.987	0.172	0.873
PC13	r	0.202	*0.257	*0.270	0.199	-0.165
	p-value	0.126	0.049	0.039	0.132	0.213
PC14	r	-0.142	-0.011	-0.150	-0.006	-0.201
	p-value	0.283	0.937	0.256	0.962	0.128
PC15	r	0.033	-0.048	-0.046	0.157	-0.008
	p-value	0.802	0.719	0.729	0.234	0.951
PC16	r	0.077	-0.048	-0.053	0.101	-0.028
	p-value	0.563	0.717	0.689	0.445	0.836
PC17	r	-0.088	-0.014	-0.045	**-0.369	-0.197
	p-value	0.506	0.919	0.738	0.004	0.135
PC18	r	0.177	*0.291	0.053	0.104	0.063
	p-value	0.179	0.026	0.688	0.433	0.638

PC19	r	-0.048	0.047	-0.093	-0.053	0.053
	p-value	0.721	0.726	0.485	0.688	0.689
PC20	r	0.002	0.018	-0.152	0.072	0.037
	p-value	0.990	0.890	0.252	0.586	0.779
PC21	r	-0.106	-0.045	-0.199	0.027	-0.061
	p-value	0.422	0.734	0.130	0.838	0.648
PC22	r	0.023	0.153	0.004	0.132	0.148
	p-value	0.864	0.248	0.973	0.318	0.263
PC23	r	0.024	0.032	0.149	0.076	0.047
	p-value	0.858	0.808	0.261	0.567	0.722
PC24	r	-0.143	-0.068	-0.218	-0.191	0.063
	p-value	0.279	0.607	0.097	0.148	0.635
PC25	r	0.127	0.084	-0.133	0.028	0.094
	p-value	0.336	0.525	0.314	0.831	0.480
PC26	r	0.055	0.022	0.041	-0.049	0.061
	p-value	0.677	0.870	0.757	0.710	0.647
PC27	r	0.051	0.045	-0.154	0.077	0.118
	p-value	0.704	0.734	0.245	0.564	0.374
PC28	r	-0.058	0.050	0.022	-0.062	0.007
	p-value	0.663	0.706	0.869	0.640	0.959
PC29	r	-0.086	-0.080	0.098	-0.037	-0.113
	p-value	0.519	0.547	0.458	0.781	0.394
PC30	r	-0.064	-0.023	0.156	0.116	0.022
	p-value	0.633	0.864	0.239	0.381	0.871
PC31	r	0.093	0.118	0.095	0.094	0.169
	p-value	0.485	0.373	0.475	0.480	0.201
PC32	r	0.090	0.142	0.111	-0.131	0.002
	p-value	0.500	0.283	0.402	0.324	0.989
PC33	r	0.216	0.243	0.146	-0.089	-0.092
	p-value	0.101	0.064	0.268	0.504	0.490
PC34	r	-0.092	-0.148	-0.175	-0.054	-0.147
	p-value	0.486	0.262	0.185	0.685	0.267
PC35	r	0.046	-0.011	0.030	0.084	-0.014
	p-value	0.731	0.932	0.822	0.527	0.915
PC36	r	0.136	0.025	0.058	-0.036	0.108
	p-value	0.303	0.854	0.662	0.785	0.416
PC37	r	-0.074	-0.001	0.046	0.052	0.058
	p-value	0.579	0.994	0.727	0.695	0.663
PC38	r	0.099	0.128	-0.004	-0.073	0.107
	p-value	0.456	0.334	0.977	0.583	0.420
PC39	r	0.150	0.012	-0.004	0.122	-0.020
	p-value	0.258	0.927	0.978	0.355	0.879

PC40	r	-0.080	-0.012	-0.175	-0.007	-0.037
	p-value	0.548	0.926	0.184	0.955	0.778
PC41	r	0.095	-0.037	0.099	0.175	-0.007
	p-value	0.472	0.779	0.457	0.185	0.961
PC42	r	-0.093	0.138	-0.021	-0.144	-0.047
	p-value	0.484	0.297	0.877	0.276	0.725
PC43	r	-0.241	-0.236	-0.114	-0.138	-0.099
	p-value	0.066	0.072	0.388	0.299	0.456
PC44	r	-0.044	0.029	-0.068	-0.039	-0.149
	p-value	0.742	0.828	0.610	0.771	0.261
PC45	r	-0.011	-0.132	-0.039	0.035	-0.024
	p-value	0.936	0.319	0.772	0.792	0.857
PC46	r	0.109	0.031	0.115	0.043	0.003
	p-value	0.409	0.818	0.387	0.746	0.982
PC47	r	0.121	0.072	-0.037	0.068	0.039
	p-value	0.362	0.589	0.781	0.606	0.768
PC48	r	0.055	0.006	0.106	0.149	0.040
	p-value	0.678	0.967	0.424	0.259	0.762
PC49	r	-0.028	-0.107	-0.040	0.029	0.006
	p-value	0.835	0.420	0.763	0.829	0.967
PC50	r	0.020	-0.013	-0.029	-0.168	0.017
	p-value	0.880	0.920	0.827	0.204	0.897
PC51	r	-0.091	-0.133	-0.067	-0.014	0.012
	p-value	0.491	0.316	0.614	0.914	0.926
PC52	r	-0.004	0.036	-0.157	0.032	-0.012
	p-value	0.975	0.784	0.234	0.810	0.930
PC53	r	0.065	-0.011	-0.054	0.053	0.092
	p-value	0.625	0.933	0.683	0.693	0.490
PC54	r	-0.157	-0.262*	-0.087	-0.005	-0.098
	p-value	0.235	0.045	0.513	0.968	0.460
PC55	r	-0.062	-0.158	-0.153	0.002	-0.095
	p-value	0.643	0.233	0.248	0.986	0.476
PC56	r	-0.153	0.052	-0.100	-0.066	-0.150
	p-value	0.247	0.698	0.453	0.618	0.258
PC57	r	-0.052	-0.071	-0.127	-0.111	-0.010
	p-value	0.696	0.591	0.336	0.403	0.940
PC58	r	-0.033	0.106	-0.061	-0.015	-0.043
	p-value	0.802	0.423	0.645	0.910	0.748

Appendix O:
Spearman's Correlation of the Ischium-Pubis Dataset

		Sex Estimation	VA	SPC	IPRR	GSN
PC1	r	**-0.596	**-0.439	**-0.404	**-0.534	**-0.404
	p-value	0.000	0.001	0.002	0.000	0.002
PC2	r	0.118	*0.291	0.190	0.164	0.146
	p-value	0.372	0.025	0.150	0.215	0.270
PC3	r	0.149	0.046	0.021	*0.286	-0.127
	p-value	0.261	0.728	0.873	0.028	0.338
PC4	r	-0.070	-0.097	0.110	-0.032	-0.031
	p-value	0.558	0.465	0.408	0.811	0.819
PC5	r	-0.037	-0.046	0.000	0.056	-0.042
	p-value	0.782	0.731	0.999	0.671	0.750
PC6	r	-0.099	-0.177	-0.145	0.059	-0.111
	p-value	0.457	0.179	0.275	0.659	0.405
PC7	r	0.125	-0.086	0.032	*0.325	*0.259
	p-value	0.344	0.519	0.811	0.012	0.048
PC8	r	0.039	0.084	-0.049	0.142	*0.315
	p-value	0.769	0.528	0.715	0.284	0.015
PC9	r	-0.039	0.080	-0.095	-0.250	-0.030
	p-value	0.830	0.546	0.475	0.057	0.824
PC10	r	0.165	-0.031	-0.100	0.133	0.022
	p-value	0.213	0.817	0.452	0.315	0.871
PC11	r	-0.124	-0.127	*-0.287	0.041	-0.147
	p-value	0.351	0.337	0.028	0.760	0.267
PC12	r	0.121	0.121	0.099	0.136	0.095
	p-value	0.362	0.361	0.454	0.303	0.476
PC13	r	0.090	0.023	0.149	-0.034	0.108
	p-value	0.496	0.863	0.260	0.798	0.417
PC14	r	0.031	0.054	-0.042	-0.017	0.039
	p-value	0.813	0.683	0.753	0.899	0.772
PC15	r	-0.070	-0.203	0.002	-0.028	-0.201
	p-value	0.600	0.123	0.986	0.832	0.126
PC16	r	-0.156	-0.140	-0.032	-0.008	0.100
	p-value	0.237	0.291	0.809	0.954	0.452
PC17	r	0.177	*0.306	0.012	0.039	0.155
	p-value	0.180	0.018	0.927	0.768	0.242
PC18	r	-0.028	0.020	-0.006	-0.118	0.010
	p-value	0.831	0.882	0.963	0.374	0.938

PC19	r	0.000	-0.189	0.105	-0.053	-0.079
	p-value	0.997	0.151	0.427	0.693	0.554
PC20	r	0.130	0.092	0.212	-0.016	0.151
	p-value	0.327	0.490	0.107	0.906	0.252
PC21	r	0.102	-0.020	0.154	-0.068	0.116
	p-value	0.443	0.881	0.244	0.610	0.383
PC22	r	-0.155	-0.059	-0.065	-0.054	-0.092
	p-value	0.243	0.657	0.626	0.684	0.486
PC23	r	-0.142	-0.210	-0.179	-0.029	-0.131
	p-value	0.283	0.110	0.175	0.828	0.324
PC24	r	0.051	-0.060	0.126	0.119	0.188
	p-value	0.701	0.654	0.343	0.371	0.155
PC25	r	-0.084	-0.069	-0.162	-0.006	0.067
	p-value	0.527	0.605	0.219	0.963	0.615
PC26	r	0.099	0.124	0.065	-0.083	0.108
	p-value	0.456	0.348	0.625	0.530	0.417
PC27	r	-0.029	-0.089	-0.116	0.056	0.036
	p-value	0.829	0.504	0.383	0.676	0.787
PC28	r	0.092	0.067	0.099	0.107	0.089
	p-value	0.489	0.613	0.455	0.419	0.500
PC29	r	0.000	0.065	0.167	0.079	-0.015
	p-value	0.994	0.625	0.206	0.554	0.913
PC30	r	0.123	0.026	0.231	0.067	0.100
	p-value	0.353	0.846	0.078	0.614	0.449
PC31	r	0.041	0.041	0.002	-0.024	0.009
	p-value	0.760	0.760	0.988	0.854	0.944
PC32	r	0.149	*0.289	0.132	-0.023	0.129
	p-value	0.260	0.026	0.319	0.864	0.329
PC33	r	0.149	-0.002	0.106	-0.034	0.067
	p-value	0.260	0.990	0.423	0.798	0.616
PC34	r	-0.111	-0.222	-0.092	0.040	0.083
	p-value	0.401	0.090	0.489	0.763	0.534
PC35	r	-0.018	0.157	0.031	-0.115	-0.063
	p-value	0.895	0.235	0.813	0.384	0.637
PC36	r	0.051	0.045	-0.012	-0.027	0.056
	p-value	0.699	0.733	0.926	0.839	0.671
PC37	r	-0.142	-0.202	*-0.277	-0.044	-0.018
	p-value	0.283	0.125	0.034	0.743	0.892
PC38	r	-0.104	-0.027	0.040	-0.102	0.103
	p-value	0.434	0.841	0.764	0.441	0.437
PC39	r	-0.097	0.035	0.039	-0.033	-0.120
	p-value	0.465	0.791	0.770	0.807	0.365

PC40	r	-0.171	-0.008	0.007	-0.023	-0.220
	p-value	0.195	0.954	0.957	0.865	0.094
PC41	r	-0.005	0.144	-0.075	-0.096	-0.107
	p-value	0.971	0.277	0.572	0.470	0.419
PC42	r	0.072	0.044	0.058	0.119	0.245
	p-value	0.589	0.743	0.661	0.368	0.062
PC43	r	0.102	0.023	0.023	0.033	0.015
	p-value	0.440	0.865	0.865	0.806	0.908
PC44	r	0.039	-0.027	-0.074	0.099	0.040
	p-value	0.768	0.841	0.579	0.457	0.762